Pattern Electroretinograpy in Peripheral Retina: System Development and Validation in Human Subjects

BY

SHRESTA PATANGAY
B.Tech., Jawaharlal Nehru Technological University, 2011
Hyderabad, India

THESIS

Submitted as partial fulfillment of the requirements
for the degree of Doctor of Philosophy in Bioengineering
in the Graduate College of the
University of Illinois at Chicago, 2018

Chicago, Illinois

Defense Committee:

John Hetling, Chair, and Advisor, Bioengineering
Jason McAnany, Ophthalmology & Visual Sciences
Heather Moss, Ophthalmology, Stanford University
James Patton, Bioengineering
Tolou Shokuhfar, Bioengineering
Thasarat Vajaranant, Ophthalmology & Visual Sciences

To, my grandfather, Narayan Rao Patangay, who started the domino effect of progress in the Patangay clan.
To my parents, who gave me everything I could ever ask for; who patiently bore all my rebellion and channeled it to make me who I am today.
To my role models – my brother and sister-in-law, who I know, will always have my back.
And to my dear friend Prashant, who in the last five years, has almost always picked me up when I was at my lowest.

ACKNOWLEDGEMENTS

I would like to thank my Advisor, Dr. John Hetling, for seeing potential in me when everyone around me did not, for giving me the space and time to learn and grow, for instilling back lost confidence and for always pushing me to do better.
– Thank you Dr. Hetling for being the best mentor and for shaping the rest of my life.

I would like thank Dr. Zahra Derafshi, a former lab member, who patiently guided me through all the tedious troubleshooting while building the system. She taught me the do's and don'ts of working in a research lab and showed me a strong work ethic that I could emulate.

My sincere gratitude to my committee members: Dr. Moss, Dr. Vajaranant, Dr. McAnany, Dr. Patton and Dr. Shokuhfar. Thank you for serving on my committee and providing insights and inputs that shaped my work.

I would like to thank Dr. Jason Park, who helped collect all the conventional pattern ERG data, for this study.

I would like to thank everybody in the Glaucoma Clinic for helping me recruit patients. Dr. Vajaranant, for allowing me to recruit them. Dr. Ruchi Shah for clarifying all my questions, Sofyia, Cristina and Magali for never missing a patient.

Last but not the least, I would like to thank all the subjects who participated in the study and made every data point happen.

LIST OF TABLES

LIST OF FIGURES.

Introduction Figures:

Specific Aim Figures:

LIST OF ABBREVIATIONS

Alzheimer's disease	AD
Amplitude	Amp
bipolar cells	BP
Confocal scanning laser ophthalmoscopy	CLSO
Diabetes mellitus	DM
Euclidean distance	ED
Electroretinogram	ERG
Ganglion cells	GC
Glaucoma hemifield test	GHT
Glaucoma patients	GP
Healthy mean	HM
Humphrey visual field	HVF
Idiopathic intracranial hypertension	IIH
Inferior-nasal	Inf - N
Intraocular pressure	IOP
International Society for Clinical Electrophysiology of Vision	ISCEV
Implicit time	IT
Mean difference	MD
Mean difference	Mdiff
Milliseconds	ms
Multiple sclerosis	MS
Nasal	N
Nasal-inferior	NI
N-Methyl-D-aspartic acid	NMDA
Nasal-superior	NS
Optical coherence tomography	OCT
Reversals per second	OPs
Phosphate buffer saline	PBS

Parkinson's disease	PD
Patter electroretinogram	pERG
Photopic candela per meter squared	Ph cd m^{-2}
Peripheral pattern electroretinogram	ppERG
Photoreceptors	PR
Retinal ganglion cells	RGC
Retinal nerve fiber layer	RNFL
Oscillatory potentials	RPS
Superior-nasal	S
Standard automated perimetry	SAP
Scotopic candela second per meter squared	sc cd s m^{-2}
Scanning laser polarimetry	SLP
Superior-nasal	Sup - N
Temporal	T or Temp
Temporal-inferior	TI
Temporal-superior	TS
Visual field	VF
Volts: V	VF
Micrometers	μm
Micrometers	μV

SUMMARY

Glaucoma, a family of disease defined by retinal ganglion cell loss, is the leading cause of blindness in the US. Early detection allows for a more favorable prognosis by allowing earlier management of the disease, thereby stopping or slowing progressive vision loss. Glaucoma is currently diagnosed through a combination of structural (optical coherence tomography, OCT), and functional (perimetry, pattern electroretinography) tests. These clinically available tests are limited to the central visual field, 20-30 degrees (full angles). Several studies [Bach et al. 1998; Hood et al. 2005; Ventura et al. 2006; Sehi et al. 2009; Banitt et al. 2013; Bach et al. 1992] demonstrate that the loss of peripheral ganglion cell function (beyond 30 degrees of visual angle) likely precedes functional loss in the central retina, at least in some patients.

It can therefore be hypothesized that a stimulus designed to target ganglion cell function in the periphery will be more sensitive to early onset of glaucoma. To test this, a novel three-dimensional pattern stimulus system was designed and prototyped. Stimulus parameters were explored, and the system was validated in healthy subjects resulting in an initial normative database. Sensitivity of the test to glaucomatous damage was assessed. To make the system clinic friendly, the system software, user-interface and testing protocols were optimized.

Part I: Introduction

Glaucoma is the second leading cause of blindness worldwide [Weinreb et al., 2014]. It is a neurodegenerative disorder that is defined by the progressive loss of retinal ganglion cells (RGC). If not identified in its earliest stages, progressive ganglion cell loss can lead to visual field deficits and ultimately blindness. This has a significant impact on health-related quality of life in affected individuals [Varma et al. 2011], resulting in a tremendous socio-economic burden. Therefore, early detection of glaucoma is a major concern amongst clinicians and researchers.

Clinical factors that are used to determine the diagnosis of glaucoma include elevated intra-ocular pressure (IOP), visual field loss, ganglion cell death, and retinal nerve fiber layer (RNFL) thinning. These changes can be identified through routine ophthalmic examinations, that include standard automated perimetry (SAP) tests and structural imaging techniques. The Humphrey visual field (HVF) analyzer is the most commonly used automated perimetry test in the clinic. It is a non-invasive psychophysical test which presents spots of light of various intensities within a defined field and requires the patient to press a hand-held button whenever light is detected. This allows for mapping of visual field deficits and detection of field losses associated with glaucoma. Structural testing methods such as the scanning laser polarimetry (SLP), confocal scanning laser ophthalmoscopy (CSLO) and the optical coherence tomography (OCT) are used to quantify changes in the retinal structure. They work by taking cross sectional images of the retina and provide clinicians with information about the shape of the optic nerve head and the structural losses associated with glaucoma. [Lucy & Wollstein., 2016]

However, the HVF and the OCT can detect glaucomatous abnormalities only after 20-50 % of the retinal ganglion cells have undergone apoptosis [Quigley et al. 1989]. Identifying

changes prior to the degeneration of neural substrate is essential to prevent irreversible vision loss; therefore, these two tests may not be best suited for early disease detection. Functional changes precede structural changes in glaucoma [Banitt et al 2013], this presents a crucial window of opportunity where indicators of ganglion cell dysfunction can be used to detect disease onset.

Earliest changes in retinal ganglion cell function are reported to begin in regions more distal to the brain [Crish & Calkins, 2011]. Functional losses are said to initiate with the failure of anterograde axonal transport (from retina to the brain) and are followed by the failure of retrograde axonal transport (brain to the retina) [Calkins and Horner., 2012; Morgan., 2004]. Functional changes thereafter are said to progress in a compartmentalized manner, meaning, the loss of axonal transport is followed by synaptic and dendritic pruning and finally cell body loss [Lui et al., 2011]. The time lag between functional abnormalities and ganglion cell apoptosis presents a crucial window of opportunity where disease management can begin before significant irreversible RGC loss [Morgan., 2012].

The electroretinogram (ERG) is the electrical response of the retina. Measuring the ERG provides a direct, informative and objective assessment of retinal function.

Depending on the light stimulus, the retinal neurons – the photoreceptors, the bi-polar cells, the amarcine cells, the horizontal cells that form the complex neural circuitry of the retina interact to produce an ERG response. Table 1 summarizes the various ERG test protocols [Bach & Poloschek, 2013]. The ERG waveform can be broken down into components, specific retinal cells contribute to the generation of each component.

Acronym	Full name	Adaptation	Stimulus	Reflecting function of
ERG	Full-field flash Electroretinogram	Dark adapted	Flash	a-Wave: rods; b-Wwave: bipolar cells
		Light adapted	Flash, flicker	Cones
mfERG	Multifocal ERG	Light adapted	Local flashes	Cones and bipolars, spatially resolved
STR	Scotopic threshold response	Dark adapted, <0.001 cd/m^2	Flash	Retinal ganglion cells
EOG	Electrooculogram	Dark + light adapted	Light rise	Retinal pigment epithelium (driven by metabolic demands from receptors)
PhNR	Photopic negative response	Light adapted	Flash	Retinal ganglion cells
PERG	Pattern ERG	Light adapted	Pattern change	Retinal ganglion cells
mfPERG	Multifocal PERG	Light adapted	Local pattern change	Retinal ganglion cells, spatially resolved
VEP	Visual evoked potential	Light adapted	(Flash) or pattern	V1 (and higher areas)
mfVEP	Multifocal VEP	Light adapted	Local pattern change	V1, spatially resolved

Table 1. Summary of clinical electrophysiological tests available. Modified from the review by Bach & Poloschek [2013], summarizing the methods used to record an electroretinogram (ERG), highlighting the ERG responses that have a retinal ganglion cell contribution. Blue shading all tests sensitive to retinal ganglion cell function. The red box indicates the test that is most sensitive to ganglion cell function.

Figure 1A shows a cross section of the retina, with ERG components generated by each cell type indicated. Figure 1B represents a typical flash ERG waveform, where the a-wave and the b-wave are largely due to the photoreceptors, and the ON-bipolar cells respectively. Any change observed in the amplitudes or implicit times of the ERG can give information about the functional integrity of the retinal structures responsible for the response.

The retinal ganglion cells are responsible for transferring in information from the retina to the brain via the optic nerve for visual processing. The cells have large or small receptive fields and get spatially tuned that is respond best to subtle changes in size [Spekreijze et al. 1973] and contrast [Enroth-Cugell & Robson 1966]. The spatial tuning properties, contrast sensitivity, and center-surround receptive field organization make the retinal ganglion cells respond strongly to a pattern stimulus, resulting in the pattern electroretinogram (pERG).

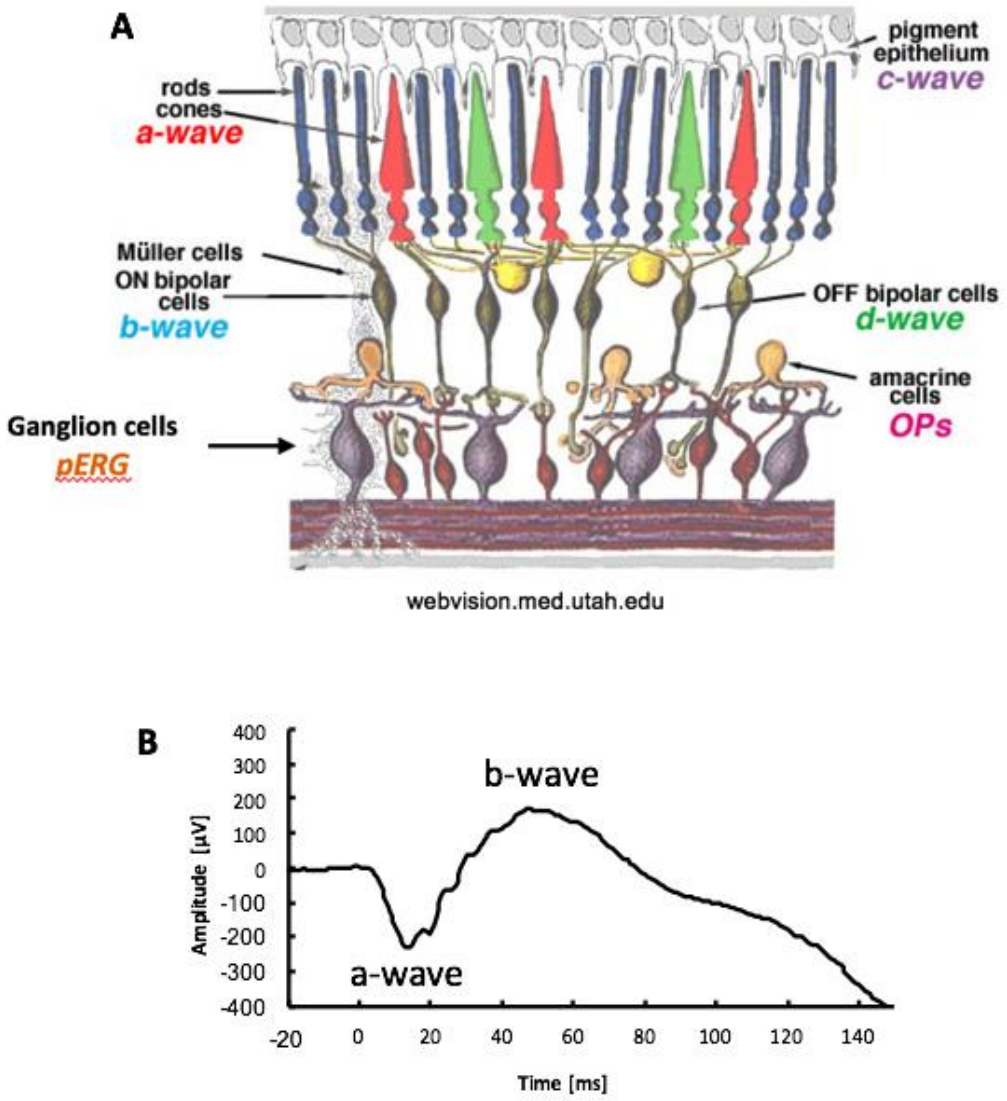

Figure 1. Cross-sectional view of the retina and associated ERG components from each cell. (A) Cross sectional view of the retinal and the ERG component elicited by each cell type. (B) A typical flash ERG response from a dark adapted human subject.

The pattern electroretinogram

The pattern electroretinogram (pERG) is recorded in response to a reversing high-contrast pattern, typically a checkerboard or grating, which has a constant time-averaged luminance. It was first recorded in the early sixties by Riggs et al. [1964]. Several studies to confirm the generators of the response followed. Reduced pERG response amplitudes in glaucoma patients as well as in the presence of pharmacological block of ganglion cells [Hood et al., 1999; Vishwanathan et al., 2000; Miura et al., 2009; Fishman et al. 2011] and experimental optic nerve transection [Maffei & Fiorentini., 1981; Maffei et al., 1985] confirmed the strong ganglion cell contribution to the pERG. Because of this, the pERG has high relative efficacy for glaucoma when compared to other electrophysiological tests of visual function [Bach & Hoffmann, 2013; Bach & Poloschek, 2013].

The pattern ERG response components.

A typical pattern ERG response is plotted in Figure 2. The transient pERG, recorded at lower reversal rates (<6 RPS) results in ~200 millisecond [ms] long response and has a smaller amplitude when compared to the flash ERG (Figure 1B). The pERG has three response peaks, a slow negative component N35, a larger positive peak P50 and a late component N95 (marked by arrows in Figure 2). The amplitudes and implicit times are evaluated within standard time windows. The P50 peak is chosen between 45-60 ms and is typically 2 – 8 μV in amplitude and, the N95 is chosen between 90 -100 ms [Bach et al., 2012]. The N95 component in the pERG is purely ganglion cell driven [Vishwanathan et al. 2000; Holder et al. 1996] while the P50 component is due to the interaction between ganglion cells and cells more distal to RGCs [Holder, 2001, Bach & Hoffman (The pattern

electroretinogram)]. Reduction in the N95 amplitude therefore reflects ganglion cell dysfunction.

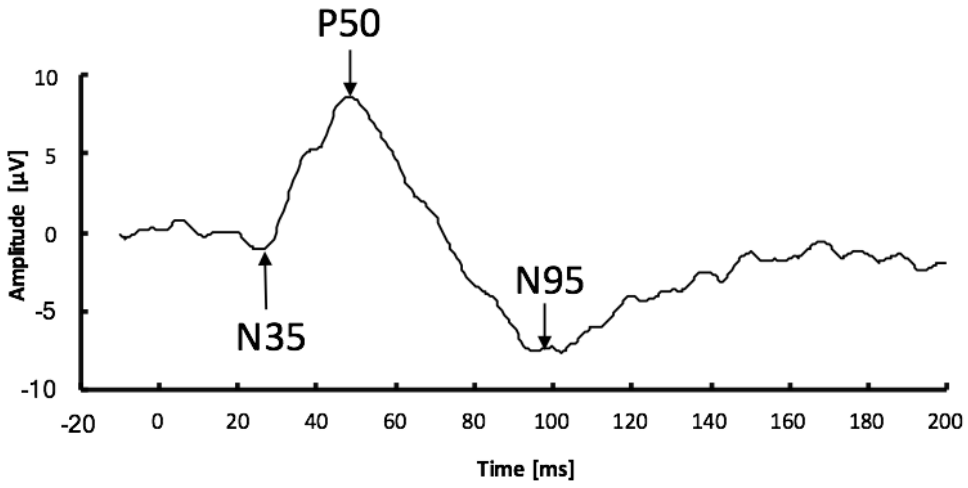

Figure 2: Figure illustrates a typical transient pattern ERG waveform elicited from a checkered ON-OFF pattern. The transient pERG waveform gas three components, the early negative N35, the positive peak P50 and the late negative peak N95. The late negative peak represents true ganglion cell function.

The Rationale.

In glaucoma, it is well documented that (compared to age-matched healthy eyes) reductions in pERG N95 amplitude precede, or exceed, reductions in structural measures (retinal nerve fiber layer thinning) or measurable defects in visual field [Bach et al., 1998; Hood et al., 2005., Ventura et al., 2006; Sehi et al., 2009; Banitt et al., 2013]. However, despite some use as an outcome measure in clinical research [Parisi et al., 2014; Parisi et al., 2015] the sensitivity and specificity of pERG have not been so high as to overcome the perceived clinical burden of performing the test for routine screening, diagnosis or monitoring of disease progression, where HVF and OCT are typically employed.

In the ERG studies cited above, measurements were made at or near the central retina (centered on the fovea). One issue that may limit the sensitivity of conventional pERG testing in glaucoma is only targeting the central 20-30 degrees of visual field (Figure 3). The reported sensitivity of pERG to early, putatively diffuse, ganglion cell dysfunction (prior to detection with other central-field tests) suggests that the locus of the earliest damage may, in some patients, be in the peripheral retina, [Hood et al. 2005; Bach et al., 1992] even beyond the commonly observed arcuate scotoma in the Bjerrum area (~10-20 degrees from fixation. Patients with abnormal sectors in the circumpapillary OCT and normal HVF suggest that the associated functional field defects are beyond the 24 degree HVF test area [Hood et al., 2013].

Given the advantages of electrophysiological testing (objective, assesses function) and the lack of a ganglion cell test that probes the currently inaccessible peripheral retina, a pERG test that elicits a ganglion cell response from the peripheral retina was is needed. Non-centralized pERG stimuli have been proposed as a means of assessing disease in the mid-peripheral retina [Aylward & Vaegan., 1990; Graham et al. 1994], but standard flat monitor sources are not ideally suited to the task.

This has created a critical need for an appropriate tool to detect and monitor the earliest changes in RGC function. A tool that will enable diagnosis of pre-apoptotic glaucoma, help monitor the disease, and evaluate the emerging neuroprotective and neurorestorative treatment options for glaucoma [Chang & Goldberg 2012; Xia et al., 2014] will have high clinical impact.

With a main goal of targeting the retinal regions where earliest glaucomatous damage is said to begin (Figure 4), a three-dimensional novel stimulus was designed. This work

focused on overcoming the limitations of an initial prototype by redesign and fabrication, characterization of the peripheral pattern ERG response by exploring various stimulus parameters, initiating the establishment of a normative database by validating the system in a group of normally-sighted subjects and testing the sensitivity of the test to glaucomatous damage in patients.

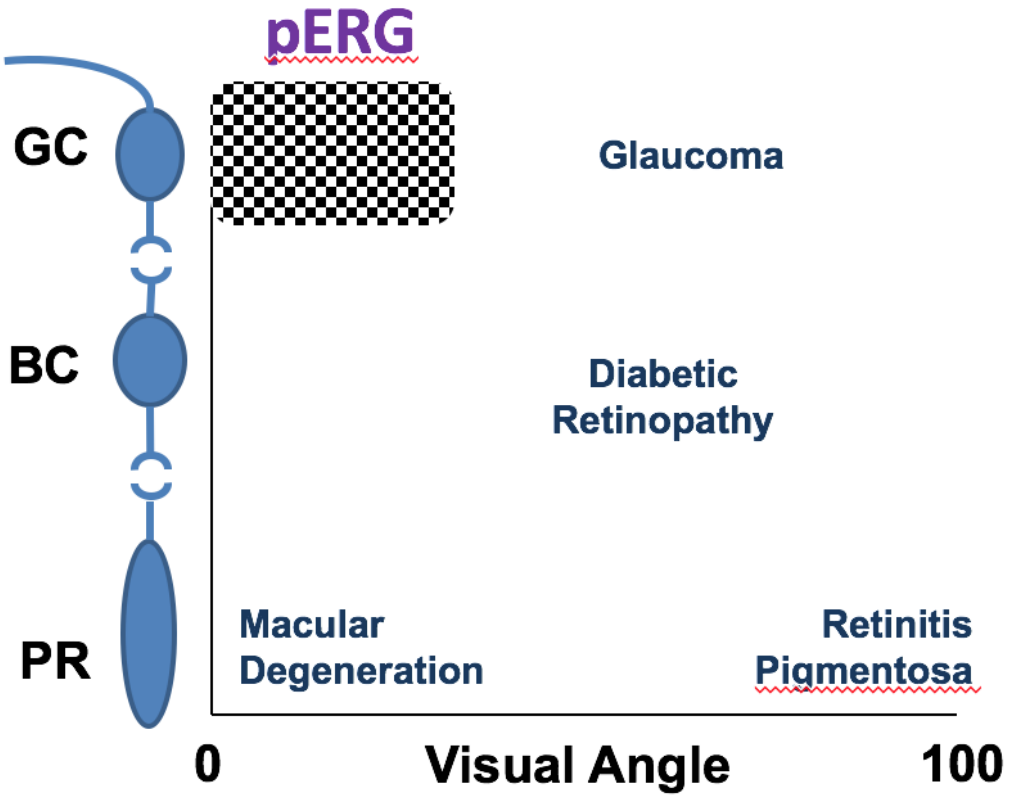

Figure 3: Illustrates the retinal locus first affected by the most prevalent blinding eye disease. The y-axis represents retinal depth (GC: ganglion cell, BC: bipolar cell, PR: photoreceptor) and the x-axis represents eccentricity in terms of visual angle. Glaucoma is said to begin in the mid-far periphery (between 30 degrees to the limits of the visual field, as illustrated. The pattern ERG stimulus (checkerboard pattern) however does not target regions outside the central retina (from 0 – 30^{o})

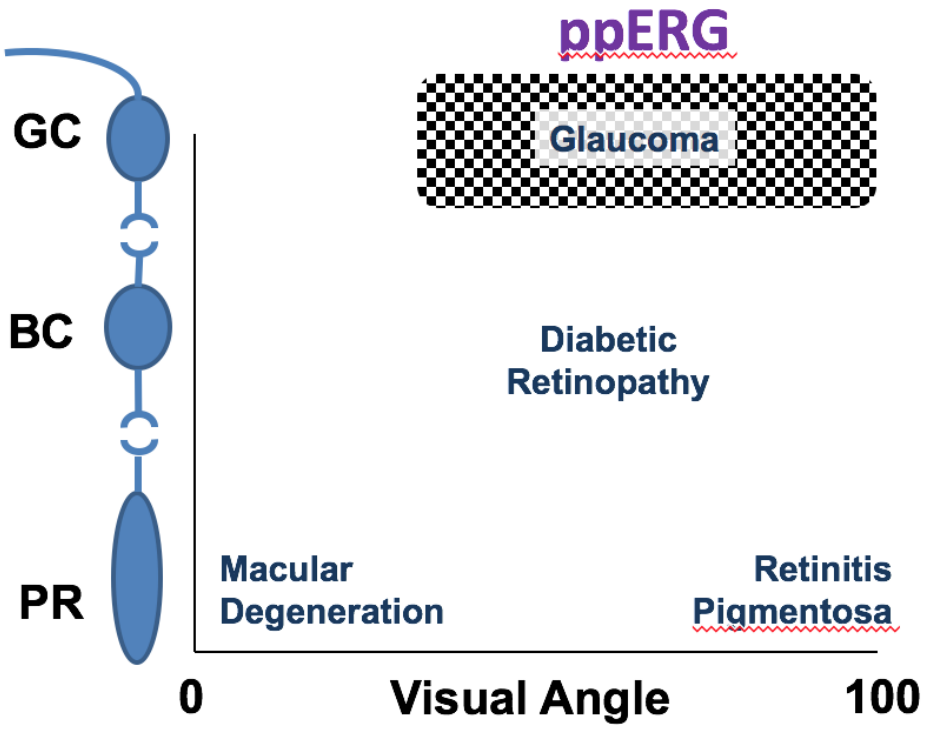

Figure 4: Illustratation the proposed region targeted by the peripheral pattern ERG stimulus. The y-axis represents retinal depth and the x-axis represents eccentricity in terms of visual angle. Glaucoma is said to begin in the mid-far periphery (between 30 degrees to the limits of the visual field, as illustrated. The peripheral pattern ERG stimulus is designed to target the mid-far periphery where early glaucomatous damage is said to manifest.

Part II: Specific Aim 1

Fabrication and characterization of a novel pattern stimulus source targeting the peripheral retina

Specific Aim 1

Fabrication and characterization of a novel pattern stimulus source targeting the peripheral retina. An existing prototype will be rebuilt to improve robustness, luminance uniformity, stimulus control, data recording and user interface.

Specific Aim 1 Motivation

Glaucomatous damage is defined by the progressive loss of retinal ganglion cells (RGC). This loss can be detected by electrophysiological testing, where, the health of ganglion cells can be measured by recoding the electroretinogram (ERG) responses elicited by these cells to different light stimuli. The retinal ganglion cells however are most sensitive to a pattern stimulus eliciting a pattern electroretinogram (pERG). The pERG responses are typically recorded when a reversing high-contrast pattern, typically a checkerboard or grating, which has a constant time-averaged luminance is presented to the eye. The pERG test is limited in a way that, it can only target the central thirty degrees of the retina, while glaucomatous damage due to RGC dysfunction is said to be diffused, primarily starting out in the peripheral retina and progressing towards the center. An electrophysiological test that evaluates retinal function in the peripheral regions currently does not exist. Evaluating ganglion cell function in these understudied regions (beyond the central 30 degrees of the visual field) will prove useful in detecting early disease onset, enabling earlier disease management, thereby minimizing vision loss.

System goals: Given the ample motivation for looking the peripheral retina and the lack of an appropriate tool, an idea of a perfect pattern ERG system is described below.

The ultimate goal is to detect the localized and/or diffused early loss of ganglion cell function, therefore a pERG stimulus that targets specific sections of the visual field and/or the entire visual field would be ideal.

The stimulus source must fulfill all constrains required for a pERG system, these are, equal number of ON and OFF checks, uniform luminance within a check, and uniform luminance across checks.

The spatial tuning properties, contrast sensitivity and center-surround receptive field organization of the ganglion cells must be considered [Nelson, 2007]. As contrast, temporal and spatial frequency effect the pERG response [Darsdo & Thompson., 1994; Zapf & Bach., 1999], the stimulus must have high contrast, with sharp borders between checks, optimum check size, and a known and controllable reversal rate.

Maintaining all these required conditions will result in a recorded signal of useful signal to noise ratio. To interpret the recorded signal real time averaging and artifact rejection must be a system component. To make the test repeatable and reliable, standardized protocols with a user-friendly interface is utmost essential.

Taking all the requirements into account, the senior design group from the Neural Engineering Vision Laboratory [Spring 2013] at the University of Illinois at Chicago built a reasonably functional stimulus source that had certain limitations. The initial prototype focused on targeting the mostly overlooked peripheral retinal regions beginning at approximately 20 degrees and extending to the limits of the visual field in all directions and was hence called the **peripheral pattern ERG (ppERG) system**.

Design of Initial prototype: To record a pattern ERG from the peripheral retina, a stimulus source that extends to the limits of the visual field is required. A three-dimensional hemispherical translucent acrylic dome of 30 cm radius was used to capture the entire visual field was. The acrylic dome was mounted inside a 32”x32”x16” wooden housing for stability (Figure1).

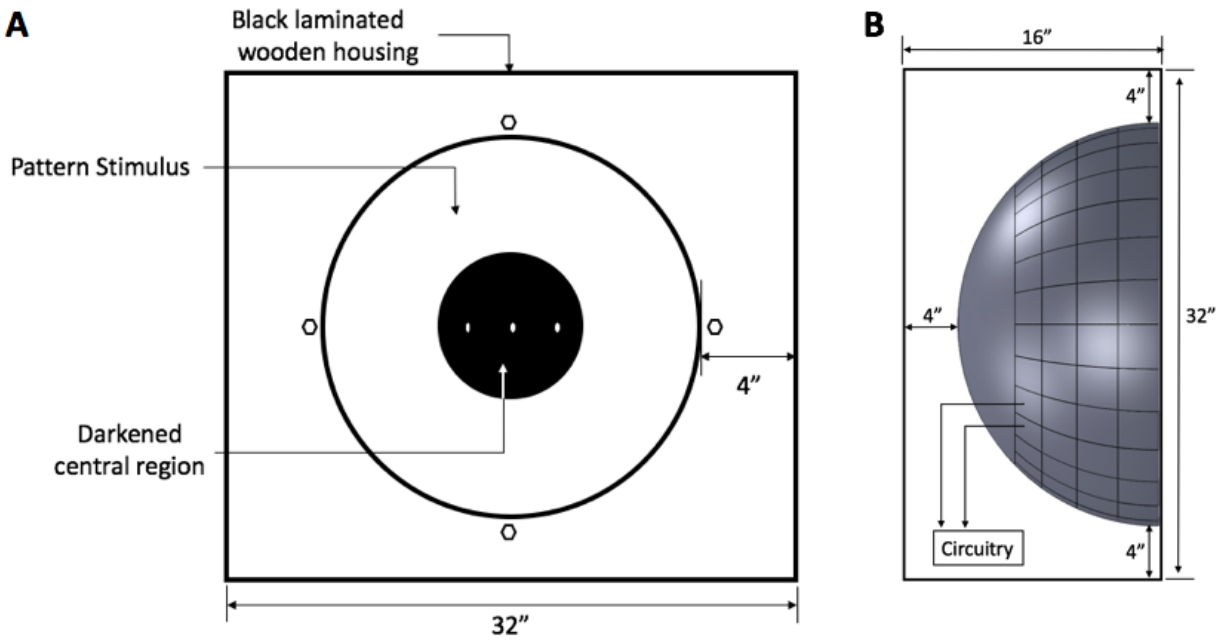

Figure 1. Schematic of the pattern stimulus source and housing. (A) Stimulus when viewed from the front, the acrylic dome is mounted inside the wooden box with the help of four bolts inserted at the top, right, bottom and left. (B) Pattern stimulus viewed from the side. The bottom of the box houses the circuity that runs the system. All units are in inches.

A checkered grid was achieved by partially tiling the dome with 120 LED units arranged in four circumferential rows and 30 radial columns. Within each row, alternate LEDs are connected in parallel resulting in two phases – A and B; individual columns connect in series. Each LED unit comprised of a plastic mount custom designed to hold a single BXRA-C0402 (Bridgelux, Fremont, CA) cool white LED (Figure 2 A-B), and standard thin film diffusers that were place between the LED and the surface of the dome. Metal fins glued to the acrylic surface encompassed each unit defined the edge of individual checks (Figure 2C). The size of each check was fixed and varied as a function of viewing distance. The checkered pattern extended from 40-170 degrees in full angle with the central 40 degrees left blank; a cross-marked ping pong ball at the apex of the dome to indicated the central fixation point. The assembled prototype is shown in Figure 3. Custom designed hardware and software powered by a microcontroller (Arduino AtMega 2560) generated an ON and OFF pattern and a preliminary peripheral pattern ERG (ppERG) response was successfully recorded. Figure 3B shows a subjected sitting at a viewing distance of 66 cm from the apex of the hemisphere. Responses were recorded at a luminance of 80 ph cd m^{-2} (ISCEV recommended standards) [Bach et al. 2012], a reversal rate of 4.26 Hz. The recorded response (blue trace), compared to the response from a conventional system is shown in Figure 4.

A

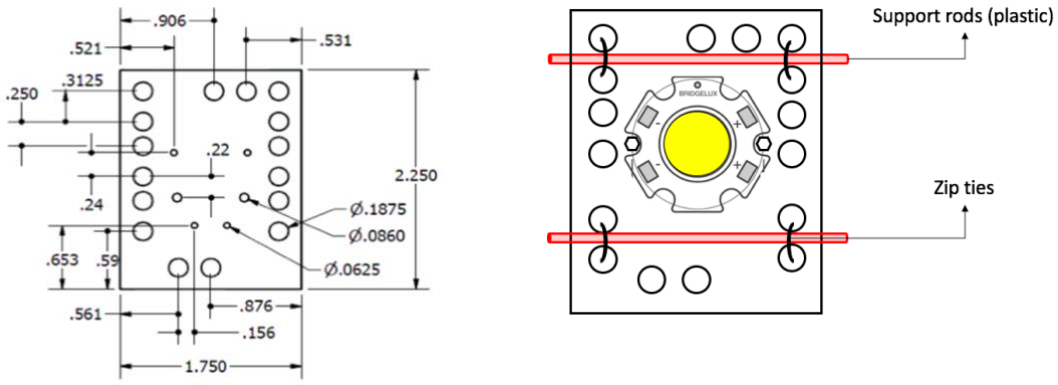
.906
.521
.531
.3125
.250
.22
2.250
.24
Ø.1875
Ø.0860
.653
.59
Ø.0625
.876
.561
.156
1.750
Support rods (plastic)
Zip ties

B

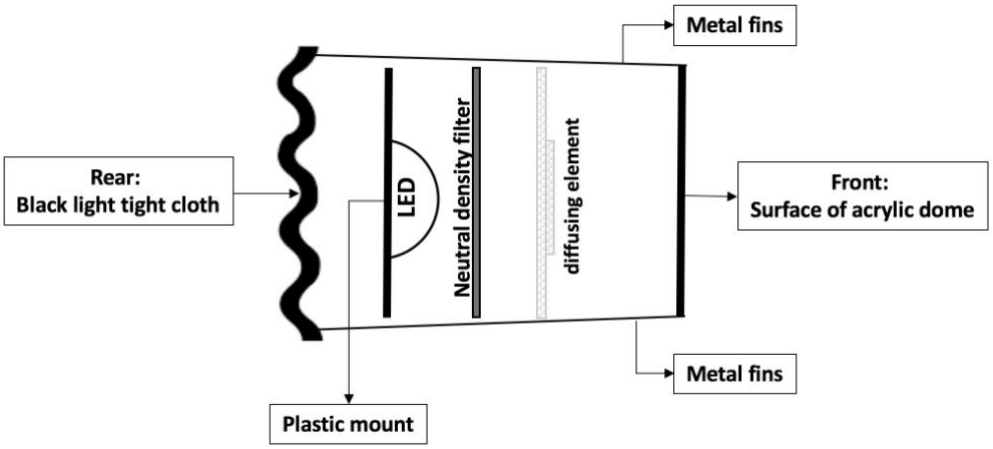
Metal fins
Rear:
Black light tight cloth
LED
Neutral density filter
diffusing element
Front:
Surface of acrylic dome
Metal fins
Plastic mount

C

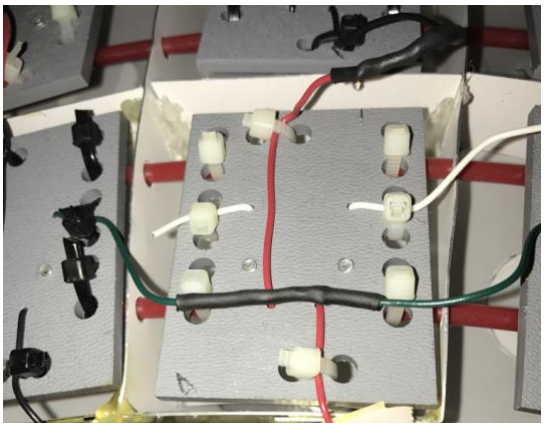

Figure 2. Schematic of LED unit. (A) (Right) Custom designed plastic LED mount was machined. The LED was screwed onto the center of the mount. Holes provided in the mount helped in routing the connecting wires. All measurements are in inches. (Left) Illustration of the LED unit. The LED was screwed to the mount using two machine screws. The mount was clasped to plastic support rods using zip-ties. The support rods ran across the circumference of each row. (B) Cross-sectional view of the LED unit. The front of the unit is the acrylic dome surface. Metal fins are glued to the back of the acrylic dome (convex side) and help in defining the edge of each check. The black light tight cloth and the neutral density filters are later additions and will be discussed in the system improvement section (C) Image of the LED unit when mounted. The metal fins defined the edge of each check. Zip-ties were used to hold all the connecting wires in place. The green (and white) wires connect the positive terminal of alternate row LEDs (in parallel). The red wires connect the negative terminals of LEDs in columns (in series).

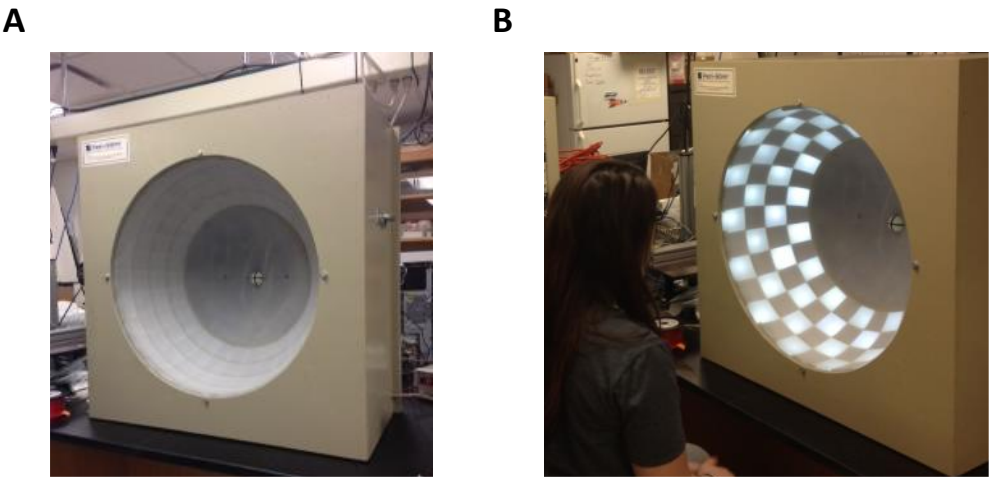

Figure 3. Initial prototype peripheral pattern ERG stimulus source. (A) Image of the prototype when the system is not powered. Four circumferential rows and 30 radial columns result in a checkered grid. The central portion of the dome is not tiled with LEDs, and has one fixation target at the apex of the dome. The entire system is held in a wooden housing. (B) Image of the prototype with a subject sitting through a recording session.

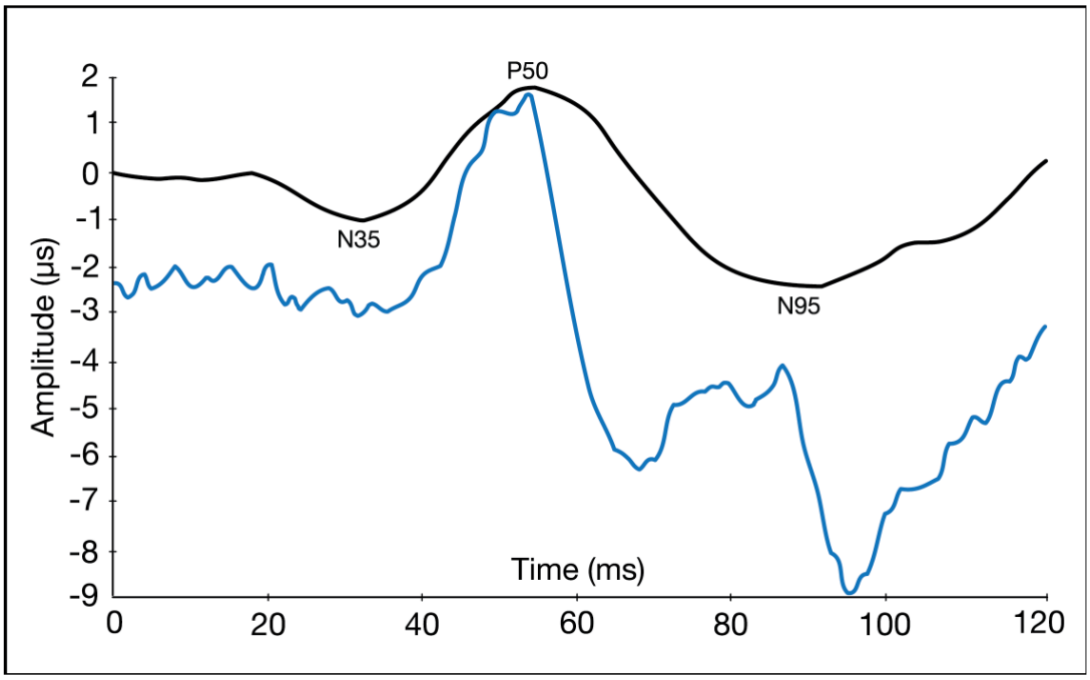

Figure 4. The first peripheral pattern ERG response. The response was recorded at a mean ON-luminance of 80 ph cd m-2 (ISCEV recommended standards), viewing distance of 66 cm and a 4.26 Hz reversal rate. Blue trace represents the peripheral pattern ERG response. The black trace the response from a convention pERG stimulus. Note the implicit times and amplitudes of both waveforms.

Although the initial prototype was capable of eliciting a peripheral pattern response similar to the conventional pERG, repeated use of the system revealed hardware malfunctions and software glitches, for example, bad LED solder connections, poorly matched pattern phase luminance, and faulty real time averaging.

To improve the overall robustness of the system, attain higher and more uniform luminances and flexible pattern control, changes in terms of hardware and software were made. This resulted in a robust peripheral pattern ERG system capable of delivering a high luminance pattern stimulus to any part of the peripheral retina. The following sections

describe in detail system modifications made to effectively record a peripheral pattern electroretinogram.

Specific Aim 1 Methods

In order to design a peripheral pattern ERG system equipped with the ideal qualities mentioned above and to mend the issues existing in the initial prototype, the following re-fabrication goals were carried out

No changes were made to the basic supporting framework of the initial prototype. That is, the three-dimensional hemisphere of 30 cm radius, the arrangement of the LEDs (to create a checkered grid), The A and B phase connections between the row LEDs, the connections of the column LEDs [Figure 5], the LED unit the wooden housing did not change. Improvements in the system were majorly made through circuit and software re-design

System Robustness.

The first step taken to improve system robustness was to identify and repair all the bad LEDs and LED solder connections. The system was powered ON and all the LED's that did not light up were marked. To make sure no LED had a loose connection the acrylic dome was removed from the wooden housing and placed upside down on a cart [Figure 6]. This gave access to all the 120 LEDs units. With the system turned ON slight force/pressure was applied on all the LED connection. LEDs that either flickered or turned OFF altogether due to the pressure were also marked. Once all the bad and loose connections were identified , each marked LED unit was removed from the grid, the LEDs electrical connections were re-soldered, the bad LEDs were replaced and the mount was put back.

The second step was to trim all the unnecessarily long wires that connected the LEDs (rows and columns). As not all the connecting wires were soldered, the third step was to re-

solder all the 120 LED connections. To do this, the connecting wires were shortened to the right amount, soldered and were insulated with heat-shrink tubing. This ensured that the wires connecting the LED units were neat, compact, robust.

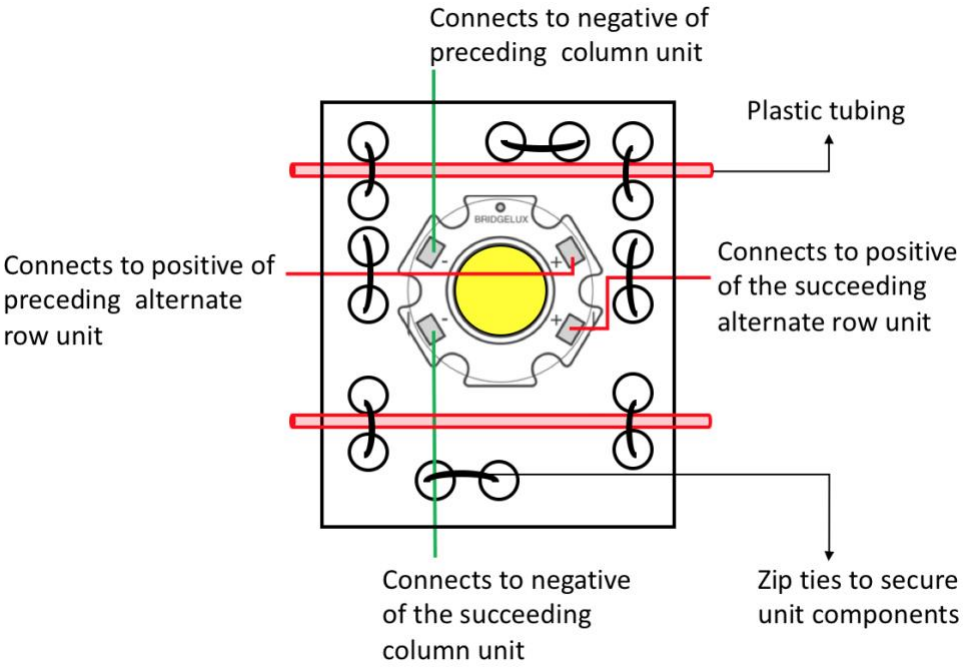

Figure 5. Connections to an LED unit. 120 LEDs are connected in parallel (rows) and in series (columns) to form a controllable ON-OFF checkered grid. The green wires that go from one LED unit to the alternate LED unit (also seen in 2C) make up one ON phase (A phase). The red wires connect the column LEDs in series.

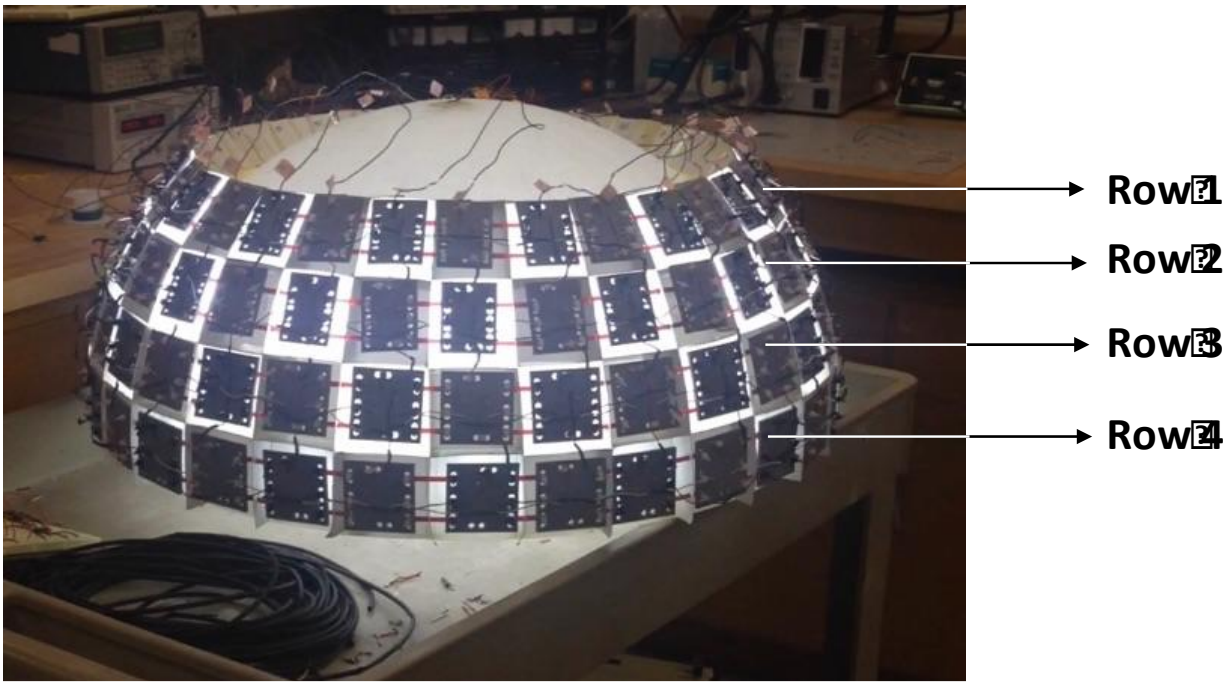

Figure 6. Distal side of the pattern stimulus source. The checkered grid one phase turned ON and the other OFF. The red plastic tubing runs across the circumference of the dome holding the row units together. Each row is labelled, with the innermost (top, in this case) being Row 1. Approximately 400 electrical connections were re-soldered and insulated with heat-shrink tubing.

Other Improvements. Each row and column was assigned a specific number and labelled accordingly (the innermost row was #1, and clockwise from the top was column #1). To reduce the transmission of light between neighbouring checks and to create a high contrast between neighbouring checks, a black light-tight cloth (Figure 2B) was tightly wrapped around the circumference of the acrylic dome before mounting it back into the housing. The central 40 degrees that corresponds with the conventional pERG monitor (14"x11") used in this study was painted matte black to avoid any stray light resulting from the light reflected from the ON LEDs onto the unlit area. White ping-pong balls that were cut in half and cross marked with a black tape were used as the three fixation targets – center, left and

right within this region. The entire set up was made to rest on a 36”x24” table with a chin rest.

The pattern ERG is said to have high inter-subject variability. Variability can be due to the changes made in the stimulus conditions and recording procedures between sessions. Standardizing recording procedures in terms of the type of recording electrode used, placement of the ground and reference electrodes, number of runs averaged and fixation decreased variability [Holopigian et al., 1988]. One of the first steps taken to standardize the recording procedures was to eliminate variations due to incorrect target fixation. To do this, a commercially available chin rest was redesigned. The base of the chin rest was replaced by a cylindrical steel post machined to have one flat side. The post was then mounted onto the table with the flat side adjoining the wooden housing. This ensured that the distance between the chin rest and the apex of the dome was 30 cm (the radius of the hemisphere), at this distance, the stimulus covered the limits of the visual field. The height of the chin rest was fixed such that when seated, the gaze of the subject (recording eye) was always tangential to the plane of the central target. The chin rest was also made interchangeable to accommodate an animal (rat) mount in order to conduct animal experiments. The animal mount was precisely machined to make sure that the height of the animal’s eye was always aligned with the central target. The updated system along with the interchangeable chin rest is shown is Figures 7A-B

A

B

Figure 7. Updated system setup. (A) System set up for human subject recording. The chin rest is incorporated to provide a stable head position during the recording. (B) System set up for animal (rat) experiments. The interchangeable chin rest replaced with a custom designed animal mount; the mount accommodated a heating pad to maintain normal body temperature (37^{o}C). Three-axis manipulator seen in the image was used to lower the recording (looped platinum needle electrode) to the eye. The recording electrode was later replaced by a DTL fiber electrode.

Pattern control – circuit design. The initial prototype was designed to be controlled by Arduino, where, the microcontroller supplied power to the LEDs, controlled the ON-OFF pattern of the LEDS, and monitored the transitions of this ON-OFF pattern. This may have caused a system overload and resulted in hardware malfunction and software issues. To reduce the tasks handled by Arduino, the circuit powering the system was redesigned to have a modular organization. Figure 8A shows the re-designed circuit and a flow of connections is shown in Figure 8B

A

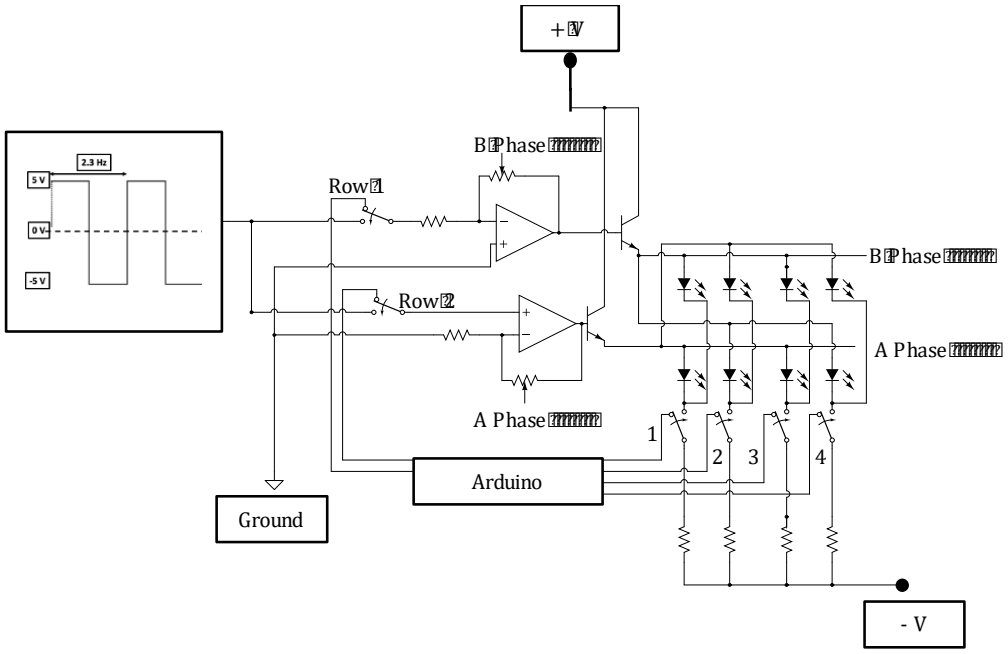

B

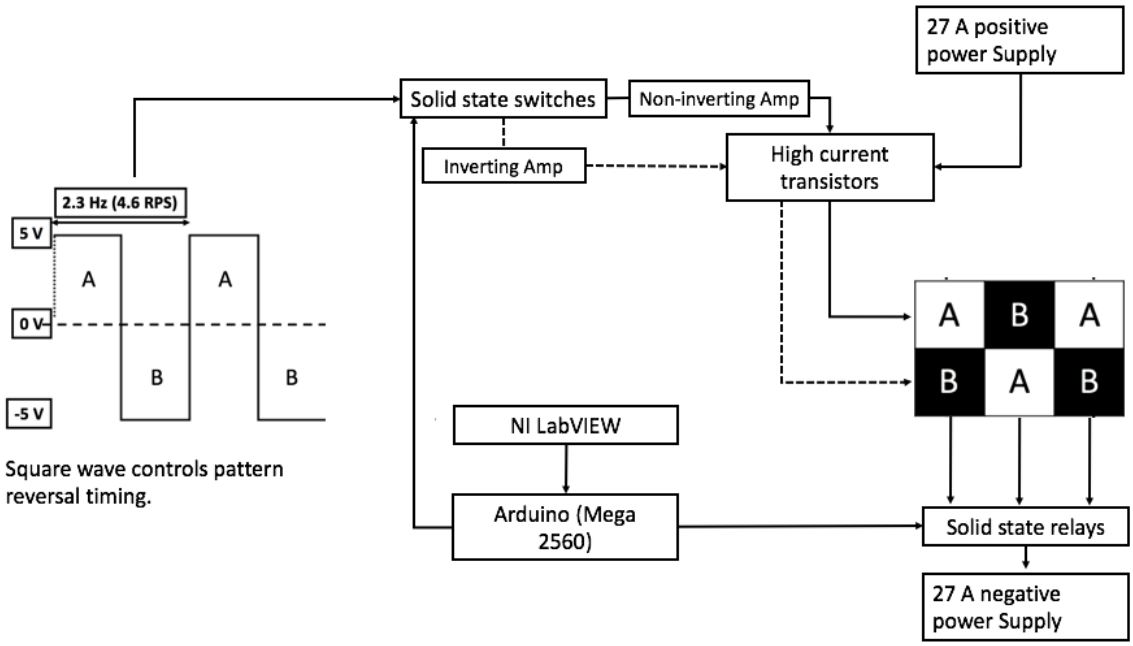

Square wave controls pattern reversal timing.

Figure 8. Pattern control – Circuit design. (A) The partial section of the re-designed circuit diagram to show the working of two rows and four columns. Circuit was created using the online software – CircuitLab (CircuitLab, Inc. Sunnyvale, CA), the green line on the phase A is analogous to the green wire seen in Figure 2C. (B) Schematic showing the flow of connections. The "A" and "B" markings on the square wave (from the function generator) depict the phase of the reversing pattern. Frequency is set at 2.3 Hz. Each row can be turned ON or OFF through solid state switches that are controlled by Arduino through LabVIEW. Inverting and non-inverting amplifiers create the ON-OFF pattern by inverting the square wave controlling half the checks. High current transistors gate the current from a programmable DC power supply at a fixed +5V voltage. The path to the negative-voltage point for each column (creates a potential difference & turn the LED ON) is gated by solid state relays that are controlled by Arduino through LabVIEW recording electrode was later replaced by a DTL fiber electrode.

The new circuit design created an addressable array allowing each row and column to be included in (or excluded from) the pattern individually. All circuit components were carefully chosen to handle high currents as the maximum current for each of the 120 LED is 1000 milliamperes (mA). The system was now powered by high current transistors (MJH6284GOS-ND, ON Semiconductors, Phoenix, AZ) that gate the current (driven by a fixed +5V voltage) from a programmable DC power supply (BK precision 9151, B&K Precision Corporation, Yorba Linda, CA) to the rows; each row has two transistors, one for each phase. Each transistor is in turn controlled by a solid-state switch (one per row; DG202BJ-E3, Vishay Intertechnology, Malvern, PA); Inverting (B phase) and non-inverting (A phase) operational amplifiers (LM741, Texas Instruments, Dallas, TX) with adjustable gain (using variable potentiometers) are used to generate the A and B phases from a single square wave input by inverting the square wave to half the checks. The path to the negative-voltage point for each column is gated by solid state relays (VO14642AT-ND, Vishay Intertechnology, Malvern, PA). The negative-voltage value is set by a second DC power supply (BK precision 9151, B&K Precision Corporation, Yorba Linda, CA) that is

programmed to predefined values; each value determines the total voltage drop across the LEDs and thus the current through the LEDs; the LED light output is proportional to the current. Therefore, the negative voltage applied determines the mean ON-luminance. The reversing pattern and pattern frequency is timed by a square wave from a function generator (Sony, Textronix, AFG310 Beaverton, OR), where the high and low phases of the square wave correspond to the state of the pattern (A phase and B phase).

Pattern control – user interface. Each row and column can be turned ON or OFF with the help of a graphical user interface (Figure 9) designed in LabVIEW (National Instruments, Austin TX). LabVIEW interfaces with Arduino to control the switches and relays. Each Arduino pin waits for the user to declare a "True" or "False" Boolean value by selecting a toggle state in LabVIEW (toggle either turned ON or OFF). If the value is "True", i.e. the toggle is turned ON, the "set pin mode" and "digital write" function (in LABVIEW) allocated to a specific Arduino pin closes the solid-state relay (by supplying + 5V voltage) allowing it to complete the circuit.

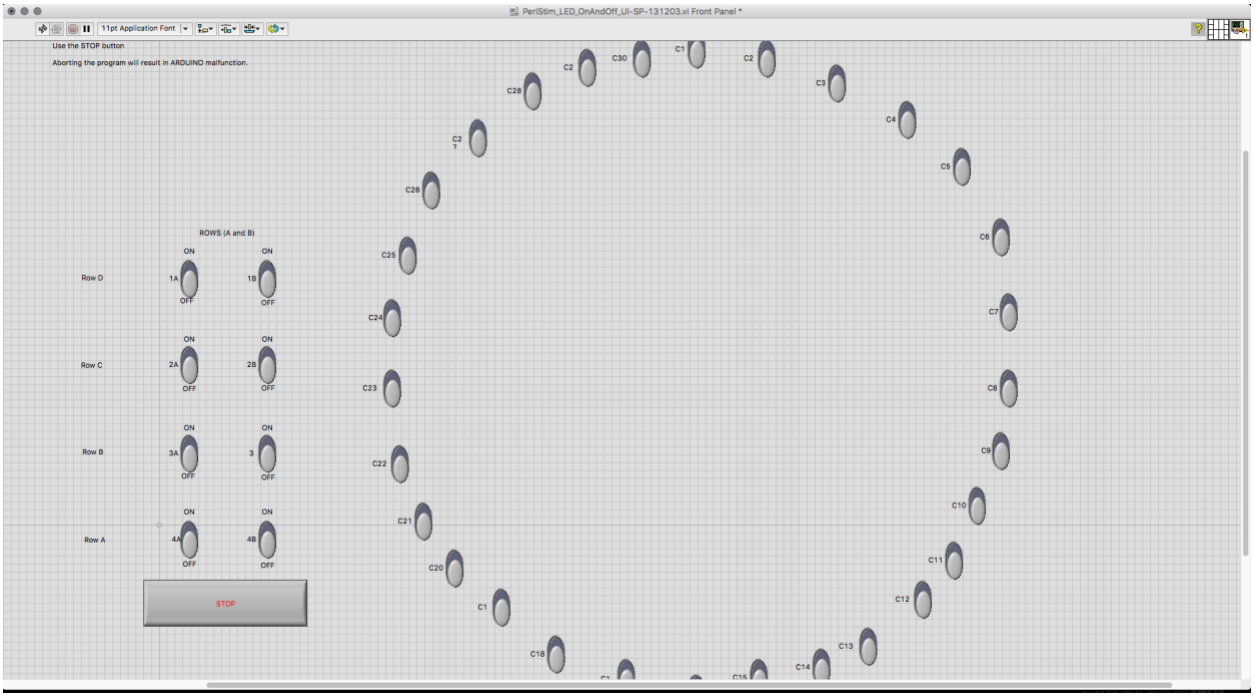

Figure 9. Pattern control – user interface. Graphical user Interface designed in LabVIEW to turn the columns and rows ON and OFF. Eight row toggles control the ON-OFF state of each phase in each row. 30 toggles, arranged in a circle control the 30 radial columns. Switching the toggle state would result in either a complete row or an entire column to turn OFF or ON. The stop button will stop the VI from running.

Luminance uniformity. A pattern ERG stimulus should have the following parameters: each phase (A and B) should have equal averaged ON-luminance, equal surface area, and the transition between phases (A to B and B to A) should occur with no all-ON or all-OFF state. Violating any of these design requirements could lead to luminance artifacts in the response. For the initial prototype, luminance uniformity of each check was managed by placing a standard thin film diffuser between the LED and the surface of the dome. The diffusing element was cut to the size of the check before placing it. A second diffusing layer, cut to the same diameter of the LED was place in the center of the first diffusing element, this created a double diffusing layer to ensure that the light from the LED was distributed evenly across the check (Figure 10). Luminance uniformity across the check was analyzed

in ImageJ (National Institute of Health, Bethesda, Maryland). A photograph that included three checks was taken. The photograph was opened in ImageJ, a line was drawn across each check. ImageJ plots the greyscale level of the pixels along the line drawn. Figure 10B shows the three checks with a line drawn across (top); the bottom of Figure 10B plots the greyscale values across the length of the line.

Luminance measurements across each check in its ON and OFF state were made using the IL 1800 photometer (International Light, Peabody, MA). Calibration readings were made in photopic candela per meter squared (ph cd m^{-2}) with a SED100 photodiode detector, R485 radiance barrel and a Y19555 photopic filter. The angle subtended by the photodetector is very small (1.5 degrees, half angle), to ensure that a maximum area of the check being measured is covered, the detector had to be placed 11.3 inches away from the check surface. To maintain consistency of the relative position of the photodetector while measuring the check luminance, a detector holder (Figure 10) was designed. This placed the photodetector unit at the appropriate distance (11.3”), ensuring that the detector covered maximum check area and did not measure any light from the neighbouring check. To match the luminance across all checks to the best possible extent, unusually bright checks (outliers) were had a neutral density filter installed. The neutral density gelatin filters (0.3, and 0.6 optical density; Rosco E-Colour #209, Rosco E-Colour #210, B and H photo, New York, NY) were placed between the LED and diffusing layer, Figure 11. Non-uniformity was also addressed by adjusting the transistor base currents using the variable potentiometers (present on the inverting and non-inverting operational amplifiers that connect to the base of the transistors), for each phase in each row (Figure 8A).

To confirm precise phase transition i.e. absence of an all-ON or all-OFF phase, careful luminance vs. time measurements using photodiodes were made. The photodiodes, in the photo voltage mode were aligned with neighbouring checks. The mean ON-luminance of the LED's was set at 1670 ph cd m^{-2} (approximately 75% of maximum current, 1000 mA), the reversal rate was set to 4.6 reversals per second (RPS) and output was monitored in LabVIEW.

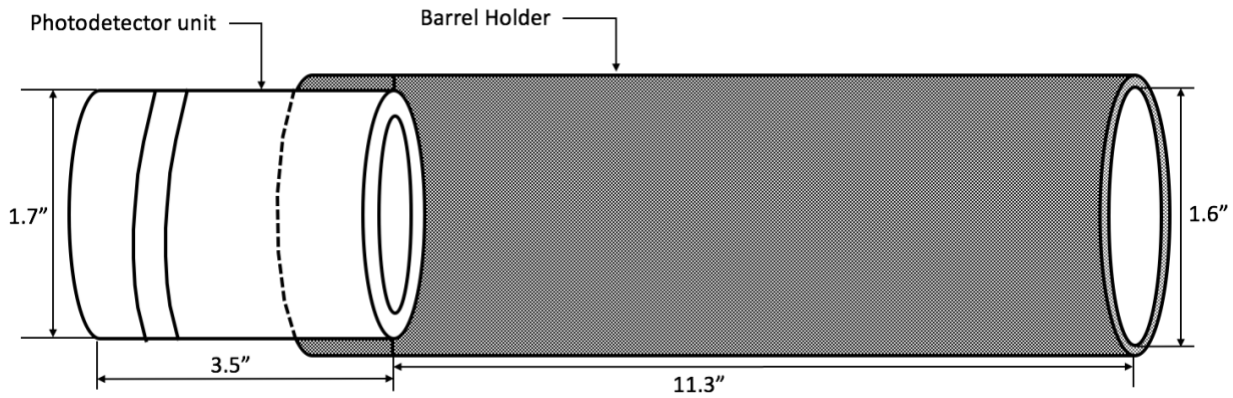

Figure 10. Luminance uniformity. Cross sectional view of a single check illustrating the placement of the double diffusing element and neutral density filter. A double diffusing element made up of two standard diffusers is placed between the LED and acrylic surface. The first diffusing layer is the same size of the check, the second diffusing layer is cut to the same diameter of the LED and is attached to the first diffusing layer using tape. The use of a double diffusing element improved the distribution of light across most checks. (B)(Top) A photograph of three checks with a line drawn across for ImageJ analysis. (Bottom) ImageJ plot; the greyscale values of the pixels along the line drawn.

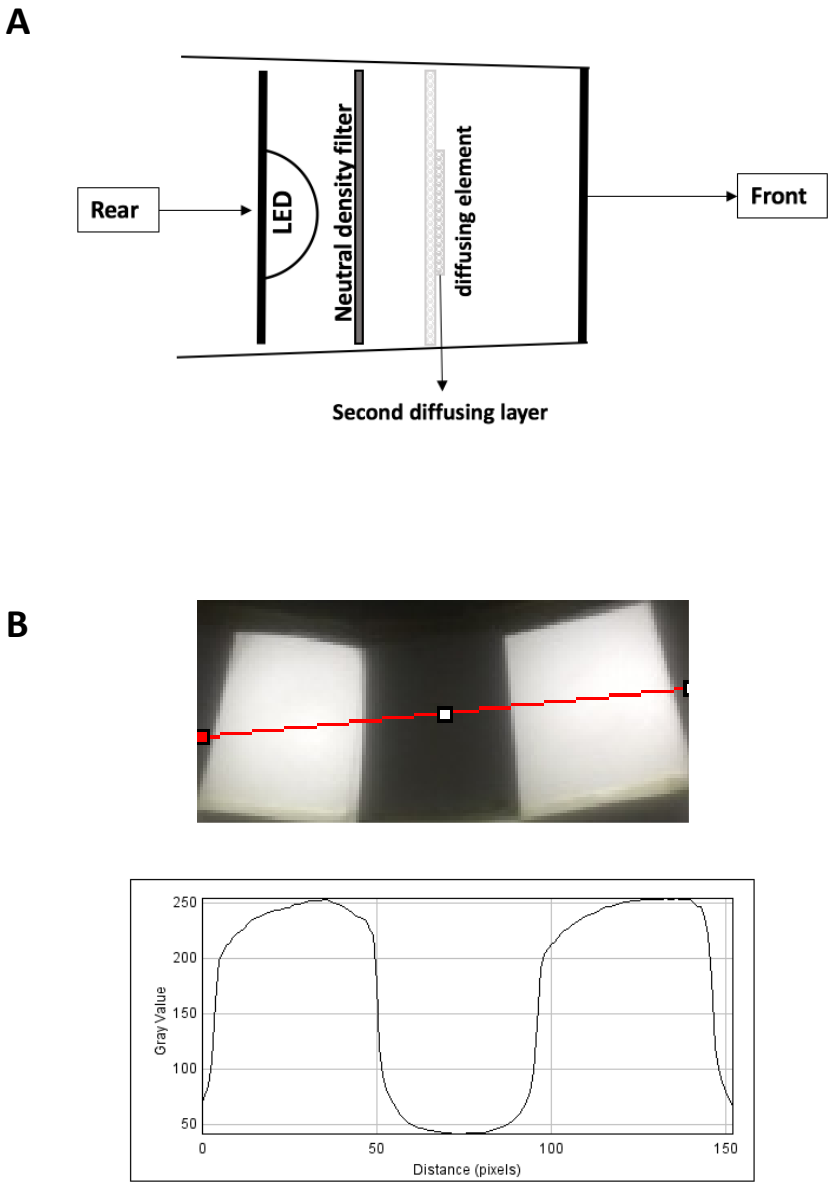

Figure 11. Schematic of the photodetector holder. The barrel holder was designed to hold the photodetector unit. This allowed the sensor to be at a fixed distance from every check and maximized the field of view of the sensor ($\pm$ 3 degrees with the radiance barrel). The diameter of the holder (1.6”) covered the shortest side of the smallest check.

Data acquisition and online signal processing. Responses were recorded binocularly or from one eye. DTL fiber electrodes (LKC Technologies, Gaithersburg, MD) were used to record the signals while adhesive skin electrodes (Ultratrace, #1690-001, Medtronic, Minneapolis, MN) were used for reference (ipsilateral temple) and ground (neck). In case of binocular recording two sets of electrodes (recording, reference and ground) were used. Each set of electrodes was connected a physiological amplifier (P511, Grass Technologies, Rockland, MA), signals were amplified 10,000x and recorded within the passband 1-1000 Hz. Data was acquired through the LabVIEW data acquisition hardware, USB 6009 (National Instruments, Austin, TX), and was digitized at 5 kHz sampling rate; this parameters was set through the DAQ assistant express VI in LabVIEW. Responses were initially recorded in five-second epochs, the ppERG signal was monitored in real time (Figure 12A); large artifacts due to blinking were noted and resulted in additional epochs being recorded until at least 200 "clean" pattern reversals were obtained for off-line averaging in MATLAB (The MathWorks, Inc., Natick, MA).

Real time monitoring and offline averaging of the data did not provide an averaged waveform immediately, therefore, to obtain a clean waveform post offline averaging, the test-operator would have to make a subjective call, based on the noise and blink artefacts, to either collect additional epochs or stop the test. This had an impact on the test time and quality

To reduce test time and improve reliability, online averaging with artefact rejection was incorporated into the existing data acquisition VI. A threshold of $\pm$ 0.4V (post amplification) was chosen to eliminate any artefacts. A pattern reversal in which the

recorded signal exceeds this threshold will not be included in the average. Data acquisition will automatically stop after 300 artefact-free pattern reversals are collected and averaged. The number of pattern reversals to record is user adjustable, and can range between 1 – 350 pattern reversals for each run. Due to the design of the online data processing block diagram (LabVIEW), the updated data acquisition VI is dependent on a global variable VI. The global variable VI parameters must be set to zero after each test-run.

A

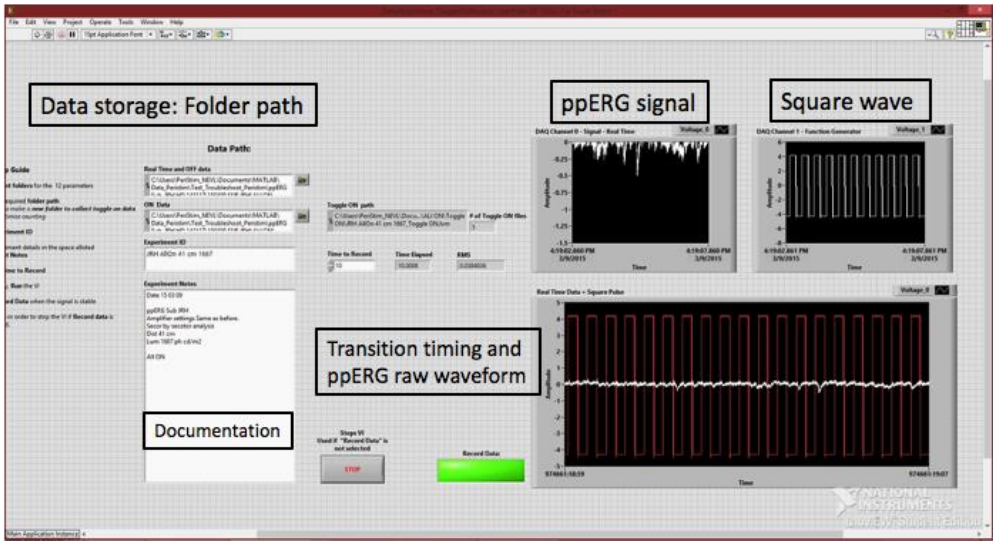

B

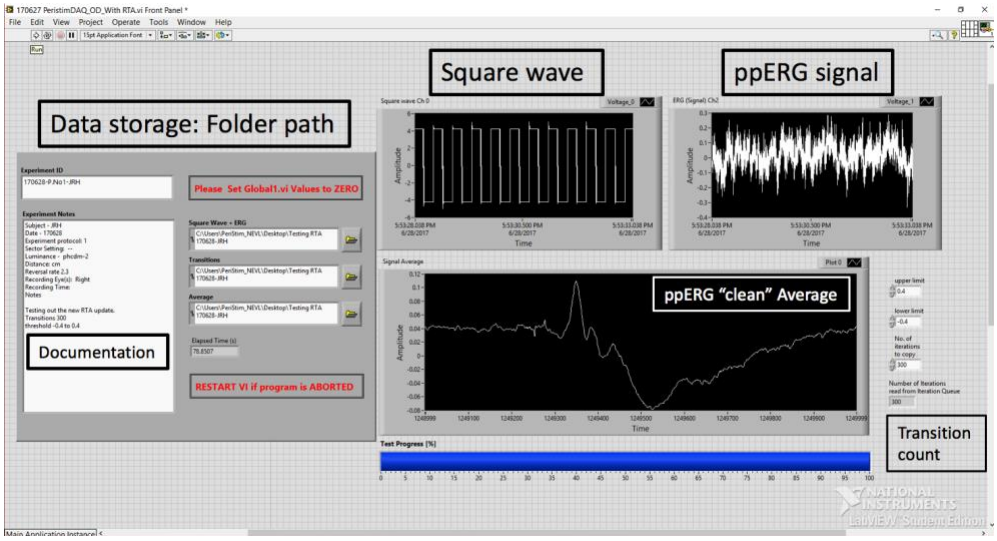

Figure 12. Data acquisition and online signal processing. (A) Image of the VI front panel prior to the incorporation of online data processing. A "Record data" toggle was switched (green button) when the ppERG stabilized. Data was recorded for 5 seconds. The waveform graphs show the transitions (top right), the pERG signal (top left) and the transitions along with the ppERG raw waveform. (B) Image of the VI front panel post incorporation of online data processing. The "Record data" toggle was removed. The waveform graphs show the transitions (top left), the pERG signal (top right) and the clean averaged waveform. A progress bar at the bottom shows the status of each test run.

Specific Aim 1 Results

System robustness. Re-soldering and insulating all the electrical connections with heat-shrink tubing resulted in good and robust connectivity between the LEDs. Labels on each row and column helped in case any troubleshooting was required; for example – if an LED check did not turn ON, it was identified by the label assigned (Row 1, column 12). The overall system redesign also made troubleshooting the system very easy; the transitions and the ON-OFF frequency is controlled by the function generator, each row has a set of switches, operational amplifiers, and transistors, each set controlls either the A phase or the B phase and a single column is controlled by a single switch, this created a modular organization, where, the problematic node could be easily identified and connections upstream or downstream could be checked.

Other improvements. The pERG amplitude is linearly related to contrast [Hans & Bach., 1999]. Contrast between neighbouring checks was increased to 96% by wrapping the black light-tight cloth around the circumference of the acrylic dome. Painting the central 40^{o} matte black reduced the light from the pattern to reflect off the surface and aided in achieving high contrast between the ON and OFF checks.

Pattern control – circuit design. Modifications made in the circuit allowed the high-output LEDs to provide luminances of ~ 15X higher than the monitors used for conventional pERG recording. Presenting a high luminance pattern will result in higher signal amplitude and therefore higher signal to noise ratio.

The system is capable of providing a range of luminances by applying different negative voltages. Four negative voltages (-3.16V, -3.28V, -3.8V, -4.22V) resulting in four mean ON-luminances (90 ph cd m^{-2}, 160 ph cd m^{-2}, 840 ph cd m^{-2} and 1670 ph cd m^{-2}) where chosen to investigate the ppERG response as a function of luminance. The luminance range varied from the ISCEV–recommended minimum (80 ph cd m^{-2}) to a luminance achievable when operating the LEDs at approximately 75% of maximum current (1000 mA, to avoid damage).

Changes could also be made with respect to the reversal rate and pattern selection. Reversal rate was managed by changing the frequency on the function generator that timed the reversing pattern. The ISCEV-recommended reversal rate for a transient pERG response is four reversals per second (RPS) [Bach et al., 2012]. A reversal rate of 4.6 RPS was chosen to avoid averaging of in-phase 60 Hz noise. As pERG components are associated with reversal rates [Bach et al., 2012; Trick GL., 1985], reversal rates of 2.3 RPS (half of 4.6 RPS) and 9.2 RPS (twice of 4.6 RPS) were also chosen to investigate ppERG responses as a function of reversal rate. A reversal rate of 4.6 RPS conformed to the ISCEV recommended standards.

Pattern control – user interface. Software updates incorporated resulted in the user having more control over the pattern, where in, specific LEDs or sections of LEDs could be turned ON or OFF. The redesign feature allowed for local stimulation of the peripheral retina,

probing local retinal regions may make the system more sensitive to localized glaucomatous damage.

Luminance uniformity. Luminance uniformity is a key factor governing the design of any pattern stimulus for pERG recording. The double-diffusing layers placed between the LED and the dome surface aided in the uniform distribution of light by eliminating any "hot-spots" in the center of each check. Figure 10B shows two ON and one OFF check and plots the luminance distribution across the checks. Luminance of each phase and row was equalized by adjusting the gain of the operational amplifiers (variable potentiometers). The neural density filters placed between outlier checks effectively reduced the luminance by cutting the transmittance accordingly (50% and 25%). The luminance across all checks was measured using the IL 1800 photometer and the mean ON-luminance between the A phase and the B phase was calculated. For a given mean ON-luminance, the standard deviation of luminance across checks was approximately 16%. Although the mean ON-luminance between phases was nearly constant (3.6% difference between A and B phase), mean ON-luminance measurements made recently showed that the standard deviation of luminance across checks increased to 32%. This increase may be due to the limited life span of the hardware components like, the LEDs, solid-state switches, operational amplifiers, potentiometers, etc.

Careful luminance vs. time measurements made for adjacent checks, confirmed an absence of all-dark or all-bright periods accompanying each pattern reversal. This can be seen in Figure 13. A transient decrease of 3.5% was seen at every other transition.

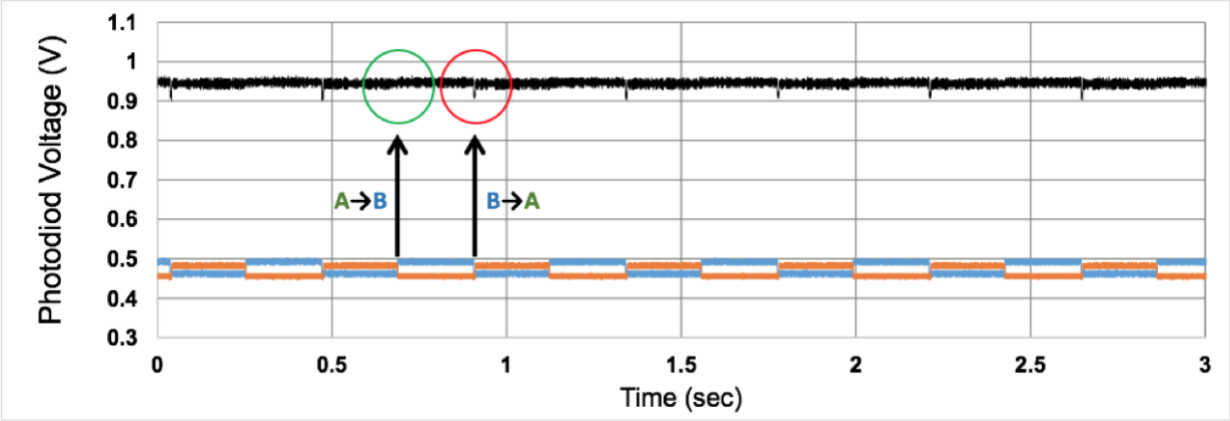

Figure 13. Luminance vs time measurements. Photodiodes placed on adjacent checks measure the luminance changes of A and B checks simultaneously. The A to B and B to A transitions are shown. Measurements were done at a ON-luminance of 1670 ph cd m^{-2} and at 4.6 RPS.

Data acquisition and online averaging. All commercial ERG recording systems provide access to the averaged clean waveform during the recording session. Incorporating such a data processing module to the existing acquisition VI made the peripheral pERG system test duration shorter. Online data processing ensured that at least 300 (user-adjustable) clean - pattern reversals were averaged in real time. As a result, the operator did not have to make a subjective call on the amount of data to collect to record a clean waveform for offline averaging, this reduced the uncertainty of the signal quality during the test. Artefacts rejection with a $\pm$0.4V ($\pm$ 40 microvolts, µV) threshold post amplification worked well to eliminate influence of blinks. This is well within the ISCEV recommended maximum range of $\pm$100 µV (for the recording the pERG). Access to the average waveform allowed for immediate interpretations and repetition of a test run in case of poor signal to noise ratio. The data acquisition user interface is seen in Figure 12B. The overall test time was typically designed to be ~1.5 - 2.0 minutes. However, the length of each run would depend

on number of pattern reversals that will be excluded due to blink artefacts, which in turn is dependent on subject compliance.

Specific Aim 1 Discussion

The main objective of this aim was to improve an existing prototype. This was achieved through numerous system improvements. Changes made in the electrical connections and circuit components provided a robust system, where many dozens of experiments were recorded with no malfunction. The updated graphical user interface to control the ON-OFF state of the LED resulted in local pattern stimulation (sector protocols, Specific Aims 2,3). Online data processing was an important addition to the system improvement as this tremendously increased the quality of stimulus, taking it a step closer to clinical use. Overall, changes made above resulted in a robust peripheral pattern ERG system capable of providing a high luminance pattern to the peripheral retina. The system was capable of providing luminances ~15X higher than standard monitors used to record pERG.

The pattern ERG responses recorded from the peripheral retina were highly novel in nature (Figure 14). The novelty of this response is explored in the following aim (Specific Aim 2) where, system validation experiments for different combinations of luminance, reversal rate, field subtended and check size are carried out. The sensitivity of the test to disease detection is measured in Specific Aim 3.

System validation and test sensitivity experiments helped to establish the ableness of the system to provide a direct, objective, repeatable and highly sensitive measure of glaucomatous damage to RGCs that can be routinely employed in a clinical setting.

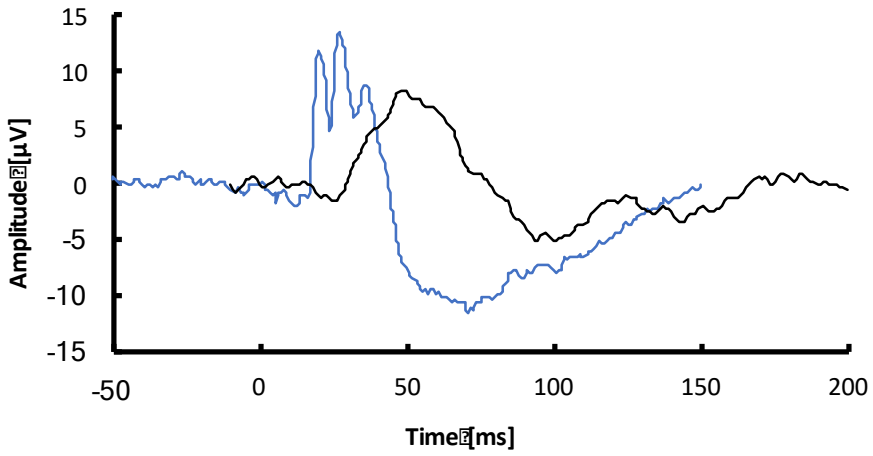

Figure 14. High luminance peripheral pattern ERG responses. The high-luminance peripheral pattern ERG response (blue trace) recorded from one subject seated at a viewing distance of 55 cm (check size of 5°), mean ON-luminance of 1670 ph cd m^{-2} and a reversal rate of 4.6 RPS. The black trace represents a conventional pattern ERG response recorded from the same subject on the same day. The pERG response was recorded at a ISCEV recommended luminance of 80 oh cd m^{-2}, with 1° checks at a viewing distance of 55 cm and a reversal rate of 4.0 RPS.

Limitations. Although improvements and changes made in the system bring it very close to the ideal pattern ERG stimulus (mentioned above: motivation), the novel three-dimensional pattern stimulus source is limited in certain ways. The central blackened region is not tiled with LEDs, this limits the system capability to probe just the peripheral regions and not the entire retina. The ON-OFF pattern is controlled by a square wave from the function generator and the inverting and non-inverting operational amplifiers, this limits the flexibility of the pattern. Any changes would require some amount of circuit rewiring. The increase of the standard deviation of the luminance (from 16 % to 32 %) is concerning.

Future upgrades. Taking these limitations into account, future system updates can involve, increasing luminance uniformity by replacing hardware components (switches, LEDs, etc.), tiling the entire hemisphere, and using software to manipulate the pattern style. This would allow in probing specific sections of the visual field and/or the entire visual field with a high luminance pattern and would be ideal for detecting earliest disease onset.

Part III: Specific Aim 2

System validation in normally-sighted subjects
(Patangay et al., 2018)

Specific Aim 2

System validation and response characterization in normally-sighted subjects. Peripheral pattern ERG responses were recorded in a small population of normally-sighted subjects (n = 11) and were compared to conventional pERG responses. The ppERG stimulus parameter space (including luminance, reversal rate and field subtended) was explored in order to identify a protocol that yielded a robust and repeatable response.

Specific Aim 2 Motivation

Specific Aim 2 focused on testing the ableness of the system. Every clinical vision test has a standardized recommended protocol that has evolved to be the most useful in informing medical decisions. As the peripheral pattern ERG system is new, the first step was to begin to explore the parameter space in order to identify the most useful protocol. As existing clinical ERG test have established normative ranges, and as the ppERG responses have never been recorded, the next thing that was done was to begin to establish a normal range for these novel responses. The ultimate goal of this work was to evaluate ppERG relative to existing clinical tests, primarily for glaucoma detection. In order to begin the process of comparing and contrasting with an established test, conventional pERG recordings in all the subjects (and patients, Specific Aim 3) were performed on the same day as ppERG recording.

There have been some initial attempts to record pERG responses from regions outside central retina. Aylward et al. used a 75° × 86° standard TV monitor. The large field subtended was achieved by increasing the stimulus area and by decreasing the viewing

distance. The authors noticed that the pERG amplitude increased with the increase of the field subtended and suggest that this quality might prove clinically useful in monitoring mid peripheral inner-retinal diseases [Aylward & Billson., 1989]. Asymmetric glaucomatous hemi-field losses were also examined by recording wide-field nasal pERG. The wide-field was obtained by reducing the viewing distance. At a reduced viewing distance the stimulus extended from 52.2° × 42.4° [Graham et al., 1994]. Responses were recorded from glaucoma patients and normal subjects; their results show that the pERG test could detect field specific losses. The functional loss arising due to selective field defects in the mid-peripheral retina was also studied by Shorstein et al. They presented a 12° × 12° stimulus in four quadrants (supranasal, supratemporal, infranasal, and infratemporal quadrants) of the visual field, and saw that in glaucomatous eyes, [Shorstein et al., 1999], responses recorded from the mid-peripheral quadrants showed reduced pERG amplitudes. Abnormalities in visual function and associated visual field losses can also be drug induced. One such example is the prescription of Vigabatrin. Vigabatrin, is an anti-epileptic drug used to treat infantile spasms and seizures. Young adults undergoing vigabatrin therapy are highly prone to peripheral visual field defects [Eke et al., 1977]. Lalonde et al. showed a strong correlation between pERG amplitudes to mid-peripheral field losses caused due to vigabatrin therapy. Mid-peripheral pERG responses were recorded using a radial checkerboard pattern extending from 30^{o} – 60^{o} [Lalonde et al., 2016].

All the above studies suggest that looking beyond the foveal and para-foveal regions into the mid and far-peripheral retina would help in detecting and monitoring early onset of

diseases effecting these largely overlooked regions. As current tools cannot extend far into the periphery, a tool to capture the function of the peripheral retina is clearly needed.

Specific Aim 2 Methods.

ppERG protocols:

ppERG Recording: Eleven normally-sighted subjects (15 eyes recorded from) were recruited. Informed consent was obtained from all subjects before participation. Procedures adhered to the tenets of the Declaration of Helsinki, and the protocol was approved by an Institutional Review Board at the University of Illinois at Chicago. The subjects had no history of eye disease, normal visual acuity, RNFL thickness within normal limits (average over all sectors: range, 75-101 μm; mean $\pm$ SD, 89 $\pm$ 8 μm), and refractive error that ranged from 0 to -5.00 diopters. Subjects ranged in age from 22 to 65 years (mean $\pm$ SD, 43 $\pm$ 15 years). Responses were recorded from one or both eyes. The ppERG signal was recorded with a DTL fiber electrode (LKC Technologies, Gaithersburg, MD) placed in contact with the cornea of the recording eye(s). A drop of proparacaine HCl was used as a topical anesthetic. Reference and ground skin electrodes were placed on the ipsilateral temple and neck respectively (Figure 15A). Table 2 summarizes the parameter values for the peripheral pattern stimulus source (ppERG) and conventional pERG stimulus source used in this study. Two sets of these electrodes, one set for each eye, were used if the ppERG was to be recorded from both eyes. Subjects were positioned at one of three viewing distances via a moveable chin rest. Once seated comfortably, the room lights were turned off and the subjects were asked to fixate on the central target during recording (Figure 15B). The mean ON-luminance was varied from 90 – 1670 photopic cd m^{-2};

Recording was done in five second epochs, and 10-30 epochs (230-690 pattern reversals) were obtained for each recording condition. Test time for each protocol rarely exceeded 3 minutes; up to five recording protocols, with breaks between, were completed for each subject. Conventional pERG recording was performed according to ISCEV standards. [Table 2, Bach et al., 2012], including correction for refractive error, on the same day.

	ppERG	pERG
Mean ON-luminance (ph cd m^{-2})	90 160 830 1670	90
Check Size	10^{o} at 30 cm 5^{o} at 55 cm	1^{o}
Reversal rate	2.3 RPS 4.6 RPS 9.2 RPS	4.0 ± 0.8 RPS
Stimulus Field (Half Angle)	35 – 85 ^{o} at 30 cm 22 – 50^{o} at 55 cm	0 – 15 ^{o} at 55 cm

Table 2. Parameter values for the peripheral pattern stimulus source (ppERG) and conventional pERG stimulus source used in this study. pERG stimulus values conform to ISCEV-recommended values

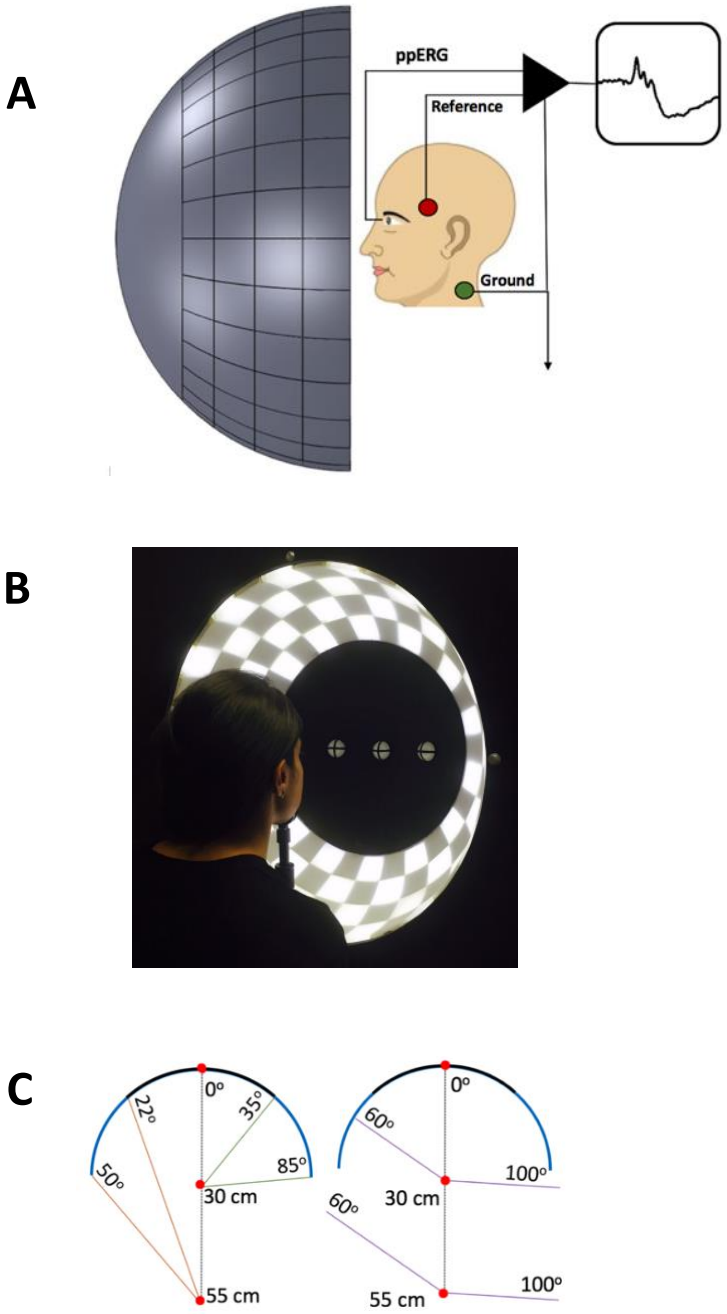

Figure 15. The general ppERG recording setup. (A) Schematic illustration of the recording setup, subject is seated at a viewing distances of 30 cm. A DTL fiber electrode was used as the recording electrode. Adhesive skin electrodes were used for reference (ipsilateral temple, red) and ground (neck, green). Signals were amplified and monitored in real time. (B) View of a subject as positioned for a recording session, subject is seated at 30 viewing distance (note position of chin rest). Fixation was always on the central target. (C) Left schematic illustrates the range of visual angles subtended by the four rows of checks (blue portions of hemisphere) at each of two

In order to identify a ppERG protocol that gave a robust and repeatable and reliable response, the following stimulus characteristics were explored.

Reversal rate: To understand the effect of change in reversal rate, transient ppERG response waveforms were recorded at three different reversal rates (2.3, 4.6, 9.2 reversals per second, RPS) for six normally sighted subjects. All subjects were seated at a fixed viewing distance of 30 cm, mean ON-luminance was maintained at 1670 ph cd m^{-2}.

Check size, viewing distance and field subtended: To understand the effect of viewing distance on the waveform, responses were obtained at three different viewing distances at a fixed mean ON-luminance (1670 ph cd m^{-2}) and reversal rate (4.6 RPS). Changing the viewing distance also affected check size and field subtended. (Table 2, Figure 15C).

Central vs. peripheral field: To isolate the effect of eccentricity only, responses were recorded with a 4x4 check pattern (check size 10^{o}, 4.6 RPS) presented in the temporal field (standard fixation target, remaining checks were dark) and central field, (subjects turned their head and fixated at the center of the 4x4 pattern, viewing distance kept constant at 30 cm).

Test/re-test and inter-subject variability. Variability between similar subjects, and test-retest repeatability for the same subject, are important considerations for efficacy of any test. In order to assess inter-subject variability, response waveforms from the eleven normally-sighted subjects (11 right eyes) were obtained with the viewing distance of 30 cm, mean ON-luminance of 1670 ph cd m^{-2}, and reversal rate of 4.6 RPS. To assess the test/ re-test repeatability, ppERG responses were obtained from one subject on three different days, with retests done 5 and 19 months from the initial test.

Exploiting regional differences in ganglion cell density. Ganglion cell density differs between the nasal and temporal retina [Curcio & Allen., 1990], therefore ppERG responses recorded from nasal and temporal hemispheres should differ in amplitude if the response is ganglion cell driven. This was tested by presenting nasal and temporal hemi-field stimuli with the ppERG system. Responses were recorded at an average distance of 41 cm, at this distance the bridge of the nose did not block any of the pattern. Mean ON-luminance and reversal rate were maintained at 1670 ph cd m^{-2} and 4.6 RPS respectively. Responses were recorded in six normally sighted subjects.

Local Pattern stimulation. Disease-related dysfunction in the retina is often sectoral rather than diffuse or global [Calkins & Horner., 2012] for this reason, local responses from the peripheral retina in three and four field sectors were evaluated.

Initially, four sectors corresponding to superior nasal, inferior and temporal fields were defined (Figure 28A). These four sectors were chosen to correspond to the four circumpapillary sectors typically defined by OCT scan, as shown in Figure 28B. Forty five-second epochs from each quadrant were recorded from 10 normally-sighted subjects, followed by recording the response to the all-ON stimulus, where the standard ppERG with the entire stimulus turned ON was recorded at the same distance.

The four sectors were later modified to correspond to the retinal nerve fiber tracts giving rise to three anatomically relevant sectors that probed the temporal, superior-nasal and inferior-nasal regions of the retina (Figure 28C–D), twenty-five five-second epochs were recorded from each sector in five normally sighted subjects, followed by all-ON.

For all sector stimuli, the stimulus was placed at a viewing distance of 41 cm from the eye, this ensured that no part of the stimulus was blocked by the bridge of the nose. Mean ON-luminance and reversal rate were maintained at 1670 ph cd m^{-2} and 4.6 RPS respectively.

With and without Acuity correction. To evaluate the effect of acuity correction on ppERG, responses were recorded from one subject with and without prescription eye glasses (-4.25 diopters, OD). The subject sat through several recording protocols (viewing distances and luminances) recorded at a fixed reversal rate of 4.6 RPS. All responses were recorded on the same day.

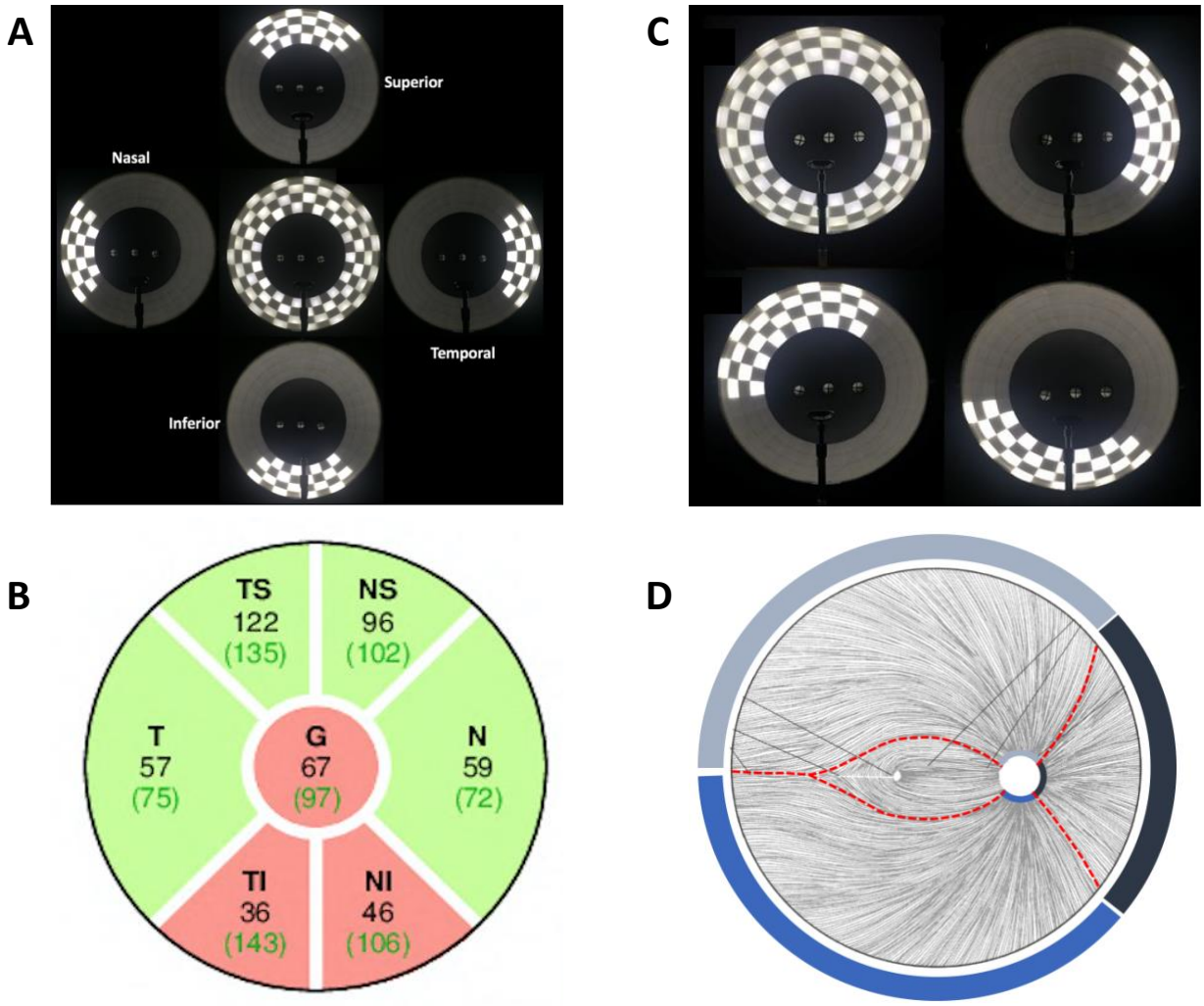

Figure 16. Sectoral stimulation capabilities of the ppERG system. (A) Four field sectors defined for a right eye. Center shows stimulus in its All-ON configuration while clockwise from top shows a subset of the peripheral check pattern presented to the subject / patient, restricted to the superior, nasal, inferior or temporal field sectors for a right eye. (B) An image of the four circumpapillary sectors (temporal (T), temporal-superior (TS), nasal-superior (NS), nasal (N), nasal-inferior (NI) and temporal-inferior (TI)) of an OCT scan for the same eye. (C) Anatomically relevant field sectors of the peripheral sector stimuli that correspond to the retinal nerve fiber tracts. Clockwise from top shows stimulus in its All-ON configuration, temporal, inferior-nasal and superior-nasal fields for a right eye. (D) Schematic illustration of the retinal nerve fiber tracts. The blue arcs (Superior-nasal, Inferior- nasal and Temporal) depict the area covered by the field sectors of the 3– D stimulus, sectors are defined by following the retinal fiber tracts (red dashed lines).

Peripheral ON response. As described in the Results section, high frequency oscillations were observed in the ppERG response. A natural question was whether these oscillations were related to the oscillatory potentials (OPs) observed in ON response ERG waveform. In order to address this question, the ppERG stimulus source was configured to present a step increase in luminance to the peripheral retina.

Previously, the circuit was set up to run half a set of LEDs in their ON state while the other half were in their OFF state, creating a checkered ON-OFF pattern. In order to generate a peripheral ON stimulus, connections were rewired to allow all the LEDs to be in the same state (ON or OFF) at the same time. Specifically, the input to the non-inverting operational amplifiers (B phase) were instead connected to the inputs of the inverting amplifiers (A phase), ensuring that all checks were in the same phase (Figure 8A, Specific Aim 1) The square wave (driving this ON-OFF state) was set at a frequency of 0.2 Hz (0.4 RPS) with a 20% duty cycle and a 5V peak to peak amplitude, this resulted in the stimulus being ON for 1 second and OFF for 4 seconds. Responses were recorded from one subject. Room lights were turned off; the pupil was dilated with one drop of phenylephrine and one drop of tropicamide, spaced 60 seconds apart. Following a 20-minute dark adaptation period, ~60 peripheral ON responses were recorded with the subject seated at a viewing distance of 30 cm from the stimulus. Mean ON-luminance was set to 744 ph cd m^{-2}, in order to approximately match the mean luminance (ON and OFF checks) presented during pattern stimulation at 1670 ph cd m^{-2}. Central ON responses (visual angle, 32^{o}) at the same luminance and viewing distance were recorded on the same day.

Effect of luminance imbalance on the ppERG. The pattern ERG is a non-linear response [Bach and Hoffmann., 2006, Principles and Practice of Clinical Electrophysiology of Vision].

Meaning, linear response components from the ON and OFF phases (A and B) will cancel each other out as a result of being equal and opposite in magnitude, resulting in the pERG response. A luminance imbalance between the phases will give rise to a luminance artifact i.e. contamination of pERG responses by the linear response components. It is therefore essential to maintain a constant mean ON-luminance while recording the pERG. In order to evaluate the effect of the presence of a luminance artifact on the ppERG response, a series of deliberate luminance imbalance will be introduced. Mean ON-luminance of the one phase will be maintained at 1670 ph cd m-2 and ppERG responses will be recorded at a viewing distance of 30 cm and 4.6RPS reversal rate for each luminance imbalance. The Luminance imbalances will be created by reducing the transistor collector-voltage for the other phase (Figure 8A, Specific Aim 1), in regular steps, resulting in a range of mean ON-luminances for that phase.

ppERG response analysis. ppERG response waveforms evoked with high-luminance patterns were distinct from typical pERG response waveforms obtained using ISCEV-recommended stimulus values. A representative waveform is plotted in Figure 17A. The most apparent novel feature in the ppERG waveform is the series of high-frequency oscillations occurring in the time range of 10-45 ms. To evaluate waveform components for amplitude and implicit time, the high-frequency components were isolated from the low-frequency components. Fourth-order Butterworth filters, with pass-bands of 1-50 Hz and 50-1000 Hz, were applied to the raw waveforms; each filter was applied twice, once forward and once backward, to avoid phase shifts in the filtered data (filtfilt function in MATLAB [Gustafsson., 1996]). The cutoff frequency of 50 Hz was found to provide the best separation of high-frequency and low-frequency peaks across the recording protocols used

here. The isolated low-frequency waveform (Figure 17B) typically included an early positive phase and a later negative phase, similar to conventional pERG waveforms (P50 and N95), but with shorter implicit times; they are referred to here simply as P and N. P was measured from baseline to the positive peak; N was measured as the difference between P and the negative trough. The isolated high-frequency waveform (Figure 17C) typically included three distinct peaks, referred to here as F1, F2 and F3. F1 was measured from baseline to peak; F2 and F3 were measured from the previous trough to peak, analogous to amplitude evaluation of flash ERG oscillatory potentials. All peak and trough amplitudes were evaluated as the maximum or minimum values, respectively, within standard time windows determined by visual examination of the range of peak times across all study participants.

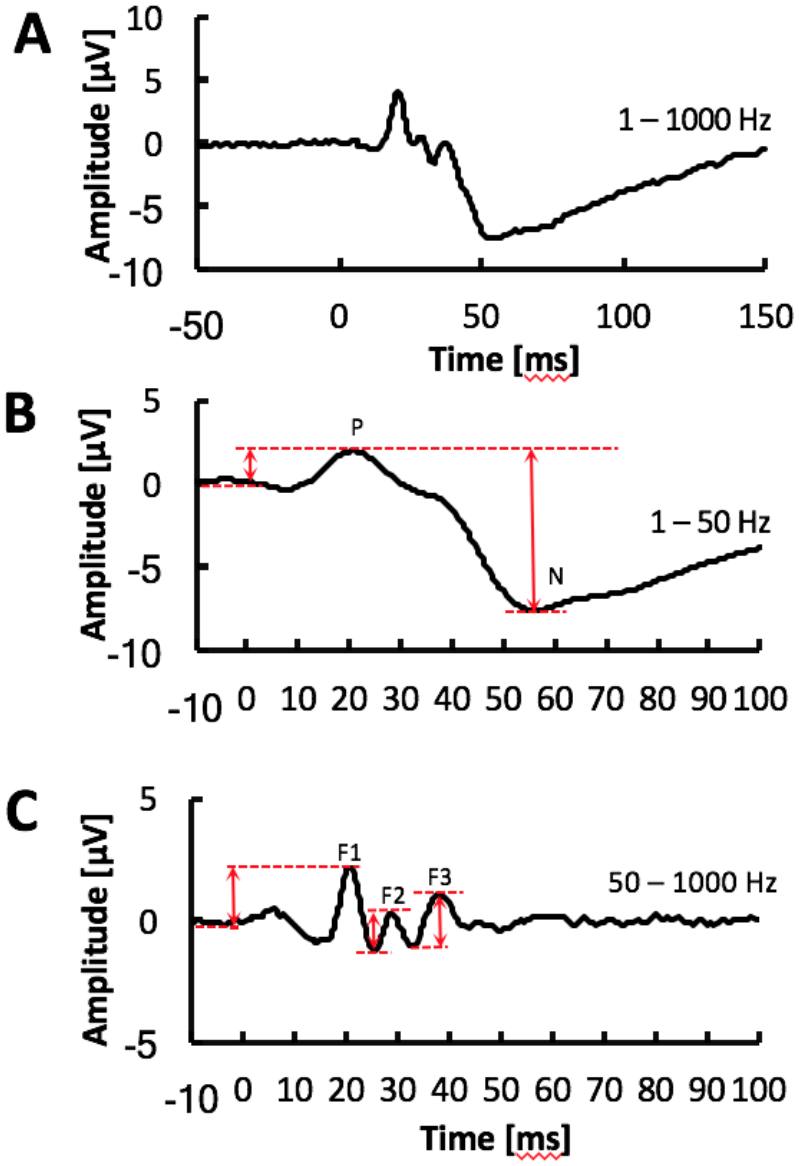

Figure 17. Evaluation of amplitudes for ppERG response waveform components. (A) Mean waveform recorded from 15 normal eyes (11 right, 4 left) with viewing distance of 30 cm and mean ON-luminance of 1670 ph cd m^{-2}. Signals were recorded with passband 1-1000 Hz. (B) Isolated low-frequency components in the passband 1-50 Hz. Amplitude of the low-frequency positive component, P, was measured from baseline to peak. Amplitude of the low-frequency negative component, N, was measured as the difference between P and the subsequent trough. (C) Isolated high-frequency components in the passband 50-1000 Hz. Amplitudes of the three high-frequency peaks evaluated as illustrated (baseline to peak for F1, trough to peak for F2, trough to peak for F3).

pERG recording and analysis.

pERG Recording: To compare peripheral pattern stimulus responses source is eliciting a responses to conventional central-field pERG, conventional pERG responses, recording conforming to ISCEV standards [ISCEV reference], including correction for refractive error, were recorded on the same day for all eleven normally sighted subjects. Responses were recorded using a commercial system (Espion E3 Electroretinography system for PSG (pattern stimulation and grating); Diagnosys LLC, Lowell, MA). DTL fiber electrodes (LKC Technologies, Gaithersburg, MD) were used to contact the cornea, referenced to a cup electrode on the ipsilateral ear. A drop of proparacaine HCl was used as a topical corneal anesthetic. Subjects fixated o

n a red fixation point at the center of the screen, responses were digitized at a 2kHz sampling rate and a total of 150 sweeps per recording epoch were obtained. The test was repeated once for better signal to noise ratio. To compare pERG responses elicited from the peripheral and central retina, conventional pERG responses were recorded using stimulus parameters that matched the ppERG system in terms of mean ON-luminance (~90 ph cd m^{-2}), viewing distance (55 cm), check size (5^{o}) and reversal rate (4 RPS)

pERG response analysis. –Amplitude and implicit time values for the pERG responses were evaluated in order to compare them to the ppERG amplitude and implicit times. Similar to the ppERG response analysis, the pERG peak and trough amplitudes were obtained within standard time windows. The P50 amplitude was measured from the average baseline (between time zero and the onset of P50) to a maximum value within a 45-60 ms window [ISCEV reference]. Visual examination of the range of N95 implicit times across all study participants extended the N95 time window by 15 ms (ISCEV recommended: 90 -100 ms).

The N95 amplitude was therefore measured from the peak of P50 to the trough of N95 within a 90-115 ms window.

Effect of NMDA on the high luminance pERG response. Pharmacological dissection experiments in a Long Evans rat was used to confirm the cellular origin of the response evoked by the large check, high luminance stimulus. The design of the experiment included five steps – pre-injection flash ERG recording, pre-injection pERG recording, intravitreal injection of NMDA (left eye) and PBS (right eye, control), post-injection flash ERG recording, post-injection pERG recording. Pre-injection responses from both eyes were recorded in order to establish a baseline for comparison. The glutamate agonist N-Methyl-D-aspartic acid (NMDA) preferentially binds to receptors on ganglion cells; PBS was used to account for effects of the injection. The post-injection flash ERG was recorded in order to monitor the effects of NMDA. Once the flash responses indicated that NMDA had taken effect, the post-injection pERG was recorded. Animals were anesthetized by administering intraperitoneal injections of 100 mg/Kg (body weight) of ketamine and10 mg/Kg (body weight) of xylezine. Proparacaine (0.5%) was used to anesthetize the cornea. A regulated heating pad was used to maintain body temperature (37-39^{o}C). A DTL fiber electrode was used as the corneal electrode; platinum subdermal needle electrodes in the cheek and nape of neck were used as reference and ground, respectively (Figure 18). Flash ERG responses (Grass P52 photo-stimulator) and pattern ERG (4x4 pattern, mean ON-luminance of 1670 ph cd m-2, 10 degree checks, central field) were recorded from both eyes before and after intraocular injections. One eye received the NMDA using volumes and concentrations reported by Xu et al. [Xu et al., 2003]; the other eye received saline as a sham control. ACC

protocol number of 14-203 was approved by the University of Illinois at Chicago for this work.

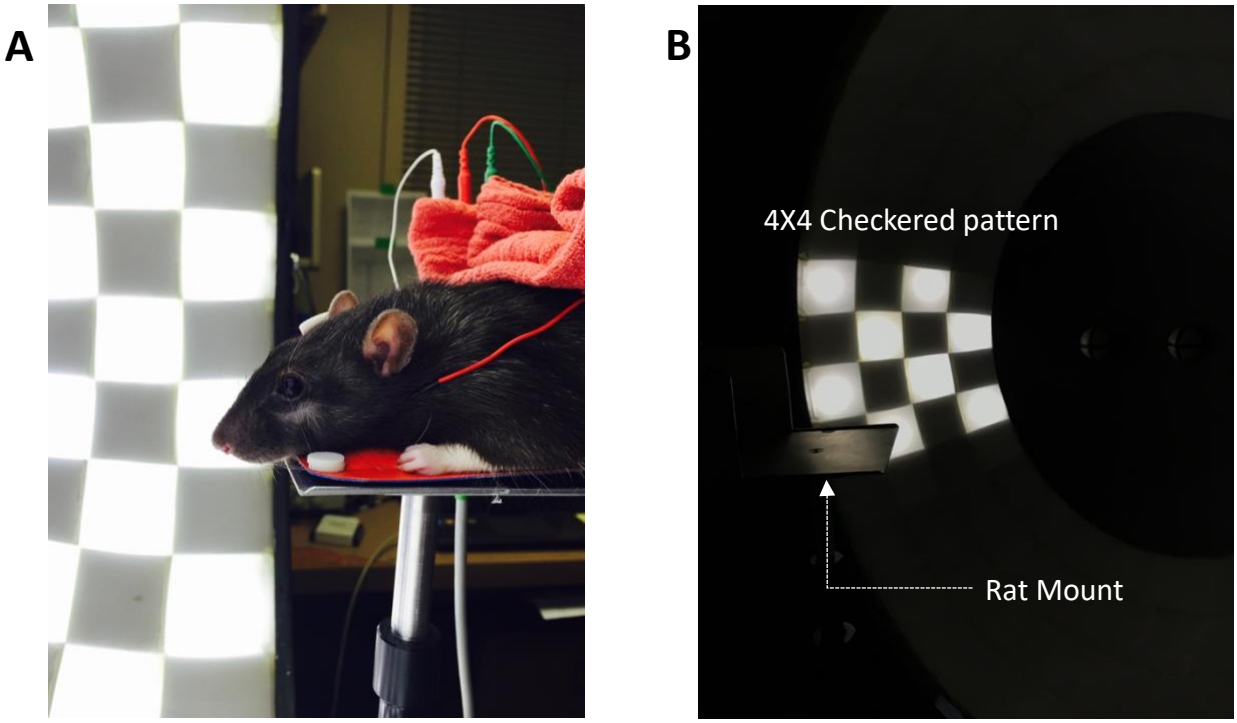

Figure 18. Rat setup to monitor effect of NMDA on the high luminance pERG response. A high-luminance pattern ERG response was recorded from one rat. (A) Anesthetized rat placed and hooked up on the custom designed rat mount, with the heating pad at the base of the mount. A DTL fiber electrode was placed on the rat eye, with platinum subdermal needle electrodes as ground (green, not visible in figure) and reference (red). Animal was placed at a distance of 30 cm from the apex of the stimulus, the mount was rotated to align the axis of the eye with the central point of the 4x4 check pattern. (B) The 4x4 check pattern presented to the rat during recording.

Specific Aim 2 Results

Comparison of ppERG and pERG response waveforms. To confirm that the custom-built peripheral pattern stimulus source elicited a response analogous to that obtained with conventional central-field pERG, responses were recorded using similar stimulus settings for both sources. Figure 19A plots the average ppERG (black) and pERG (green) waveforms obtained from six normally-sighted subjects when the mean ON-luminance and viewing distance were matched (90 ph cd m^{-2} and 55 cm, respectively); at 55 cm, the ppERG stimulus falls in the mid-periphery (22^o-50^o, Figure 15C). The remaining stimulus difference was check size (5^o for ppERG and 1^o for pERG). Under these conditions, both the ppERG and pERG waveforms are dominated by early positive and later negative peaks, the primary differences being the earlier peak times, and "ripples" visible on the leading edge of the positive component, for the ppERG response. To examine the effect of signal filtering, the average ppERG response in Figure 19A was digitally filtered to match the pERG passband (1-100 Hz), and replotted in Figure 19B (black trace); note the absence of high-frequency ripples on the leading edge. The green trace in Figure 19B is the pERG waveform obtained when the check size was increased to 5^o to match the ppERG stimulus source. With luminance, check size, and signal filtering matched, the central and peripheral pERG waveforms are quite similar; the remaining differences are the slightly earlier positive component peak time, and the earlier and broader negative peak, for the ppERG responses

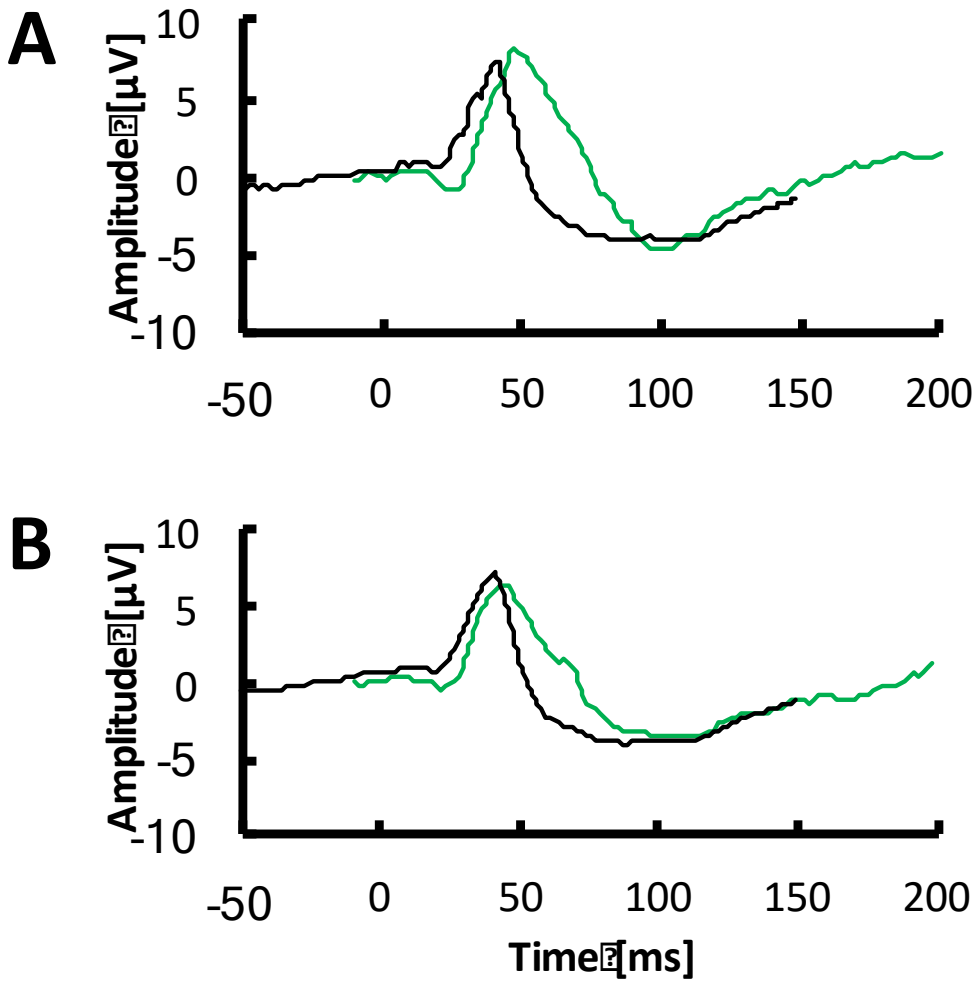

Figure 19. Comparison of ppERG and pERG response waveforms. Waveforms are average of six normally-sighted subjects. (A) Response waveforms for ppERG (black trace, 5° checks, 1-1000 Hz passband, field subtended 22°-50°) and pERG (green trace, 1° checks, 1-100 Hz passband, field subtended 0-15°), with both systems set to ~4 RPS and mean ON-luminance of ~90 ph cd m^{-2}. (B) Response waveforms obtained when reversal rate (~4 RPS), luminance (~90 ph cd m^{-2}), check size (5°) and passband (1-100 Hz) were matched; fields subtended as in panel A. Black trace, ppERG; green trace, pERG.

Test-retest, inter-subject variability. Consistency across similar subjects, and test-retest repeatability for the same subject, are important considerations for efficacy of any test. Response waveforms from the eleven normally-sighted subjects (11 right eyes) are plotted in Figure 20A (black traces, red trace is average waveform). These responses were obtained with the viewing distance of 30 cm, mean ON-luminance of 1670 ph cd m^{-2}, and reversal rate of 4.6 RPS. There is a general similarity of waveform shape from subject to subject; this can be more clearly seen in panels B and C of Figure 20, which plot the isolated low-frequency and high-frequency components for each subject, respectively. The highest variability occurs in the amplitude of the N component, followed by F2; F2 showed a slight negative correlation with age (-0.06 μV $year^{-1}$, not shown), but N did not. Panel D plots the pERG responses recorded in the same subjects on the same days, for comparison (green trace is average waveform).

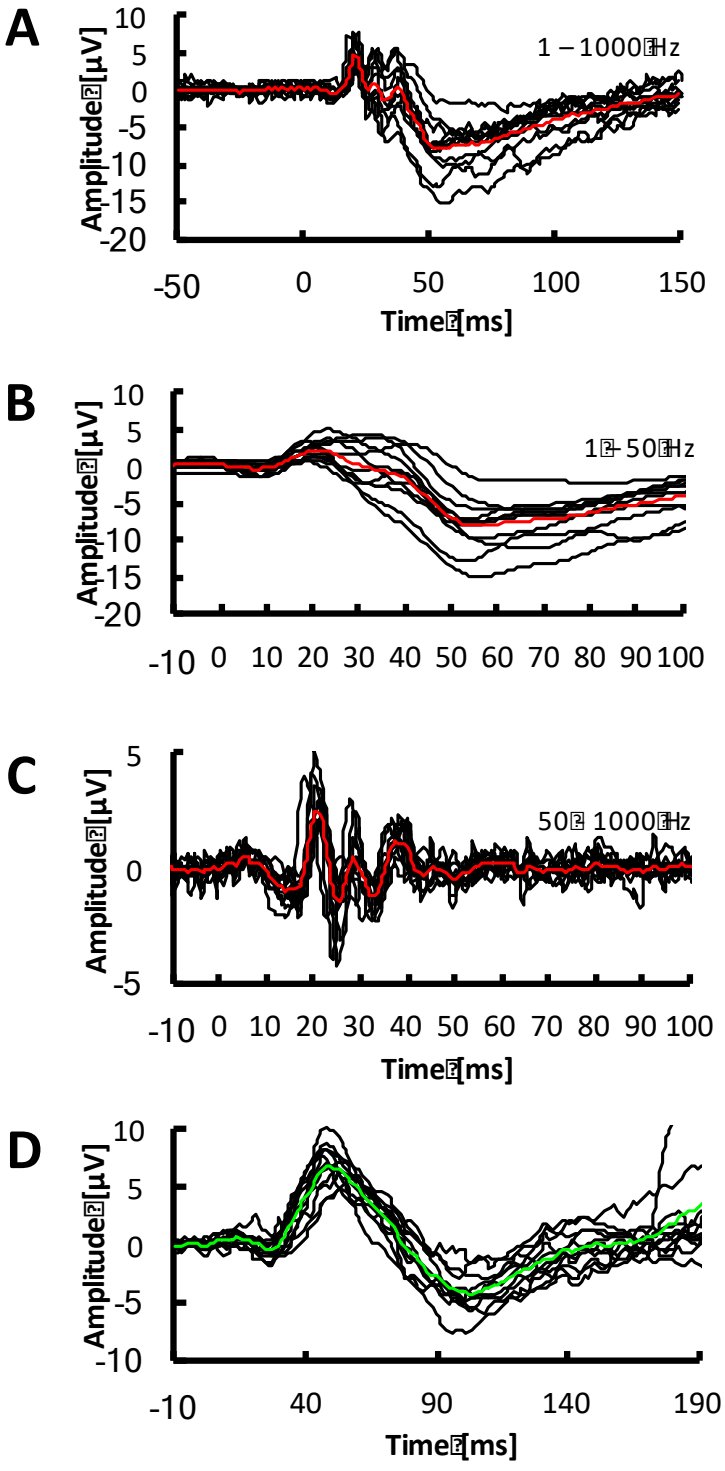

Figure 20. Inter-Subject variability in ppERG and pERG responses. (A) ppERG response waveforms recorded from 11 right eyes with viewing distance of 30 cm and mean ON-luminance of 1670 ph cd m^{-2}. Red trace is the average of the 11 black waveforms. (B) Isolated low-frequency components of the waveforms in panel A. (C) Isolated high-frequency components of the waveforms in panel A. (D) Conventional pERG responses, stimulus parameters as given in Table 2, same subjects as in panel A. Green trace is the average of the 11 black waveforms.

The high-frequency components in the ppERG response somewhat resemble flash-ERG oscillatory potentials (OP's) in shape, though OP's are ten times larger in amplitude; a comparison is made in panel F of Figure 21. The average isolated OP waveform for one subject is plotted in black (dark adapted subject, flash strength = 2.3 sc cd s m^{-2}). The four peaks typical at this flash strength are labeled. The red trace plots the average isolated ppERG high-frequency components from the same eye. Panels D-E plot the raw (passband 1-1000 hz) and isolated-low frequency components (passband 1-50 Hz) for the two responses. The number of peaks in the ppERG response was consistently three within the parameter space limits investigated here, and the oscillations occurred at slightly lower frequency than is typical for flash ERG OP's. A more direct comparison was made by examining the ppERG high frequency components relative to the peripheral ON response oscillations (Figure 21C). The black trace represents peripheral ON response oscillations isolated at a passband of 50-300 Hz; ~80 peripheral ON responses were recorded from one subject. The black trace plots the average ppERG response recorded from the same subject on five different days. ppERG responses were recorded at a viewing distance of 30 cm, mean ON-luminance of 1670 ph cd m^{-2} and a 4.6 RPS reversal rate. Panels B-C plot the raw (passband 1-1000 Hz) and isolated-low frequency components (filter passband 1-50 Hz) for the two responses. Like the flash OPs, the peripheral ON response OPs were somewhat similar yet distinct in appearance. Further investigation using pharmacological dissection may be needed to confirm the origins of ppERG high frequency components.

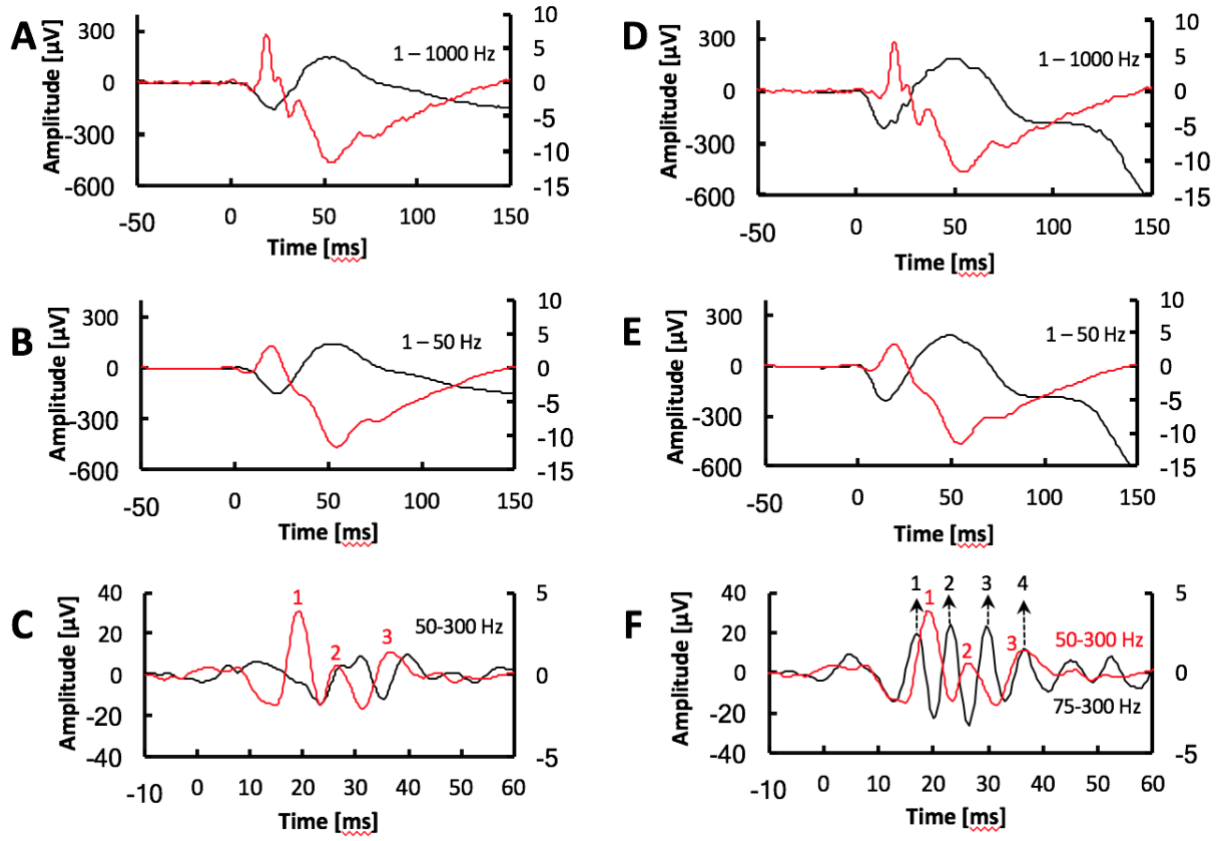

Figure 21. Comparison of ppERG, flash ERG and peripheral ON response waveforms. Peripheral ON and patter ERG responses are recorded from one normally sighted subject seated at a viewing distance of 30 cm with a mean ON luminance of 740 ph cd m^{-2} for peripheral ON recording and 1670 ph cd m^{-2} for ppERG recording. (A) Black trace plots the average of 80 peripheral ON responses (left axis) and the red trace plots the average of ppERG responses across 5 sessions (right axis). (B) Isolated low frequency components of the peripheral ON (black trace) and ppERG responses (red trace) (filter passband 1-50 Hz). (C) Isolated high frequency components of the peripheral ON plotted in black (left axis) compared to the isolated ppERG high frequency components (red trace, right axis) (filter passband 50-300 Hz). ppERG high-frequency components (F1-F3) numbered in red. Panels D-F plot flash ERG response against the ppERG response for the same individual. (D) Black trace (left axis) is an average of 10 flashes recorded at a luminance of 2.3 sc cd s m^{-2}. Red trace (right axis) plots the average ppERG responses. (E) Isolated low frequency components of the flash ERG (black trace, left axis) and ppERG responses (red trace, right axis). (F) Isolated high-frequency ppERG components (filter passband 50-300 Hz) plotted in red (right amplitude axis) compared to the isolated oscillatory potentials (OP's, black trace, filter passband 75-300 Hz, left amplitude axis) isolated from flash ERG response. Pattern transition, and flash presentation, respectively, occurred at time zero. OP's numbered in black, ppERG high-frequency components (F1-F3) numbered in red, ppERG stimulus parameters as in panel A-C.

Amplitude and implicit time values for all pERG and ppERG components are summarized in Figure 22; here the ppERG stimulus was viewed from 30 cm and had mean ON-luminance of 1670 ph cd m^{-2}; the pERG stimulus was consistent with the ISCEV standards (Table 1). Under these conditions, the amplitudes of P50 are significantly larger than those for P. There was no significant difference in negative component amplitudes (N95 vs. N), but because N95 and N amplitudes are measured from the peak of the preceding positive component (P50 and P, respectively), N typically reached greater negative values at peak than N95. Implicit times of P and N were significantly shorter than P50 and N95, respectively.

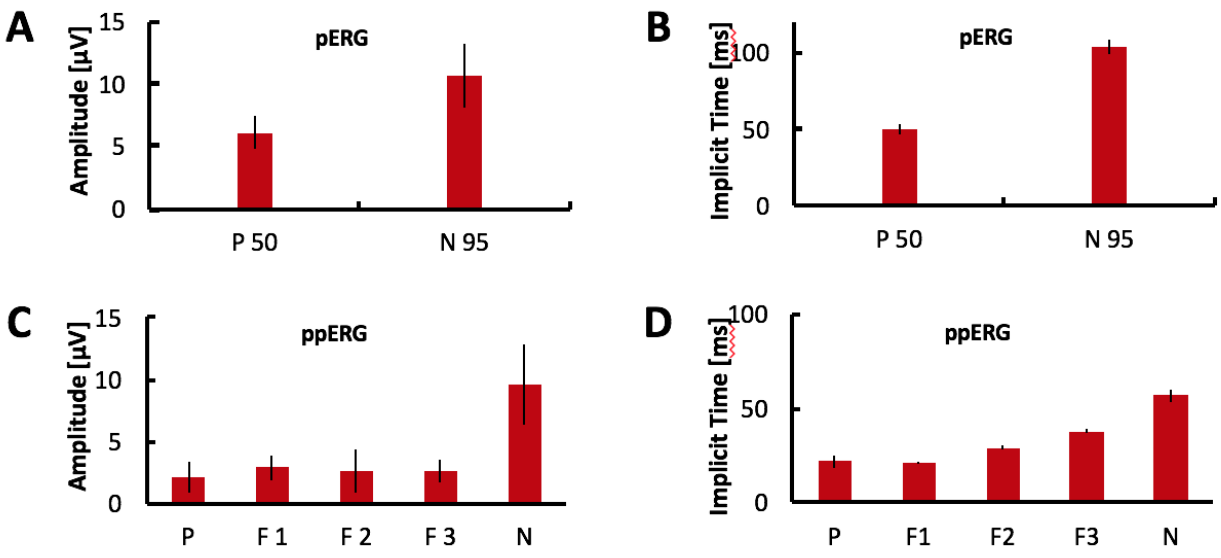

Figure 22. Amplitudes and latencies for the ppERG response components (P, F1, F2, F3, N) and pERG response components (P50, N95). Responses evaluated for the 11 right eye responses are plotted in Fig. 8. All responses obtained at a viewing distance of 30 cm and mean ON-luminance of 1670 ph cd m^{-2}. Bar heights plot mean, error bars plot $\pm$ one standard deviation. N95 and N amplitudes were not significantly different ($p = 0.11$). Differences between P50 and P, amplitude and implicit time, and between N95 and N implicit time, were significant ($p < 0.001$); paired, two-tailed t-test.

Test/re-test reliability and Intra-session repeatability is essential for detecting subtle disease related changes in the signal over time. In order to test the ppERG test repeatability response waveforms were obtained from one subject on three different days, with re-tests done 5 and 19 months after the initial test (Figure 23A). Test-retest repeatability was very good; similar results were obtained in all six healthy subjects for which re-test responses were obtained (3-19 months between tests, $0.58 < r^2 < 0.98$). This degree of repeatability is encouraging for monitoring longitudinal changes in individuals. Reliability of the pERG response is also dependent on the quality of intra-session repeatability [Porciatti et al. 2004]. To test the intra-session repeatability and to assess ppERG reliability, three runs of ppERG responses were recorded from one subject in a single session. The results presented in Figure 23B show high intra-session repeatability [$0.97 < r^2 < 0.99$]. Each waveform is an average of 300 transitions recorded at a viewing distance of 30 cm, mean ON luminance of 1670 ph cd m^{-2} and 4.6 RPS reversal rate.

ppERG responses were recorded from one eye in seven normally-sighted subjects and both eyes in four normally sighted subjects. Correlation between the pairs of eyes was calculated in order to evaluate the potential for bias caused by the inclusion of responses from both eyes in one subject to the global average waveform (i.e. $n = 11$ vs $n = 15$)

The ppERG responses obtained from left and right eyes (OS and OD responses obtained simultaneously) of four different subjects are plotted in Figure 23C. The correlation between pairs of eyes (OS vs. OD) was high, $r^2 = 0.93 + 0.05$ (mean + one standard deviation).

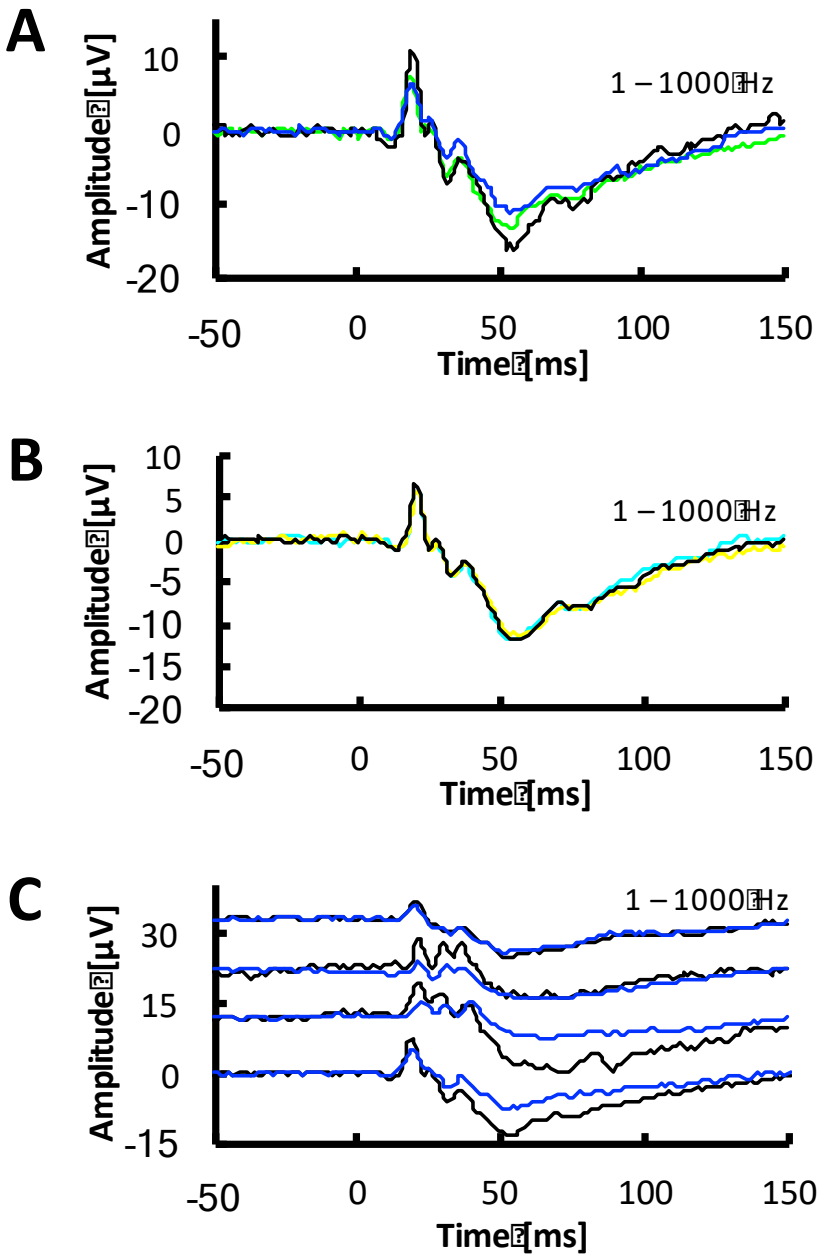

Figure 23. Test-retest variability, and left-right eye correlation. (A) ppERG response waveforms recorded in one subject on three different days. Responses plotted in blue and green recorded 5 and 19 months, respectively, after the response plotted in black. Responses obtained at a viewing distance of 30 cm and mean ON-luminance of 1670 ph cd m^{-2}. (B) Plots ppERG responses from three consecutive runs (green: run 1, yellow: run 2, black: run3). Each run is an average of 300 transitions. (C)Responses obtained from right (black) and left (blue) eyes of four subjects, recorded simultaneously, stimulus conditions as in panel A. Waveforms for three subjects offset vertically for clarity.

A main goal of this work was to identify a ppERG protocol that yielded in a robust repeatable response, and that was complementary to conventional pERG protocols. This was accomplished by exploring the parameter space available with the ppERG system. Parameters of the novel ppERG stimulus that could be varied were the mean ON-luminance, reversal rate, field subtended, and check size (confounded with viewing distance, as described below). These parameters were varied in a systematic way and the effects on the ppERG response components were analyzed.

ppERG vs. luminance. Response waveforms obtained at a fixed viewing distance (55 cm) and reversal rate (4.6 RPS), and four different values for mean ON-luminance, are plotted in Figure 24. Panel A plots the mean waveforms obtained from six normally-sighted subjects; panels B and C plot the isolated low-frequency and high-frequency components, respectively. The effect of increasing luminance is most evident in the leading edge of the P component (likely pre-axonal contribution), and in the evolution of the high-frequency components (F1-F3), with the strongest dependence shown by F1. These dependencies are summarized in panel D of Figure 24. Implicit time for the P component became shorter at higher luminances, but the other components showed little dependence, as shown in panel E of Figure 24.

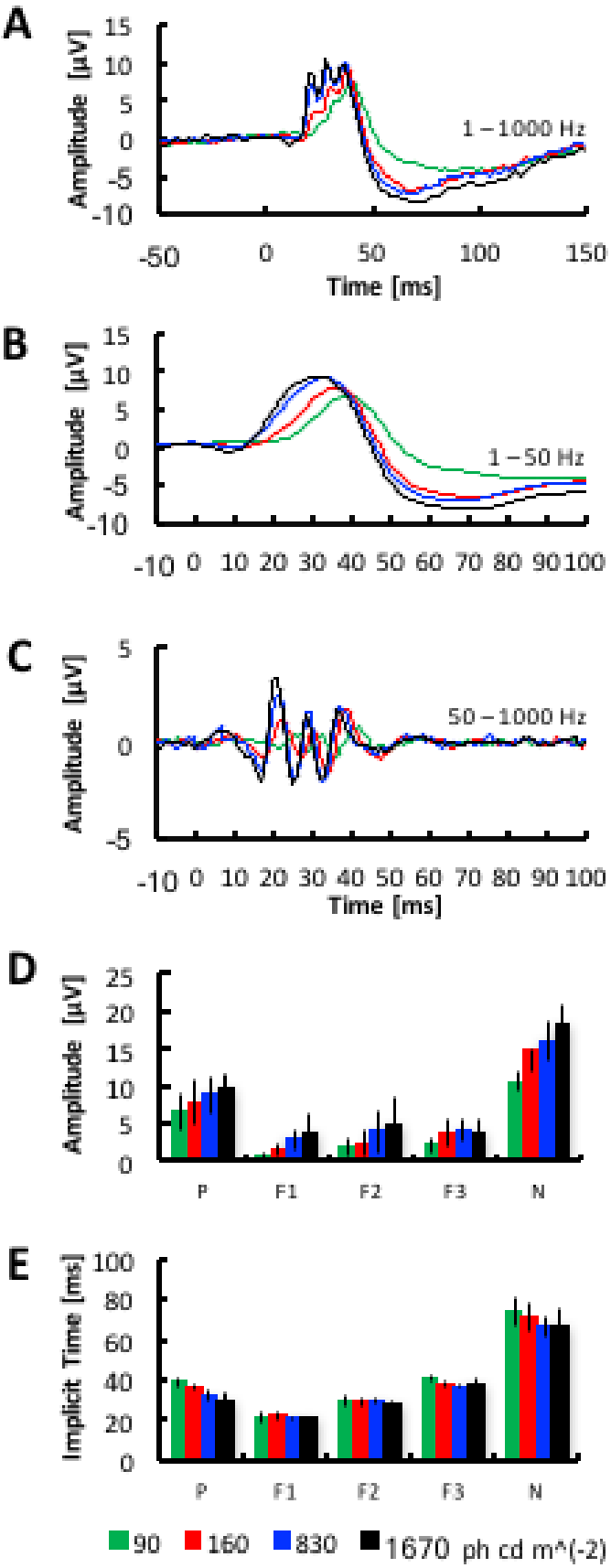

Figure 24. Effect of luminance on ppERG responses. Each waveform is the average response from six subjects; viewing distance fixed at 55 cm, reversal rate of 4.6 RPS. (A) Responses obtained when mean ON-luminance = 90 (green), 160 (red), 830 (blue) and 1670 (black) ph cd m^{-2}. (B) Isolated low-frequency components of the waveforms show in panel A. (C) Isolated high-frequency components of the waveforms shown in panel A. (D) Response feature amplitudes for each luminance; bar heights plot mean, error bars plot $\pm$ one standard deviation. (E) Response feature implicit times for each luminance; bar heights plot mean, error bars plot $\pm$ one standard deviation

ppERG vs. reversal rate. Response waveforms at a fixed viewing distance (30 cm) and mean ON-luminance (1670 ph cd m^{-2}) were recorded at three reversal rates (2.3, 4.6 and 9.2 reversals per second, RPS); these responses are plotted in Figure 25. Panel A plots the mean waveforms obtained from six normally-sighted subjects; panels B and C plot the isolated low-frequency and high-frequency components, respectively. As reversal rate increased, P amplitude increased slightly, and N amplitude decreased significantly, -0.9 μV RPS^{-1} (linear regression, $r^2 = 0.91$); the fall-off of N amplitude is steeper than has been observed for N95 in conventional pERG (-0.3 μV RPS^{-1} over the range 2-7 RPS) [Berninger & Schuurmans., 1985]. High-frequency ppERG response components were less sensitive to reversal rate over the range investigated; the greatest fall-off was seen for F2 between 4.6 and 9.2 RPS. Implicit time of the ppERG components showed little dependence on the change in reversal rate This is can be seen in Figure 25E.

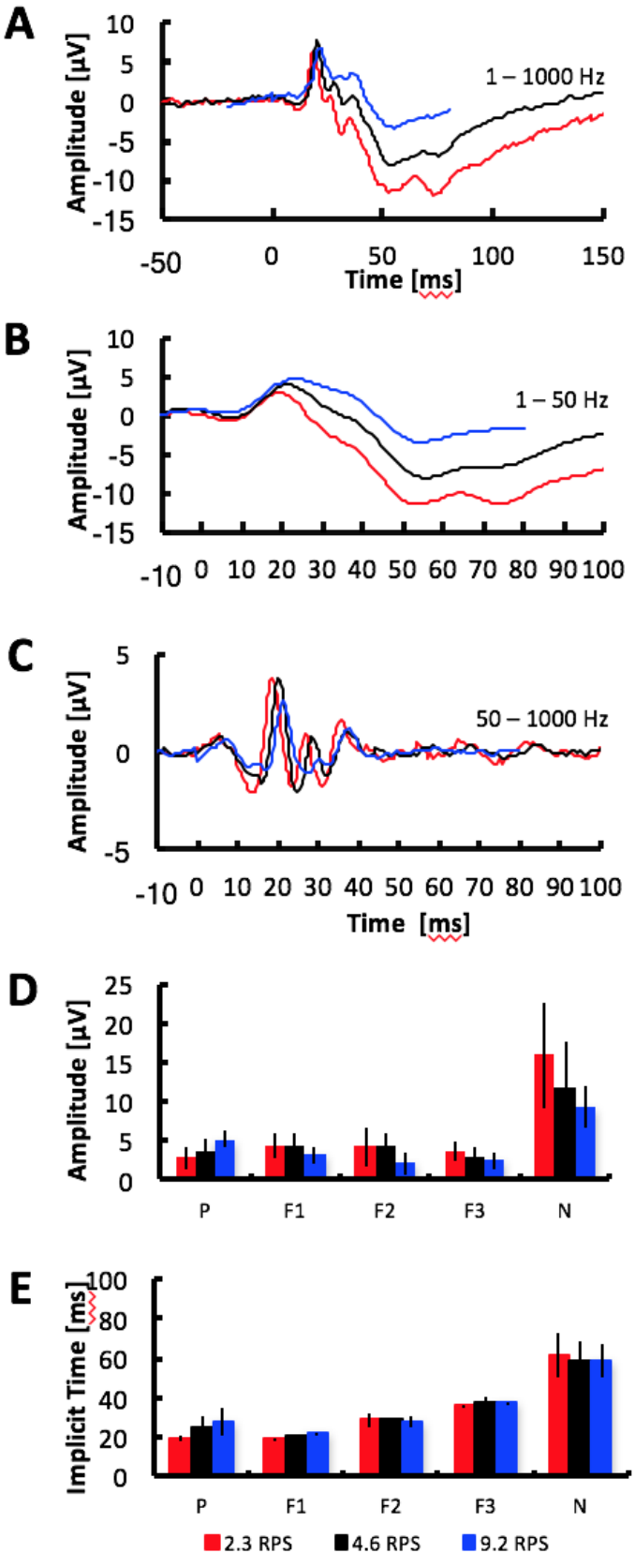

Figure 25. Effect of reversal rate on ppERG responses. Each waveform is the average response from six subjects; viewing distance of 30 cm, mean ON-luminance of 1670 ph cd m^{-2}. (A) Responses obtained for reversal rates of 2.3 (red), 4.6 (black) and 9.2 (blue) reversals per second (RPS). (B) Isolated low-frequency components of the waveforms show in panel A. (C) Isolated high-frequency components of the waveforms shown in panel A. (D) Response feature amplitudes for each reversal rate; bar heights plot mean, error bars plot $\pm$ one standard deviation. (E) Response feature implicit times for each reversal rate; bar heights plot mean, error bars plot $\pm$ one standard deviation.

ppERG vs. field subtended. Response waveforms obtained at a fixed mean ON-luminance (1670 ph cd m^{-2}) and reversal rate (4.6 RPS), and three different viewing distances, are plotted in Figure 26. Recall that viewing distance influences both the field subtended by the stimulus and apparent check size (Table 2, Figure 15C). Panel A of Figure 26 plots the mean waveforms obtained from six normally-sighted subjects; panels B and C plot the isolated low-frequency and high-frequency components, respectively. As the field subtended by the stimulus becomes more central (with increasing viewing distance), the amplitude of P increases, but the high-frequency components are nearly unchanged. These trends are summarized in panel D of Figure 26. The N component peaks at approximately the same negative value for each distance (panel B), however the amplitude of N, which is measured from the peak of P, also increases with increasing viewing distance (panel D). Implicit times for P and N are shortest at the closest viewing distance, where the stimulus is presented farthest in the periphery (panel E).

To isolate the effect of eccentricity only, responses were recorded with a 4x4 check pattern (check size 10^{o}, 4.6 RPS) presented in the temporal field (standard fixation target, remaining checks were dark) and central field, (subjects turned their head and fixated at the center of the 4x4 pattern, viewing distance kept constant at 30 cm). The results are shown in Figure 27 for mean ON-luminances of 90 and 1670 ph cd m^{-2}. Waveforms in Panels A and C plot the average response for six subjects; green traces plot pERG responses from large 10^{o} checks (90 ph cd m^{-2}, 30 cm viewing distance) for comparison. At both luminances, the positive contribution to the waveform is significantly reduced with peripheral stimulation (red traces), allowing the N component to reach greater negative values (at earlier implicit times) with respect to baseline. This trend is more clearly seen in

Figure 26B which plots the isolated low frequency components, the trailing edge of P (defined by a sum of positive and negative contributions) is most sensitive to eccentricity of the pattern. This suggests that with peripheral stimulation the N component is less corrupted by pre-axonal corneal-positive contributions, and is more purely a reflection of axonal ganglion cell activity.

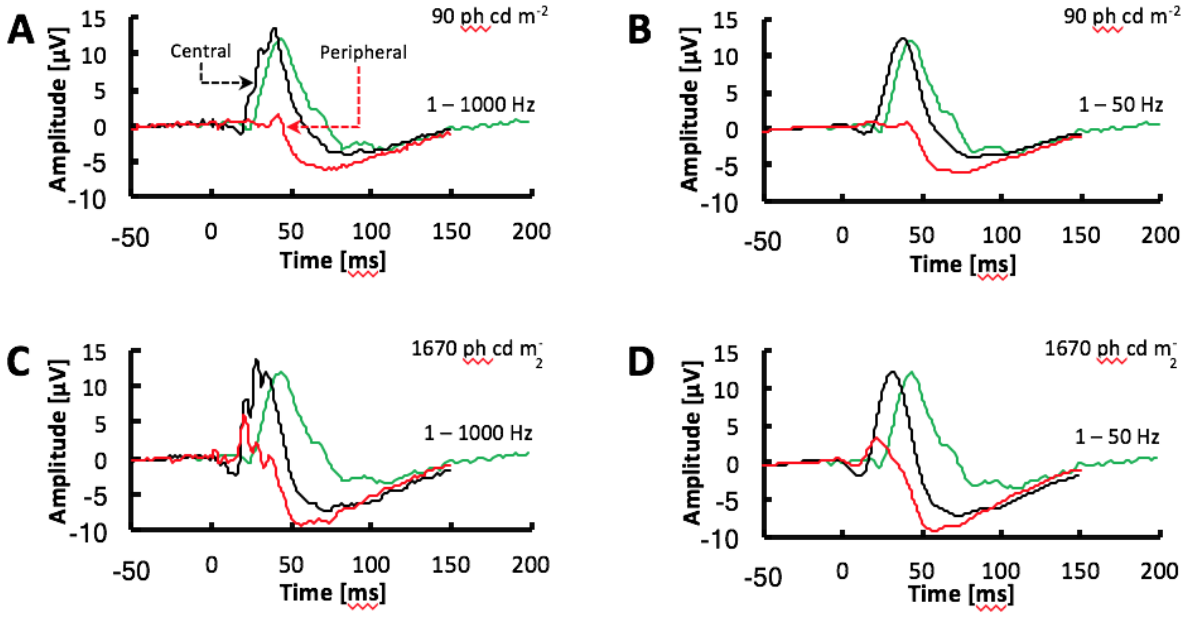

Figure 27. Effect of field subtended by a high-luminance pattern stimulus. A 4x4 check pattern was presented to the central or temporal field at a fixed viewing distance of 30 cm, by altering direction of gaze. Each waveform is the average response from six subjects. (A) ppERG response waveforms obtained with mean ON-luminance of 90 ph cd m^{-2}; central field response (black), temporal field response (red). (B) Isolated low-frequency components of the waveforms shown in A, colors as in A. (C) ppERG response waveforms obtained with mean ON-luminance of 1670 ph cd m^{-2}; colors as in A. (D) Isolated low-frequency components of the waveforms shown in C, colors as in A. In all panels, green trace plots response waveform from the pERG system with large 10° checks (90 ph cd m^{-2}, 30 cm viewing distance) for comparison.

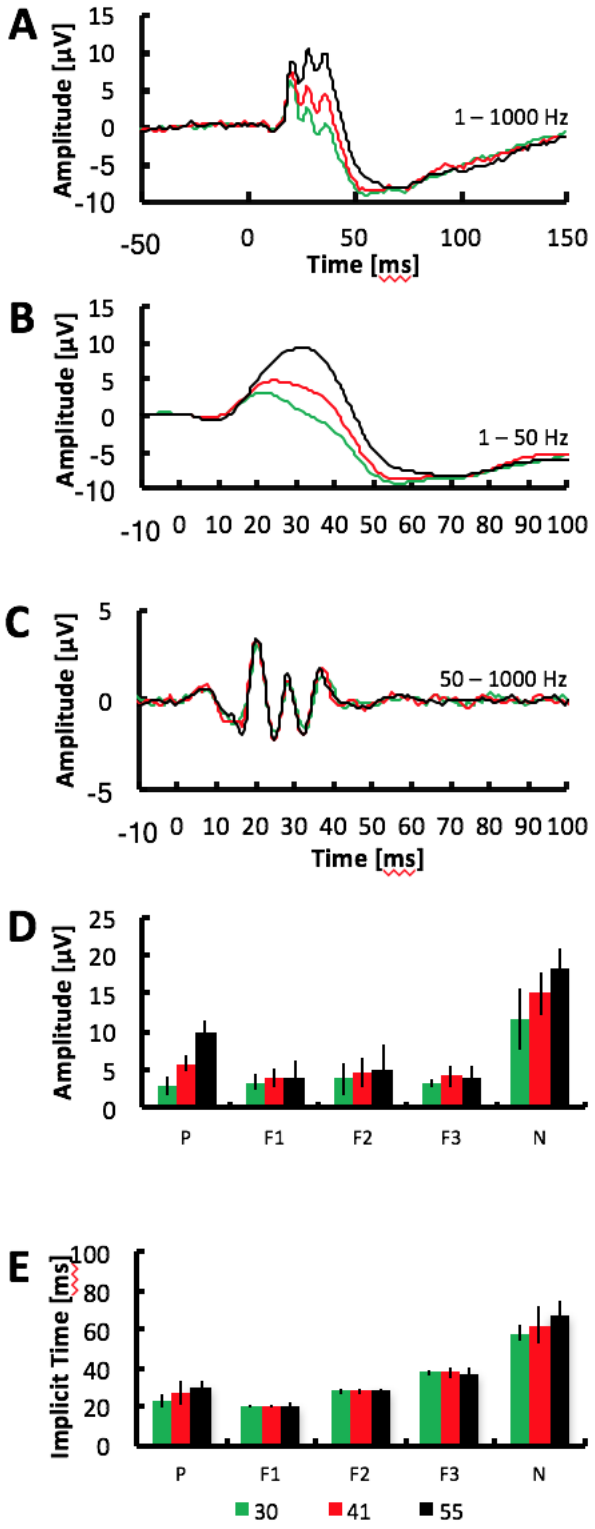

Figure 26. Effect of viewing distance on ppERG responses. Each waveform is the average response from six subjects; mean ON-luminance fixed at 1670 ph cd m^{-2}, reversal rate of 4.6 RPS. (A) Responses obtained when viewing distance = 30 cm (green), 41 cm (red), or 55 cm (black). (B) Isolated low-frequency components of the waveforms show in panel A. (C) Isolated high-frequency components of the waveforms shown in panel A. (D) Response feature amplitudes for each viewing distance; bar heights plot mean, error bars plot $\pm$ one standard deviation. (E) Response feature implicit times for each viewing distance; bar heights plot mean, error bars plot $\pm$ one standard deviation.

Local Pattern Stimulation. Disease-related dysfunction in the retina is often sectoral rather than diffuse or global; for this reason, we evaluated local responses from peripheral retina in four field sectors. Average waveforms obtained from superior, nasal, inferior and temporal quadrants of peripheral retina in nine right eyes are plotted in Figure 28A-C. For these tests, the stimulus source was moved to the nearest distance at which the entire stimulus was visible for all subjects (no part blocked by the bridge of the nose), which was 41 cm. As seen in panel D of Figure 28, amplitude differences between sector responses are dramatic, with the largest P and N amplitudes from the temporal field, and the smallest from the nasal field, qualitatively consistent with temporal-nasal differences in ganglion cell density. Sectoral responses allow for calculation of intra-subject ratios, which can reduce the influence of variance in absolute amplitude differences between subjects, and possibly highlight sectoral damage due to disease. The coefficient of variation (standard deviation divided by mean, CV) for N amplitudes was 49% (average value across the four sectors, central bars of panel D). However, the CV for ratios of sector response amplitudes (where S', N', I', and T' represent the N amplitude of each sector divided by the sum of N amplitudes of the remaining three sectors) was reduced to 27%. This reduced inter-subject variability demonstrates the narrowing of normative ranges when using intra-subject ratio values.

Modifying stimulus sectors to reflect the path taken by the retinal nerve fiber to the peripheral retina (Figure 16C-D) gave rise to three field sectors: temporal, superior-nasal and inferior-nasal. Figure 29 plots the mean waveforms across five normally sighted subjects for each of the three sectors and the all-ON configuration. Responses were recorded at a distance of 41 cm, mean ON-luminance of 1670 ph cd m^{-2} and 4.6 RPS

reversal rate. Responses from the temporal field (nasal retina) had the largest P and N amplitude consistent with the results presented above (Figure 28). Responses from the superior-nasal field (inferior-temporal retina) had reduced P and N amplitudes. This may be due the decrease in ganglion cell densities in the peripheral temporal and inferior retinal regions [Curcio & Allen., 1990].

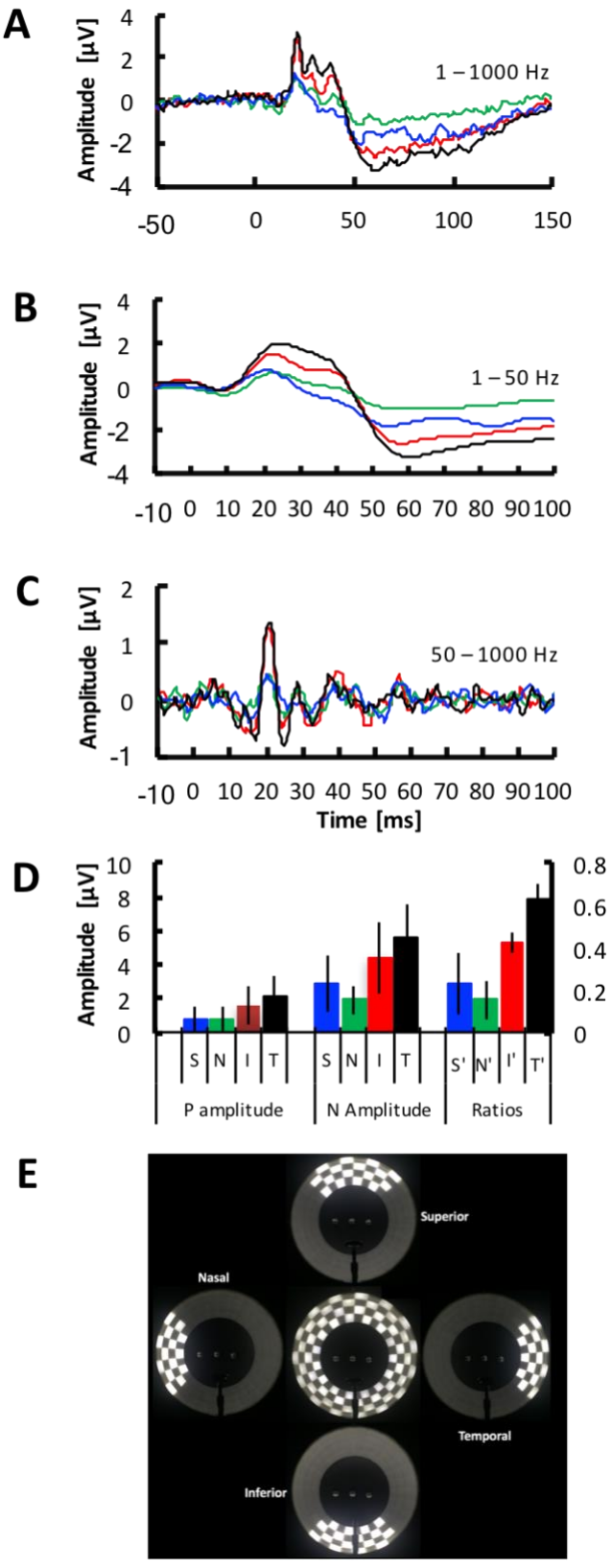

Figure 28. Pattern ERG responses evoked from four sectors of peripheral retina. The 30 columns of the stimulus were divided into four sectoral stimuli to probe the superior (S), nasal (N) inferior (I) and temporal (T) fields. All tests done at a viewing distance of 41 cm, luminance of 1670 ph cd m^{-2}, and reversal rate of 4.6 RPS. (A) Mean waveforms from nine right eyes evoked by presenting the stimulus to each of the four sectors: superior (blue), nasal (green), inferior (red), and temporal (black). (B) Isolated low-frequency components of the waveforms shown in panel A. (C) Isolated high-frequency components of the waveforms shown in panel A. (D) Mean amplitudes of the P and N components recorded in each sector, error bars plot $\pm$ one standard deviation. Right group of bars plot the ratios of N amplitudes for each sector (see text); error bars plot $\pm$ one standard deviation. (E) Photographs of the sector stimuli, with the "all on" configuration shown in center; field designations for a right eye.

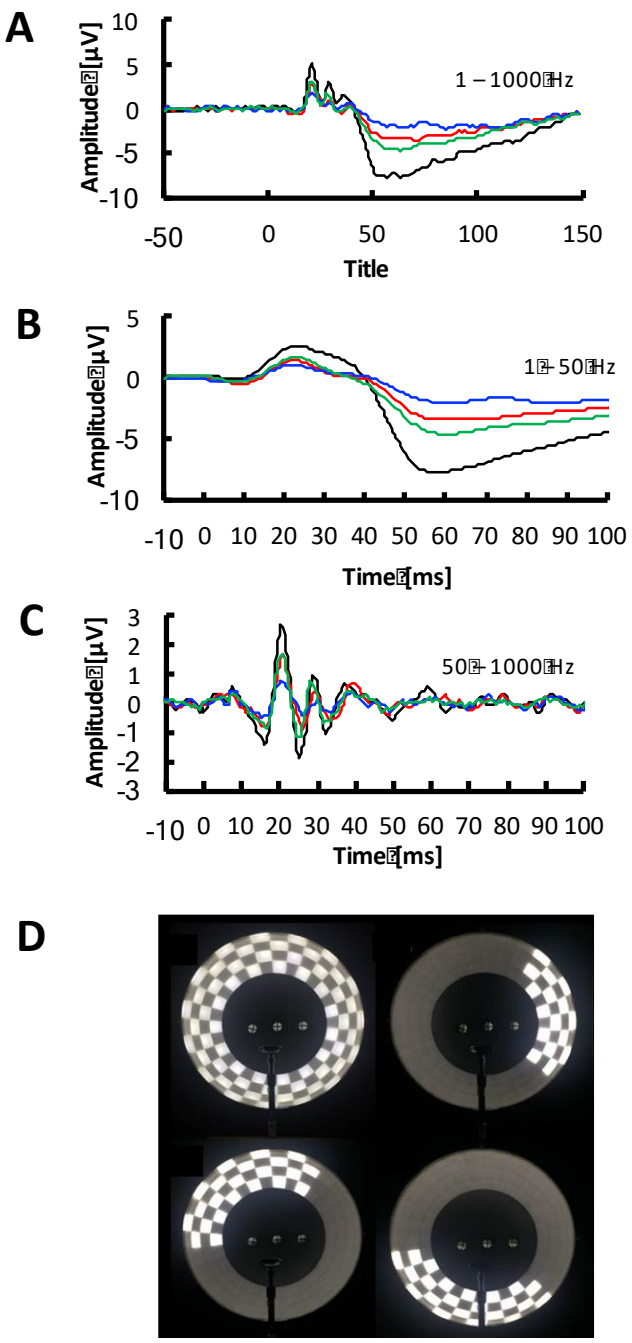

Figure 29. Pattern ERG responses evoked from three sectors of peripheral retina. The 30 columns of the stimulus were divided into three sectoral stimuli to probe the superior-nasal (S-N) inferior-nasal (I-N) and temporal (T) fields. Recording from each sector was done at a viewing distance of 41 cm, luminance of 1670 ph cd m^{-2}, and reversal rate of 4.6 RPS. (A) Mean waveforms from five right eyes evoked by presenting the each of the three sectors: superior-nasal (blue), inferior-nasal (red), and temporal (black) consecutively. (B) Isolated low-frequency components of the waveforms shown in panel A. (C) Isolated high-frequency components of the waveforms shown in panel A. (E) Photographs of the sector stimuli, with the all ON shown on the upper left corner followed by temporal field (upper right), inferior-nasal field (bottom right) and superior-nasal field (bottom left) for a right eye.

With and without Acuity correction Conventional pERG response waveforms show an evident reduction in amplitudes with the loss of visual acuity [Arden & Berninger., 1988; Arden et al., 1984], for this reason subjects are required to wear the appropriate optical correction while undergoing the test. To evaluate the effect of abnormal visual acuity on the ppERG waveforms, responses were recorded from one subject with and without prescription eye glasses. The subject sat through 12 recording protocols comprising of three viewing distances (30 cm, 41 cm and 55 cm) and four mean ON-luminances (90 ph cd m^{-2}, 160 ph cd m^{-2}, 830 ph cd m^{-2} and 1670 ph cd m-2) recorded at a reversal rate of 4.6 RPS. All responses were recorded on the same day. Figure 30 plots a subset of recorded responses. Comparison of ppERG response with and without acuity correction showed minimal differences in amplitudes except at a viewing distance of 30 cm (Figure 30A). At this distance, responses recorded without correction (black trace) were relatively larger than those recorded with corrective eye glasses (red trace). This may be because, at a viewing distance of 30 cm, the stimulus extends to the limits of the visual field (far periphery, Specific Aim 1, field subtended figure) resulting in some part of the pattern being blocked by the presence of the eye glass frames. Increasing the viewing distance results in the pattern not being hindered by the eye glass frames. This eliminates the reduction in ppERG amplitude when responses are recorded with corrective eye glasses (Figure 30B-C), suggesting that the ppERG response may not be strongly dependent on refractive error.

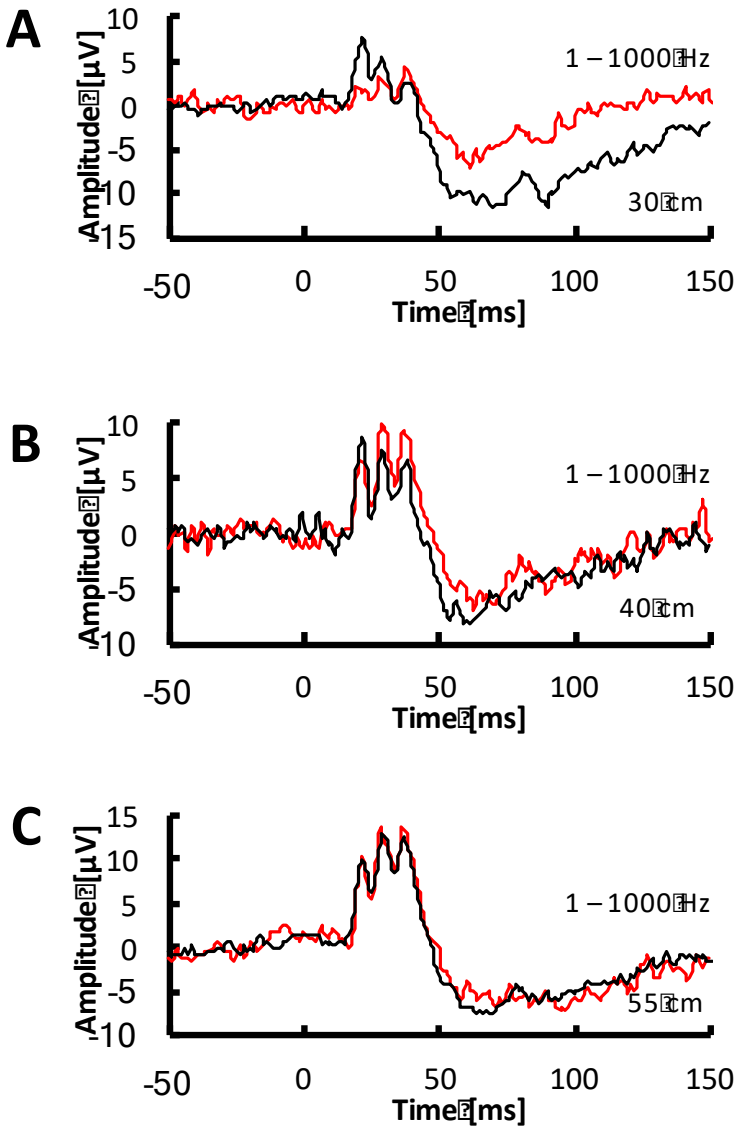

Figure 30. Effect of acuity correction on ppERG response waveforms. ppERG responses were recorded from one subject with and without prescription eye glasses. Subject sat through multiple protocols. Results from a subset of recording protocols are presented here. Figures A-C show ppERG response waveforms recorded at three different viewing distances with a mean ON-luminance of 1670 ph cd m^{-2} at each distance. In all cases, black traces represent responses recorded with acuity correction, red traces represent responses recorded without acuity correction. (A) ppERG response recorded with the subject seated at a viewing distance of 30 cm from the central fixation point. (B) ppERG responses recorded when the viewing distance is increased to 41 cm. (C) ppERG responses recorded when the viewing distance is increased to 55 cm.

Effect of NMDA on the high luminance pERG response. To confirm the cellular origin of response evoked by the large check, high luminance stimulus source, pharmacological dissection experiments in a Long Evans rat was done. Figure 31 presents results obtained in response to 15 flashes before and after the injection of NMDA. The black trace represents the pre-injection flash ERG recorded after 5 minutes of dark adaptation. The red trace represents post-injection flash ERG recorded 20 minutes after the administration of NMDA. The increase in the b-wave amplitude and elimination of the oscillatory potentials confirmed the effect of the drug. Following the effect of NMDA, high luminance pERG responses were recorded from a 4x4 central pattern presented to the left eye and right eye (control). Figure 32B shows the effect of NMDA on the high luminance pattern ERG. The positive component of the response as seen in the red trace, becomes larger in amplitude as a result of the negative ganglion cell component being blocked by NMDA. Black trance shows the pERG response before NMDA injection. The right eye received PBS as a sham control, Figure 32A presents results obtained before (black trace) and after (red trace) the injection of saline. All pERG responses are an average of twenty 25-second epochs, yielding 2300 pattern reversals.

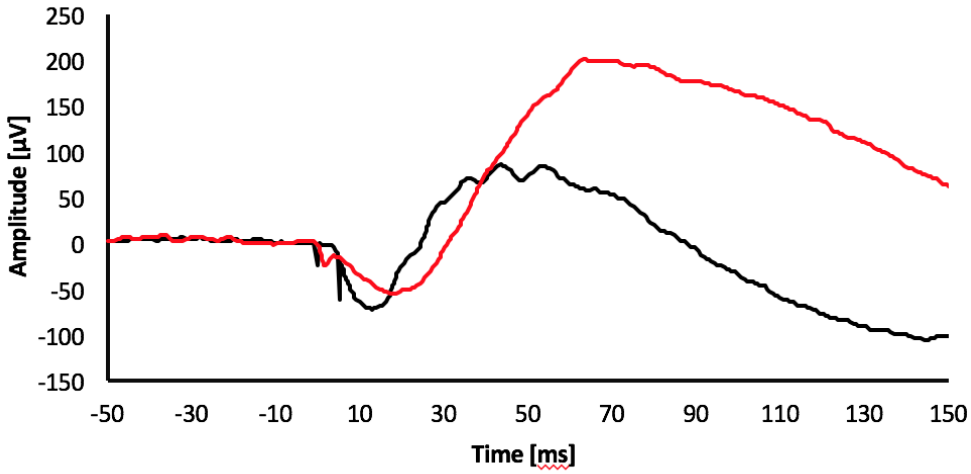

Figure 31. Pharmacological dissection of the flash ERG; pre and post NMDA. Black trace: flash response before the injection of NMDA recorded after 5 ms of dark adaptation, Red trace: The flash response 20 min after injection of NMDA. Response is an average of 15 flashes recorded with one minute intervals between each flash.

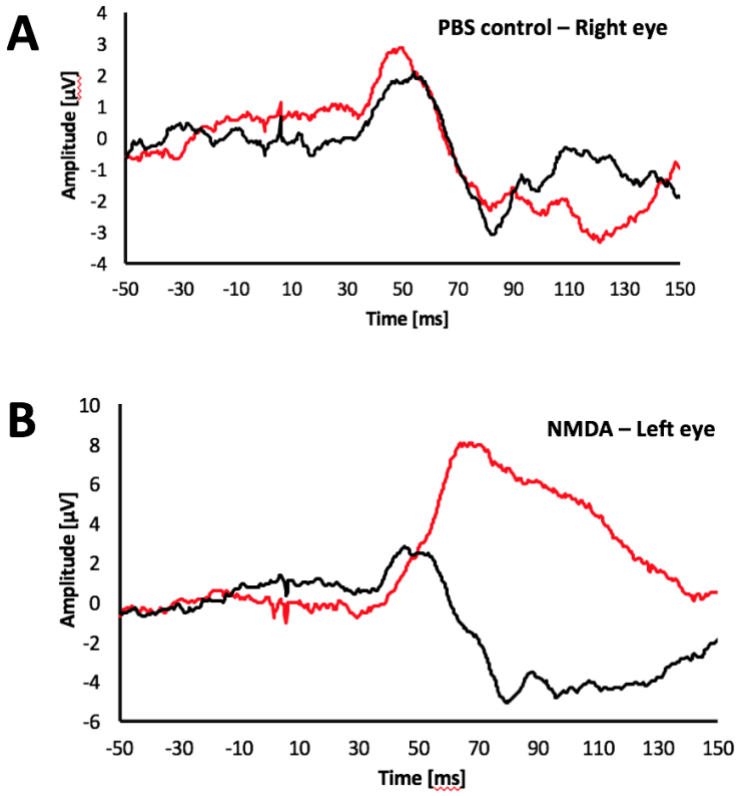

Figure 32. Effect of NMDA on the high luminance pERG response. (A) High luminance pattern ERG responses recorded from the right (control) eye. Black trace: The response before the intravitreal injection of PBS while red trace shows the response after the injection of PBS. (B) High luminance pattern ERG responses recorded from the left eye before (black) and after (red) intravitreal injection of NMDA.

Specific Aim 2 Discussion.

Functional changes in the far-peripheral retina are relatively under-studied, in large part because of a lack of suitable tests. Full-field flash ERG probes the entire retina, however local dysfunction in the periphery can have a relatively small effect on the response, resulting in amplitude changes that fall within the normal distribution. Goldmann perimetry can map the boundaries of the visual field, but is an indirect measure and suffers

from poor repeatability. A dearth of objective tools for studying the peripheral retina, along with evidence of peripheral retina functional loss in early glaucoma, motivated the design of a pattern ERG stimulus source that would enable objective measurement of ganglion cell function beyond 20 degrees of visual angle. This novel system is now available to study inner-retina functional changes in the peripheral retina, where ganglion cell diversity, density, morphology, orientation and connectivity differ substantially from central retina.

The two novel capabilities of the ppERG stimulus employed here are peripheral-field stimulation and high-luminance patterns, with mean ON-luminance ~15X that achievable with standard pERG computer monitor sources. With increasing eccentricity of the stimulus field, the positive contribution to the response waveform is reduced (Figures. 13, 14), resulting in a late negative component (N) that is possibly a more pure reflection of axonal ganglion cell activity due to the lack of opposing corneal-positive contributions. With increasing luminance, the ppERG response components become larger in amplitude (Figure 24), including the evolution of high-frequency components not seen under ISCEV-recommended recording conditions. A comparison between ppERG high-frequency components and flash-ERG oscillatory potentials is muddied by the very different stimuli (reversing pattern with constant mean-ON luminance vs. full-field flash on a dark background), but the similarities in the two responses should be considered. The number of prominent OP peaks, and the time of the first OP peak, vary with flash strength, but the frequency (i.e. time between peaks) is relatively preserved over a wide range of stimulus strengths. Similarly, time between peaks of the high-frequency ppERG components was not sensitive to pattern luminance, reversal rate or field subtended. A possible origin of the

high frequency components is a local on-response arising from the centers of the relatively large checks. This hypothesis is opposed by the observation that the F1-F3 amplitudes were essentially unchanged when apparent check area was reduced by 75% (Figure 26C). The absence of an ON response is also confirmed by comparing the dissimilarities between the ppERG high-frequency components to the peripheral ON response oscillatory potentials (Figure 21C). Presence of an ON response would result in similar waveforms that differ only in amplitude. However, the strong dependence of F1 amplitude on pattern luminance (Figure 24C, D) is reminiscent of the dependence of the first major OP on flash strength. It will be of interest to study the ppERG response in diabetic retinopathy patients with reduced OP amplitudes.

One consideration for ppERG testing is the effect of low acuity in the peripheral field. Contrary to ISCEV recommendations, no corrective lenses were worn during the ppERG test, regardless of prescription (with the exception of one contact lens wearer). Correction for refractive error in the far periphery would be challenging as the error varies with eccentricity. Fortunately, comparison of responses with and without correction showed minimal differences in response amplitudes (Figure 30), suggesting that the ppERG response is not strongly dependent on refractive error. This may be due in part to the relatively large check sizes used (5-10 degrees), and deserves further study. The optimum check size for detecting glaucoma with central patterns is approximately one degree, and falls off significantly with larger checks [Bach et al. 1988]; the optimal check size for peripheral patterns would be expected to be somewhat larger due to the larger average receptive fields for peripheral ganglion cells, and should be determined systematically.

An important potential advantage of the ppERG stimulus source used here is the ability to probe field sectors of the peripheral retina (Figure. 16-17). Probing local areas of retinal function has the potential to increase the sensitivity of any test, by increasing the effect size compared to healthy for localized dysfunction, and by narrowing normal ranges through evaluation of relative values within an eye. Internally-referenced measures have been used to increase the sensitivity of pERG [Bach & Sereining., 2013], perimetry, OCT, and flash ERG, to sectoral functional and structural changes in glaucoma. Using an internally-referenced measure of ppERG N amplitude yielded a coefficient of variation that was approximately one half of that seen with absolute N amplitudes; this approach should be explored in glaucoma where structural and functional changes are known to be sectoral.

Part IV: Specific Aim 3

Assessment of ppERG test sensitivity

Specific Aim 3

Assessment of ppERG test sensitivity. ppERG and pERG responses will be recorded, and evaluated for relative sensitivity to glaucomatous damage in a small population of glaucoma patients (n = 10).

Specific Aim 3 Motivation. Glaucoma is defined to the progressive loss of retinal ganglion cell (RGC) function eventual loss of RGC death. Recent insights into the pathophysiology of glaucoma reveal degenerative events along the entire length of RGC axonal projections from the retina to the brain [Calkins 2012; Davis et al. 2016]. Earliest dysfunction in ganglion cells can be due to a host of changes, such as reductions in anterograde and retrograde axonal transport [Crish et al., 2010; Dengler-Crish et al., 2014], impaired neurotransmitter release [Smith et al., 2016], loss of synaptic connectivity, and changes in dendritic architecture affected by molecular stressors [Morquette & Di Polo, 2008; Morgan 2012; Calkins & Horner, 2012], all of which eventually lead to the structural degeneration of RGC substrate and ultimately result in cell death.

The considerable time lag between the onset of functional loss and the clinically detectable structural degeneration makes it hard to capture the onset of the disease. Though pERG reflects ganglion cell function and can possibly detect the functional loss that begins in axonal regions closer to the brain, it is limited to the central 30 degrees of the visual field. This limitation does not allow it to access any peripheral and/or diffused glaucomatous degeneration [Calkins & Horner, 2012, Bach et al. 1992, Fitzgibbon and Taylor, 1996]. Detecting peripheral or diffused dysfunction prior to the structural changes could help

identify disease onset and provide a therapeutic opportunity to prevent irreversible vision loss. To achieve this, a novel high luminance peripheral pattern ERG stimulus source was developed (Specific Aim 1). A motivation for developing the ppERG stimulus source was to evaluate sensitivity to glaucomatous damage of the ppERG test (a measure of peripheral – field RGC function) compared to conventional central-field pERG. The ppERG system (Specific Aim 1) was able to produce a robust and repeatable responses in normally-sighted subjects (Specific Aim 2).

Specific Aim 3 was motivated by two main goals. The first goal was to evaluate the sensitivity of the newly developed system to detect peripheral ganglion cell dysfunction. Proof of concept was achieved by recording ppERG responses from a small cohort of glaucoma patients and comparing them with the normally-sighted responses.

The second goal was to choose a best protocol from the ppERG stimulus parameter space available. Although the pERG is an objective test to assess retinal function, it is highly underutilized because of the difficulty to perform the test. To make the ppERG test convenient for the operator and patient, an optimum protocol that will give maximum information within a short period of time is required.

Specific Aim 3 Methods

Subjects. Eleven glaucoma patients and one glaucoma suspect were recruited from the Glaucoma Service and the General Eye Clinic at the University of Illinois at Chicago (UIC). ppERG responses were also recorded from one type-2 diabetes mellitus (DM) patient and one idiopathic intracranial hypertension (IIH) patient recruited from the University of Illinois Hospital and Health Sciences System and the Neuro-ophthalmology Clinic at UIC,

respectively. Informed consent was obtained from all subjects before participation. Procedures adhered to the tenets of the Declaration of Helsinki, and the protocol was approved by an Institutional Review Board at the University of Illinois at Chicago. All glaucoma patients were selected based on retinal nerve fiber layer (RNFL) thinning as examined in Heidelberg SD – OCT scans (Heidelberg Engineering, Germany) and/or abnormal mean deviation values ("outside normal limits") obtained from the 24-2 SITA-standard strategy (Humphrey Field Analyzer, Carl-Zeiss Meditec, Dublin, CA, USA). Patient age, RNFL thickness and mean deviation values for all patients are summarized in Table 3.

A

Healthy - ID	Age	MD	% RNFL
H 1	32	-0.74	92
H 2	49	-0.59	93
H 3	26	-2.06	96
H 4	27	-0.82	88
H 5	38	0.25	96
H 6	22	NA	101
H 7	58	0.33	NA
H 8	65	0.54	NA
H 9	48	-2.74	NA
H 10	62	NA	89.58
H 11	40	NA	77.32
Average	42.45	-0.8	91.61
St-Dev	15.06	1.1	6.65

B

Patient ID	Age (years)	MD	% RNFL
GP 1	53	-4.05	71.57
GP 2	74	-3.89	95.51
GP 3	72	0.94	70.53
GP 4	53	-7.02	NA
GP 5	41	-4.03	76.68
GP 6	59	-4.78	68.39
GP 7	73	-2.63	90.46
GP9	73	-6.32	106.31
GP10	38	-5.56	90.72
GP11	58	NA	50
GP 12	41	-9.07	69.07
GP 13	67	-1.09	NA
Average	58.5		
St-Dev	13.51		

Table 3. Age (in years), mean deviation and percent retinal nerve fiber layer thickness values for normally-sighted subjects (n = 11)(A) and glaucoma patients (n = 12)(B)

ppERG Recording: Exploration of stimulus parameter space in terms of mean ON-luminance, field subtended, and reversal rate in normally sighted subjects (Specific Aim 2) resulted in the shortlisting of four recording protocols (30 cm, 1670 ph cd m^{-2}; 55 cm, 1670 ph cd m^{-2}; 30 cm, 90 ph cd m^{-2}; 55 cm, 90 ph cd m^{-2}) for the patients (protocol ranking). A viewing distance of 55 cm (check size: 5^{o}) and a mean ON-luminance of 90 ph cd m^{-2} was chosen to conform to the ISCEV recommended standards. For the ppERG stimulus to probe the far peripheral retina with a high luminance pattern, a viewing distance of 30 cm (check size: 10^{o}) and a mean ON-luminance of 1670 ph cd m^{-2} was chosen (Specific Aim 2, Figure 15C). Responses were sequentially recorded from both luminances at each distance. For all protocols, reversal rate was set at 4.6 RPS. Seven patients sat through all four protocols within a single session. Five patients, who participated late in the study, underwent only one protocol (all-ON, 30 cm, 1670 ph cd m^{-2}). Conventional pERG responses following ISCEV recommended standards were recorded on the same day. A subset of patients (n = 3) also underwent the three-sector local pattern stimulation protocol. Recording procedures (electrode placement, fixation and data acquisition) were constant throughout all subjects (normally-sighted subjects and patients, Specific Aim 2, ppERG and pERG recording and local pattern stimulation).

ppERG Test sensitivity.

Cluster analysis: To compare pERG and ppERG responses from glaucomatous and healthy eyes, cluster analysis was used. Amplitudes and implicit times for P, N, F1, F2, F3 response components were obtained by isolating the novel high-frequency components from the low-frequency components (ppERG response analysis, Specific Aim 2, Figure 17). Obtaining the amplitude and implicit time for each of the five peaks (P, N, F1, F2, F3)

resulted in ten feature values that described the ppERG response waveform. Each feature was taken as an axis in a ten-dimensional space (10-D). The mean location of normally-sighted subjects was determined, and then the ten-dimensional Euclidean distance between this mean and each of the subjects and glaucoma patients was determined. A similar analysis was performed for the six parameters obtained from the conventional pERG responses (6-D space that included the amplitudes and implicit times of N35, P50, N95). To understand the influence of just the high frequency components in glaucomatous eyes, the average distances from the healthy mean using the high-frequency component features were also analyzed for all glaucoma patients. To compare the sensitivities of both tests (pERG and ppERG) with equal number of features, a four-dimensional cluster analysis with just the amplitudes and implicit times of P and N for ppERG and P50 and N95 for pERG was performed

Linear regression analysis: To further compare the relative sensitivities of pERG and ppERG to structural changes, the correlation of these tests with retinal nerve fiber layer (RNFL) thickness was evaluated. As the patient and normal groups were not age-matched, each RNFL thickness was first converted to percent of normal for that person's age group; percent values for the global RNFL thickness were determined for all subjects (normally-sighted and patients). Linear regression analysis between the percentage RNFL thinning and Euclidean distance was performed.

ppERG protocol ranking. A main objective was to determine which ppERG protocol provided the best separation between patient responses and healthy eye responses, and which response features were most useful in achieving that separation. A mean difference (MDiff) value was calculated, as shown in Eq. 1. The MDiff value represents the average

distance of the five glaucoma patient responses (initially recruited into the study) from the mean healthy eye response, and reflects the "usefulness" of a given response feature, obtained with a given protocol, to identify a response as outside of the healthy eye distribution.

Eq. 1

$$MDiff_{Feature,Protocol} = \frac{\sum_{x=1}^{5}\left|(\bar{F}_{Healthy} - F_{Patient\ x})\right|}{5\sigma_{Healthy}}$$

In Equation 1, the difference between the healthy mean and each patient was calculated for a feature value F; these five differences were summed, and then normalized by dividing by five times the standard deviation (σ) of the healthy eye responses. The MDiff value was calculated for each feature, for each protocol, resulting in 40 values. To evaluate the "usefulness" of each protocol, the ten MDiff values for each protocol were summed. To evaluate the "usefulness" of each response feature in separating abnormal responses from normal, the MDiff values for each feature were summed across the four protocols.

Local Pattern Stimulation.

Glaucomatous ganglion cell dysfunction is said to progress sectorially following a retinotopic sequential pattern. Retinotopic mapping revealed that the retinal nerve fiber tracts of the temporal, superior and inferior-temporal optic nerve head project from the periphery, and are distinct from those that terminate within the macula. The fibers from the nasal optic nerve head project from the macula (Figure 36A-B) [Fitzgibbon & Taylor 1996]. As degradation is believed to usually start from the periphery and progress towards the central retina [Calkins & Horner 2012], early onset of dysfunction in these regions may be more prone to detection by probing local areas of retinal function. To test this, ppERG

responses were recorded from anatomically relevant field sectors (local pattern stimulation, Specific Aim 2) in three glaucoma patients.

For the field sectors to be associated with the retinotopic map, ppERG sectors were defined by turning only a portion of the stimulus ON (Specific Aim 2, Figure 16C). This could be achieved through pattern control (Specific Aim 1), where individual checks of the stimulus could be turned ON and OFF using a graphical user interface in LabVIEW. For the right eye, the temporal field (nasal retina) included columns 4 – 11, inferior-nasal field (superior-temporal retina) included columns 13 – 22 and the superior-nasal field (inferior-temporal retina) included columns 24 – 3. For the left eye, the temporal field (nasal retina) included columns 20 – 27, inferior-nasal field (superior-temporal retina) included columns 9 – 18 and the superior-nasal field (inferior-temporal retina) included columns 28 – 7. Columns 23, 12 (right eye) and columns 8, 19 (left eye) were not included in order to maintain equal number of ON and OFF checks within each sector. Responses from the field sectors were compared to the RNFL thinning (OCT scans) and visual field defects (HVF) for all three patients.

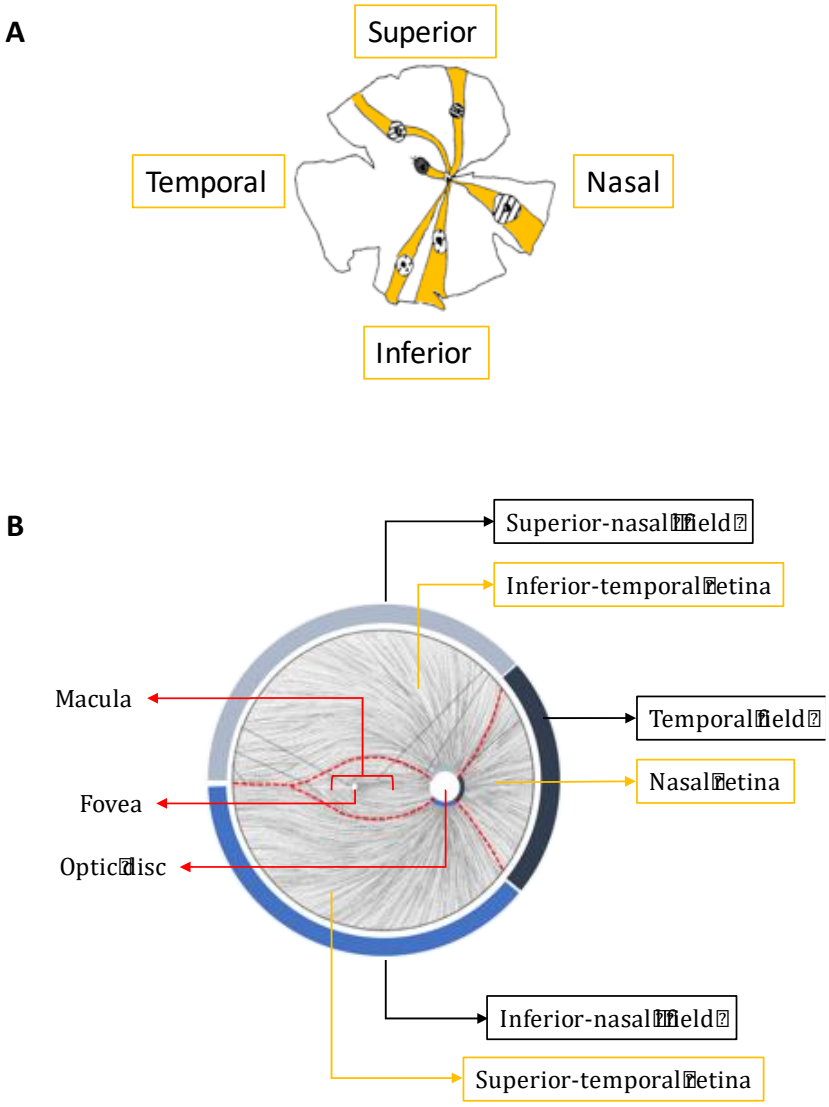

Figure 36. Topographic organization of the retinal ganglion cells. (A) Retinal nerve fiber tracts traced with the help of carbocyanine dyes [Fitizgibbon & Taylor., 1996;]. Tracing revealed the topographic organization of retinal ganglion cells. Foveal fibers were occupied regions of the temporal retina, while temporal fibers were directed towards the superior and inferior regions. The image was modified to clearly show the path of retinal fiber tracts to the superior and inferior-temporal regions and the nasal retina are highlighted in yellow). The organization of retinal ganglion cells into distinct sectors resulted in the idea of local pattern stimulation using defined portions (sectors) of the ppERG stimulus source. (B) Rendition of the retinal fiber tracts taken from [Oyster CW., 1999] The blue arcs (Superior-nasal, Inferior-nasal and Temporal) indicate the range of RNFL fiber tracts that relate ppERG Sector stimuli to circumpapillary OCT sectors (bounded by red dashed lines). The superior, inferior and temporal retinal fibers extend

Specific Aim 3 Results

ppERG Test sensitivity – Cluster analysis. To determine ppERG test sensitivity a cluster analysis using the feature values extracted from the response waveforms of both groups (glaucoma patients and normally-sighted subjects) was performed. Table 4A-B summarizes the amplitude and implicit time value of all feature components (ppERG and pERG) in both subject groups. The pERG values were extracted from responses recorded under standard ISCEV recommended conditions The ppERG values were extracted from responses recorded with the 30 cm, 1670 ph cd m^{-2} protocol. The N amplitude values varied across the patients for both test. As seen in the Figure 33, there was significant overlap of amplitude and implicit time values between patients and normally-sighted individuals for both tests; separation between normal eyes and glaucomatous eyes was best when based on amplitude for pERG, and when based on implicit time for ppERG. These observations suggest a diversity of functional deficits affecting positive and negative contributions to the pERG response within this small patient sample.

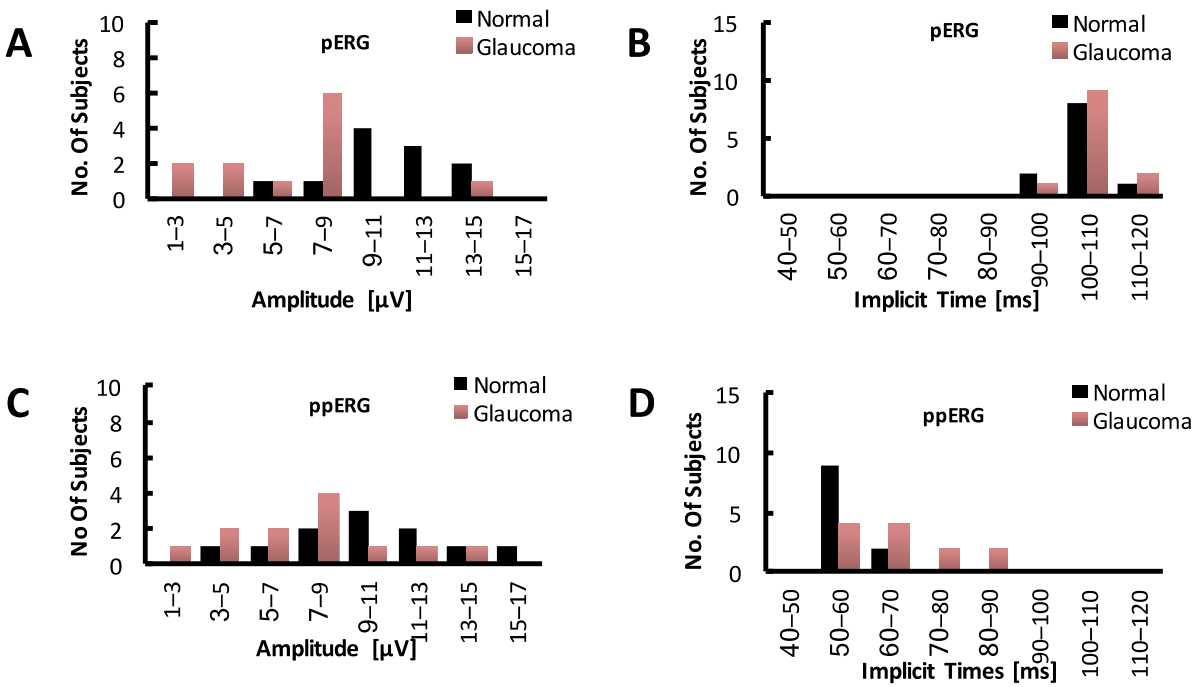

Figure 33. Distribution of pERG and ppERG negative response component amplitudes and implicit times in normal (n = 11) eyes and glaucomatous eyes (n = 12). All ppERG responses obtained with viewing distance of 30 cm and mean ON-luminance of 1670 ph cd m-2. (A) pERG N95 amplitude. (B) pERG N95 implicit time. (C) ppERG N amplitude. (D) ppERG N implicit time.

To compare the relative sensitivities of the two test to glaucomatous damage a cluster analysis (based on the feature values) was performed. The results of the cluster analysis were a distance from the healthy mean in the feature space, calculated for each study participant. These distances are summarized in the histograms of Figure 34. Panel A plots the distances based on the pERG response data of five glaucoma patients and six normally-sighted subjects and, three of the five glaucoma patients appear well within the normally-sighted subject distribution. Panel B plots the distances based on the ten ppERG feature values obtained with the 30 cm, 1670 ph cd m^{-2} protocol from the same group; all five glaucoma patients are clearly separated from the healthy eye responses. To understand the

influence of just the ppERG high frequency components to glaucomatous damage, Euclidean distance of these features are plotted in a six-dimensional space. Figure 34C shows that the high frequency components are modestly influenced by glaucomatous damage in the small population of patients ($n = 5$) analyzed here.

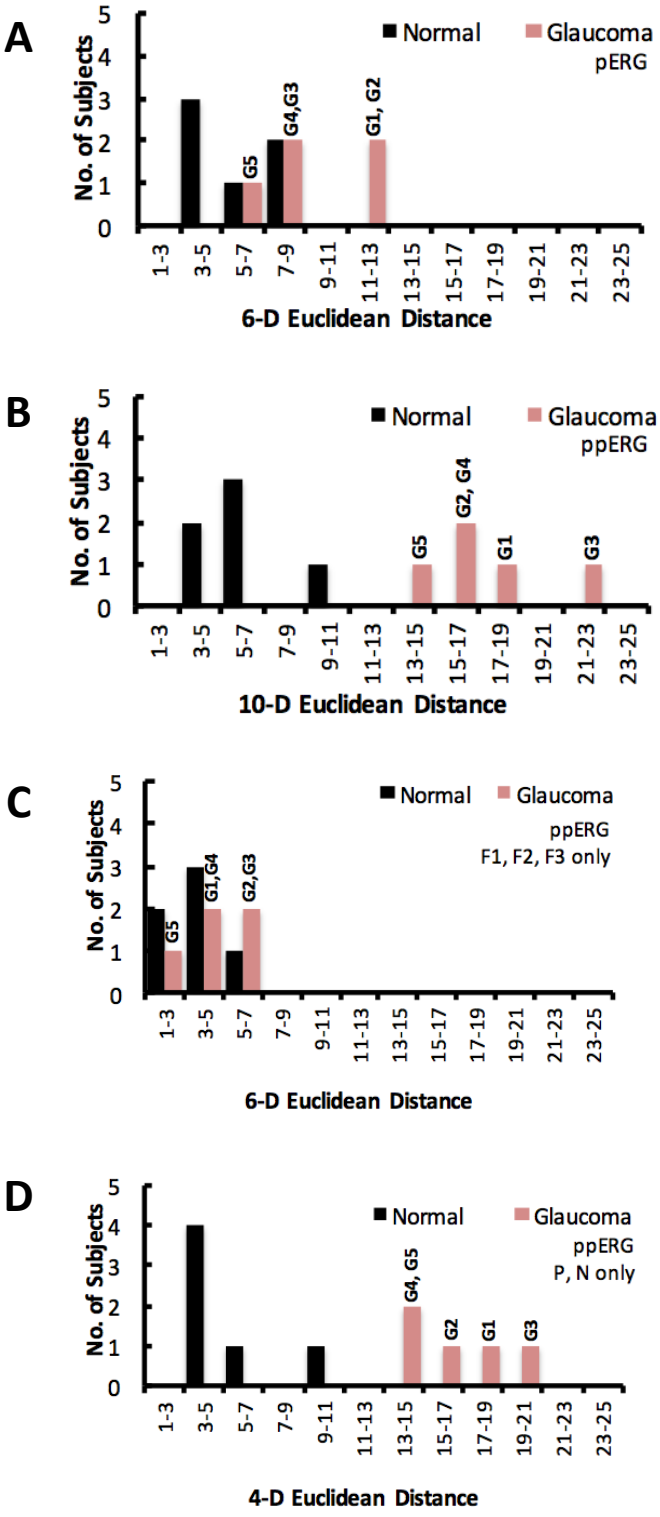

Figure 34. Cluster analysis histograms. The x-axis in each panel is the Euclidean distance in the feature space from each study participant to the mean location of normally-sighted subjects (n = 6). Patient labels (GP 1-5) refer to Table 3 (A) Separation obtained using six pERG features (amplitudes and implicit times of N35, P50 and N95) under standard ISCEV conditions (Table 1). (B) Separation obtained using the ten ppERG features (amplitudes and implicit times of N, P, F1, F2, F3) extracted from responses obtained with the (30, 1670) protocol. The increased dimensionality in the cluster space from 6D in pERG to 10 D in ppERG did not automatically lead to larger differences from normal (Euclidean distance) for the ppERG test (demonstrated by the similar average Euclidean distances for the normally-sighted subjects 6.2 and 5 for pERG and ppERG respectively) (C) Separation obtained using only the six features extracted from high-frequency ppERG response components (amplitudes and implicit times of F1, F2, F3). (D) Separation obtained using only the four features extracted from low-frequency ppERG response components (amplitudes and implicit times of P and N).

Until more is known about the involvement of the high frequency ppERG components, all future analysis used the P and N component of the ppERG response and P50 and N95 component of the pERG response for consistent comparison.

The cluster analysis in a four-dimensional space for twelve glaucoma patients and eleven normally-sighted subjects for both test is plotted in Figure 35A-B. Including all four response parameters i.e. amplitudes and implicit times provided good separation between normal eyes and glaucomatous eyes for ppERG but not for pERG. It should be noted that the normally-sighted subjects were not age-matched to the glaucoma patients in this initial study, however both tests (pERG and ppERG) were evaluated with the same subject and patient groups allowing comparison of relative sensitivity. Table 4 summarizes amplitudes, implicit times and 4 – D Euclidean distance values for both normally-sighted individuals (Table 4A) and glaucoma patients (Table 4B)

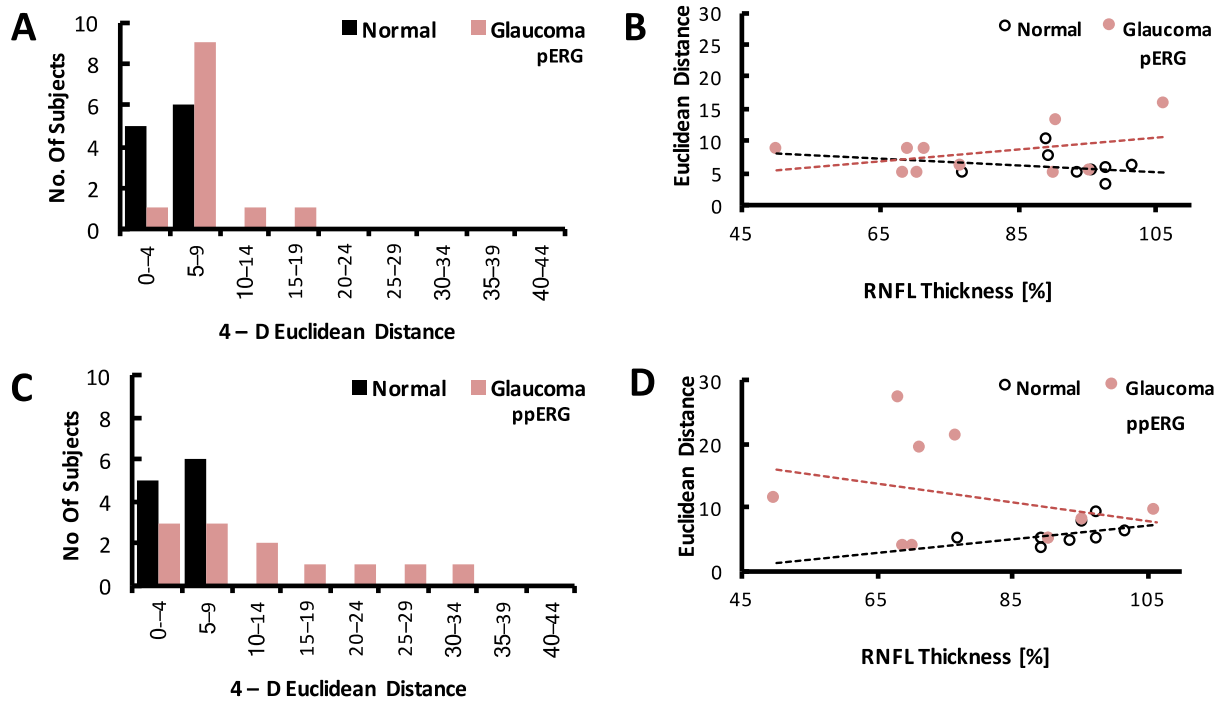

Figure 35. Cluster analysis based on amplitudes and implicit times of ppERG and pERG response waveforms for normally-sighted subjects (n = 11) and glaucoma patients (n = 12). For ppERG, viewing distance was 30 cm and mean ON-luminance was 1670 ph cd m-2. For pERG, standard ISCEV-recommended stimulus settings were used (Table 2). (A) Euclidean distance from the mean normal response for the pERG test. (B) Euclidean distance vs. RNFL thickness for the pERG test, RNFL thickness converted to % of normal for each participants' age group. Normal eye responses and glaucoma eye responses fit with separate linear trendlines, slopes = -0.05 and 0.08, respectively. (C) Euclidean distance from the mean normal response for the ppERG test. (D) Euclidean distance vs. RNFL thickness for the ppERG test, RNFL thickness converted to % of normal for each participants' age group. Normal eye responses and glaucoma eye responses fit with separate linear trendlines, slopes = 0.10 and -0.15, respectively.

A

Healthy ID	P amplitude [μV]		P Implicit times [ms]		N amplitude [μV]		N Implicit times [ms]		Euclidean Distance	
	ppERG	pERG	ppERG	pERG	ppERG	pERG	ppERG	pERG	ppERG	pERG
H 1	4.02	7.17	21.73	48.50	11.60	12.30	53.67	100.00	4.43	4.80
H 2	3.22	6.10	19.25	46.00	15.20	10.76	54.05	104.00	7.40	4.31
H 3	1.64	7.14	20.00	48.00	13.74	14.71	56.13	102.00	5.01	5.27
H 4	2.81	6.25	24.15	46.50	9.10	9.25	60.90	98.00	5.78	7.49
H 5	0.21	5.78	24.88	49.00	6.26	11.66	57.80	101.50	9.20	2.79
H 6	3.84	8.88	26.07	48.00	9.30	14.38	60.13	104.00	6.72	5.46
H 7	1.33	4.47	20.80	53.50	8.81	9.17	55.40	104.00	4.21	4.69
H 8	0.80	4.89	19.80	56.00	10.46	7.93	56.00	109.00	2.64	9.52
H 9	1.50	5.85	24.40	51.50	3.40	11.75	59.00	108.00	7.93	5.18
H 10	0.24	4.68	18.20	53.50	7.25	6.63	53.60	110.50	3.59	9.75
H 11	1.59	5.41	18.80	48.50	9.47	10.17	53.60	99.50	4.40	4.95
Average	1.93	6.06	21.64	49.91	9.51	10.79	56.39	103.68	5.57	5.84
St-Dev	1.35	1.29	2.76	3.23	3.30	2.51	2.70	4.06	2.02	2.18

Table 4. Amplitudes and implicit times of the four feature values (P and N amplitudes and implicit times) used to calculate the Euclidean distances for pERG and ppERG responses. (A) summarizes information for normally-sighted subjects (n = 11).

B

Patient ID	P amplitude [μV]		P Implicit times [ms]		N amplitude [μV]		N Implicit times [ms]		Euclidean Distance	
	ppERG	pERG	ppERG	pERG	ppERG	pERG	ppERG	pERG	ppERG	pERG
GP 1	-0.99	3.48	21.00	50.50	3.98	4.81	74.80	98.00	19.45	8.67
GP 2	2.09	2.03	26.40	51.50	7.04	7.66	50.00	104.50	8.34	5.40
GP 3	1.03	5.74	25.00	51.50	7.75	8.07	56.80	107.50	3.92	4.96
GP 4	11.35	4.73	40.40	50.50	14.16	8.87	80.00	112.50	31.93	9.14
GP 5	2.89	7.78	37.80	47.00	7.36	15.68	70.20	103.00	21.39	5.99
GP 6	9.28	6.17	26.20	52.00	11.89	8.18	82.40	107.00	27.51	4.71
GP 7	2.60	3.02	24.40	49.00	10.37	8.30	60.60	106.50	5.15	4.92
GP 9	0.57	0.78	20.80	60.00	2.54	1.42	62.80	108.50	9.60	15.52
GP 10	0.42	1.86	18.60	57.50	5.81	2.91	56.60	109.50	5.02	13.08
GP 11	3.20	3.49	26.80	48.50	4.45	3.06	65.60	101.00	11.77	8.69
GP 12	0.70	4.03	21.00	53.50	5.78	8.35	55.60	111.00	4.06	8.75
GP 13	2.62	1.82	31.20	51.50	7.28	6.34	68.20	104.00	15.37	6.36
Average									13.63	8.02
St-Dev									9.56	3.41

Table 4. Amplitudes and implicit times of the four feature values (P and N amplitudes and implicit times) used to calculate the Euclidean distances for pERG and ppERG responses. (B) Summarizes information for the glaucoma patients (n = 12).

ppERG Test sensitivity – Linear regression analysis: The Euclidean distance from the normal mean for each subject and patient are plotted against age-normalized RNFL thickness in panels B and D of Figure 35. For both tests, normal eye responses and glaucomatous eye responses were fit with separate regression lines Linear regression analysis revealed that the slopes for normal (-0.05) and glaucomatous eyes (0.08) were nearly zero for the pERG test, as was the slope for normal eye responses for the ppERG test (0.10). However, glaucomatous eyes with RNFL thickness below approximately 70% of normal had distinctly abnormal ppERG responses. For the small patient group evaluated here, the high-luminance ppERG test is shown to be relatively more sensitive to glaucomatous damage than the conventional central-field, low-luminance pERG.

ppERG protocol ranking. Despite being an excellent method to objectively detect the functional loss of retinal ganglion cells, the pERG test, though clinically available is highly underutilized. This may be because of the need for a skilled test-operator and high patient compliance to obtain a reliable pERG response [Porciatti et al. 2004]. In order to increase the clinical viability of the ppERG test, to give maximum information within a short test time, an optimum protocol is needed. To identify this optimum protocol, protocol ranking was done. Ranking resulted in the 30 cm viewing distance, 1670 ph cd m^{-2} mean ON-luminance protocol to be the best. The 30 cm, 1670 ph cd m^{-2} protocol most fully exploits the novel capabilities of the ppERG system (far-peripheral stimulation, high luminance, Figure 15C, Specific Aim 2). This protocol also gives the best separation in cluster analysis, between normally-sighted subjects and glaucoma patients. Ranks of the other protocols are summarized in Table 5.

Feature values were also ranked to identify the most useful feature component. The amplitude and latency of the low-frequency components (P and N) provided the best separation; the amplitude of F3 and latency of F1 were the next most "useful" features. These values are seen in Table 6.

Protocol	(30, 1670)	(30, 90)	(55, 1670)	(55, 90)
∑MDiff	14.0	8.9	12.7	9.5

Table 5. Mean difference values summed across features, for each ppERG protocol employed. Protocols identified by (viewing distance, luminance).

Feature	N Amp	N IT	P IT	P Amp	F3 Amp	F1 IT	F1 Amp	F2 IT	F2 Amp	F3 IT
∑MDiff	8.5	6.9	6.2	6.0	4.1	4.0	3.2	2.7	2.2	1.3

Table 6. Mean difference values summed across protocols, for the ten response features analyzed. Features are evaluated amplitudes (Amp) or implicit times (IT) of response waveform peaks (N, P, F1, F2, F3).

Local Pattern Stimulation.

Sensitivity of the ppERG test to local glaucomatous damage was assessed by probing localized regions of the peripheral retina. Figures 5,6,7 plot the results, where retinal regions targeted by ppERG, pERG, HVF and OCT are illustrated. The visual field covered by the pERG monitor ($\pm 15^{o}$, gray square) and HVF 24-2 stimulus (yellow dots) are superimposed on a rendition of the retinal fiber tracts [Oyster., 1999]. Relative to this, the ppERG stimulus is capable of targeting regions farther out into the periphery (40 – 170 degrees, Specific Aim 2, Figure 15C). The range of the RNFL fibers that relate ppERG sectors to the OCT sectors are indicated by the three blue arcs (Superior-nasal (light blue), Inferior-nasal (medium blue) and Temporal (dark blue)) and are bound by red dashed lines.

Figure 37A-C presents the responses to ppERG sector stimuli recorded from the right eye of a mid-stage glaucoma patient (GP 12, red trace). The ppERG response is compared to a global mean of five normally sighted subjects (black trace). The largest reduction in amplitude is seen in the super-nasal field (inferior-temporal retina), Figure 37A. This is consistent with OCT scans (Figure 37A) and HVF results (Figure 37D) for that sector. ppERG amplitudes for the inferior-nasal and temporal fields (Figure 37B-C) were reduced, in disagreement with the corresponding OCT scans and HVF sectors, which showed normal results. There is an overall reduction of the ppERG (all-ON configuration, 30 cm, 1670 ph cd m^{-2}, Figure 37E) and pERG responses (Figure 37D),

N amplitude ratios for GP 3 (Figure 38F) are within the normal range for all sectors; inferior-nasal (GP 3: 0.53; HM: 0.55 ± 0.03); superior-nasal sectors (GP 3: 0.23; HM: 0.29 ± 0.9) and temporal sector (GP 3: 0.87; HM: 0.75 ± 0.18).

N amplitude ratios for the glaucoma suspect (GP 13) (Figure 39F) are within one standard deviation of the healthy mean; inferior-nasal (GP 13: 0.57; HM: 0.55 ± 0.03), superior-nasal sectors (GP 13: 0.30; HM: 0.29 ± 0.9), temporal sector (GP 13: 0.68; HM: 0.75 ± 0.18).

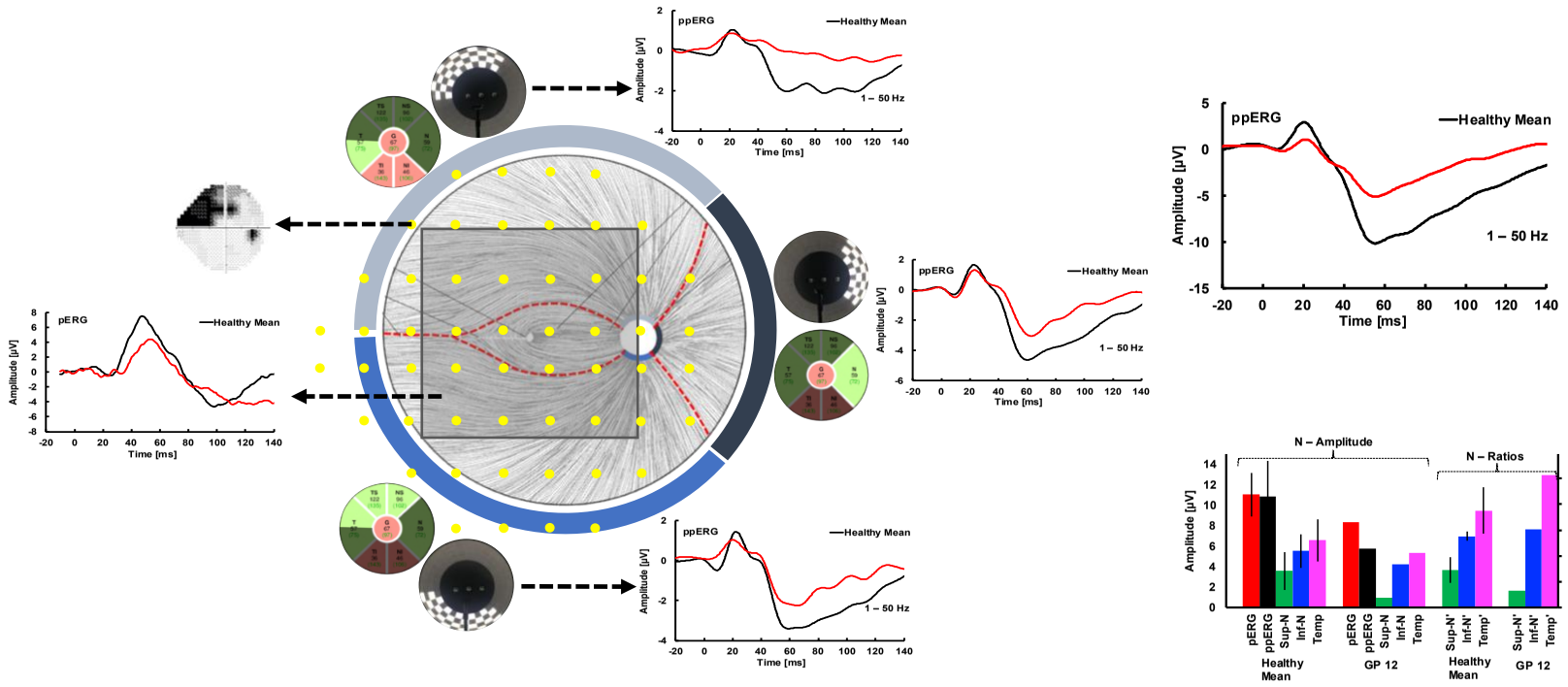

Figure 37. Schematic illustration of retinal regions targeted by ppERG, pERG, HVF and OCT. The blue arcs (Superior-nasal, Inferior-nasal and Temporal) indicate the range of RNFL fiber tracts that relate ppERG Sector stimuli to circumpapillary OCT sectors (bounded by red dashed lines). Yellow dots indicate the HVF 24-2 stimulus. The grey square indicates the pERG stimulus field ($\pm 15^{o}$). (A-C) Responses to ppERG Sector stimuli recorded from the right eye of a mid-stage glaucoma patient (red trace). (D) HVF for this patient (mean deviation: -9.07 dB; glaucoma hemi-field test (GHT): outside normal limits) and pERG responses from the corresponding eye. (E) Response to 30 cm 1670 ph cd m^{-2} ppERG protocol from the same patient (red trace), compared to the healthy mean (black trace, $n = 5$). (F) N component amplitudes elicited by pERG, ppERG Ring and ppERG Sector stimuli, compared to the healthy mean ($n = 5$, error bars plot $\pm$ one standard deviation). Ratios of N amplitude (each sector response divided by the sum of the other two), evaluated to assess asymmetry in functional changes.

Figure 38A-C present the responses to ppERG sector stimuli recorded from the right eye of a glaucoma patient with normal visual field (GP 3, MD 0.94) and abnormal RNFL thickness. There is no significant difference in the pERG and pERG amplitudes and implicit times from the healthy mean (back trace, Figure 38D and 38E). However, the ppERG sector response amplitudes are reduced by ~ 1.5 microvolts (μV) in each sector (red trace) compared to the healthy mean (back trace). These abnormalities are consistent with the OCT scans but are not seen in the HFV results.

Figure 39A-C present the responses to ppERG sector stimuli recorded from the left eye of a glaucoma suspect (GP 13, red trace). Along with the reduction in temporal (-2 μV) and inferior-nasal fields (-1.4 μV) N amplitudes, there is an increase in the N implicit times when compared to the normally sighted subjects (black trace). This is seen in the all-ON configuration, 30 cm, 1670 ph cd m^{-2} ppERG responses as well (Figure 39E). The considerable reduction of the P50 amplitude (Figure 39D) may be due to a more central dysfunction, however this is not manifested in any visual field loss.

Asymmetry in functional changes within sectors are evaluated by calculating N amplitude ratios. The N amplitude of each sector is divided by the N amplitude sum of the other two sectors. A summary of pERG, ppERG amplitudes and N amplitude ratios of the patients compared to healthy mean is ($n = 5$, error bars plots $\pm$ one standard deviation) shown in Figure 37F, 38F and 39F. N amplitude ratios for the mid-stage glaucoma patient (GP 12) are abnormal when compared to the ratios of the healthy mean (more than one standard deviation, Figure 37F, "*").

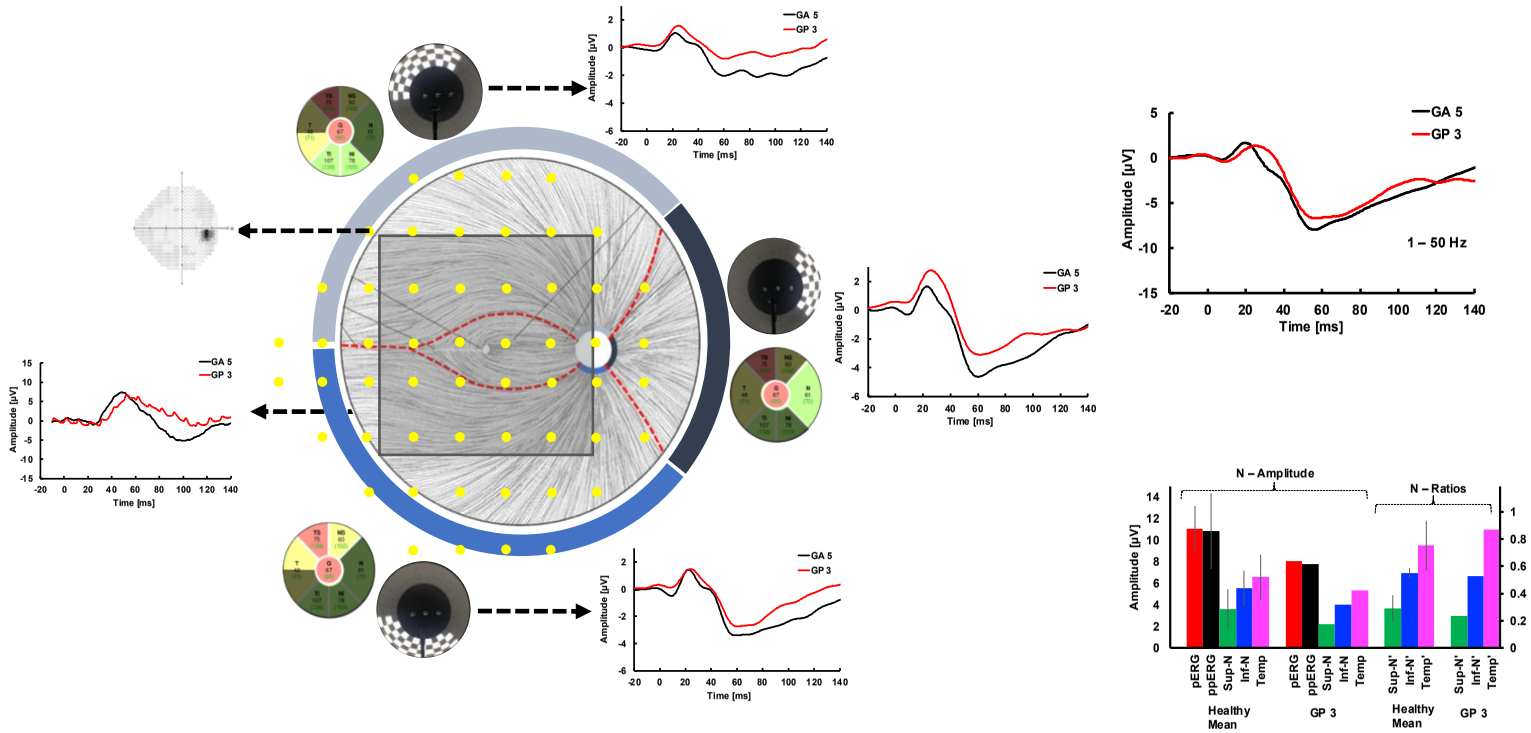

Figure 38. Schematic illustration of retinal regions targeted by ppERG, pERG, HVF and OCT. (GP 3). Same construction as Figure 37, for a glaucoma patient with abnormal sectors in OCT but normal visual field test results. (A-C) Responses to ppERG Sector stimuli recorded from the right eye (red trace). (D) HVF results (mean deviation: 0.94 dB; glaucoma hemi-field test (GHT): within normal limits) and pERG responses from the corresponding eye. (E) Response to 30 cm 1670 ph cd m^{-2} ppERG protocol from the same patient (red trace), compared to the healthy mean (black trace, n = 5). (F) N component amplitudes elicited by pERG, ppERG Ring and ppERG Sector stimuli, compared to the healthy mean (n = 5, error bars plot ± one standard deviation). Ratios of N amplitude (each sector response divided by the sum of the other two), evaluated to assess asymmetry in functional changes.

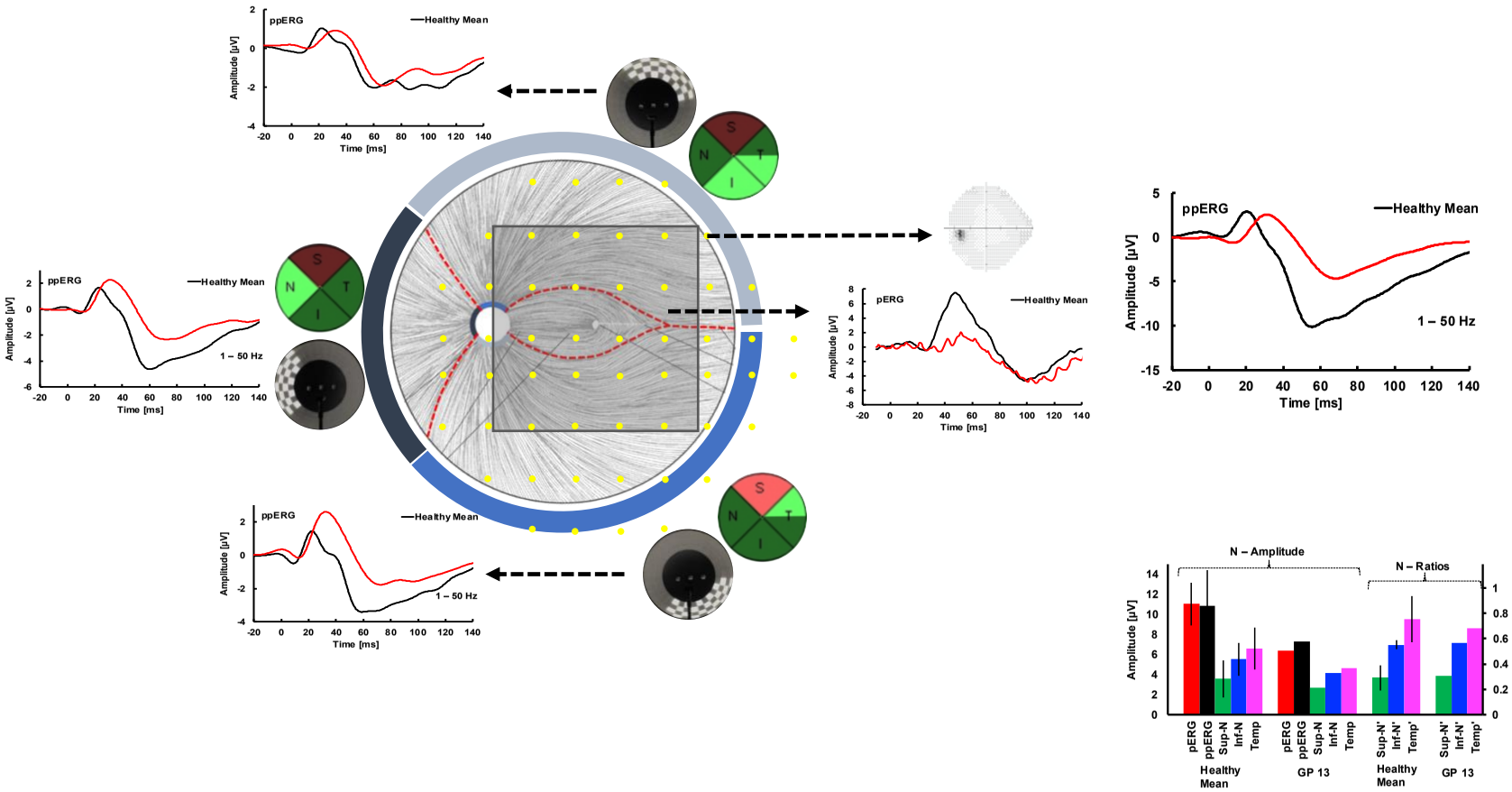

Figure 39. Schematic illustration of retinal regions targeted by ppERG, pERG, HVF and OCT. (GP 13). Responses were recorded from the left eye. A-C. Responses to ppERG Sector stimuli (red trace). (D) HVF 24-2 was normal (Mean deviation: -1.09 dB, GHT: within normal limits) and pERG responses from the corresponding eye (red trace). (E) Response to 30 cm 1670 ph cd m^{-2} ppERG protocol from the same patient, compared to the healthy mean (black trace, n = 5). (F) N component amplitudes elicited by pERG, ppERG Ring and ppERG Sector stimuli, compared to the healthy mean (n = 5, error bars plot ± one standard deviation). Ratios of N amplitude (each sector response divided by the sum of the other two), evaluated to assess asymmetry in functional changes.

ppERG response waveforms: Other patient populations.

Diabetes. Reduction in amplitudes and increase in implicit times of the oscillatory potentials have been observed in diabetic patients prior to the development of diabetic retinopathy. [Luu et al. 2010; Pescosolido et al. 2015; Tzekov et al. 1999]. To observe if the ppERG high frequency components undergo similar changes in amplitude and implicit times as the affected OPs, ppERG responses were recorded from one diabetic patient and are compared to the healthy mean (n = 11). Figure 40A-C plots responses (red trace) recorded from the 30 cm, 1670 ph cdm^{-2} protocol with a reversal rate of 4.6 RPS, black trace represent the waveform recorded from the healthy mean. Amplitudes are reduced and implicit times are increased, consistent with the changes observed in oscillatory potentials of diabetic patients [Li et al., 1992; Movasat et al.,2008], this supports further data collection from more patients.

Idiopathic intracranial hypertension: Idiopathic intracranial hypertension (IIH) is caused by the mechanical compression of retinal ganglion cells (RGC) resulting in early peripheral RGC dysfunction. This dysfunction and associated field defects can be detected by electrophysiological methods, such as the pERG and perimetry tests like the HVF. However, both tests are limited to the central 24 degrees, while RGC dysfunction in IIH patients is said to manifest in the peripheral retina [Moss et al. 2015] The peripheral pattern electroretinogram may prove useful in detecting the onset of peripheral ganglion cell loss in IIH patients. In order to test this, ppERG responses were recorded from one IIH patient at two viewing distances and a mean ON-luminance of 1670 ph cd m^{-2}. Responses are summarized in Figure 9. For this patient, the larger ppERG N amplitude, measured from the

peak of P to the trough of N (within set time windows, Specific Aim 2) (Figure 40B) may be due to an increase in the positive P component (Table 7 – ppERG P amplitudes).

Although ppERG assesses the peripheral retinal ganglion cell function, any claims regarding the sensitivity of the test to RGC loss in IIH patients would need a larger sample set.

	P amp		P IT	
	ppERG	pERG	ppERG	pERG
Healthy Mean	1.927	6.056	21.643	49.909
IIH patient	10.245	6.4476	25.8	52.5
	N amp		N IT	
	ppERG	pERG	ppERG	pERG
Healthy Mean	9.508	10.792	56.389	103.682
IIH patient	13.582	7.8994	75.8	113.5

Table 7. ppERG P and N amplitudes and implicit times and pERG P50 and N95 amplitudes and implicit times compared with that of the healthy mean (n = 11) for the one patient

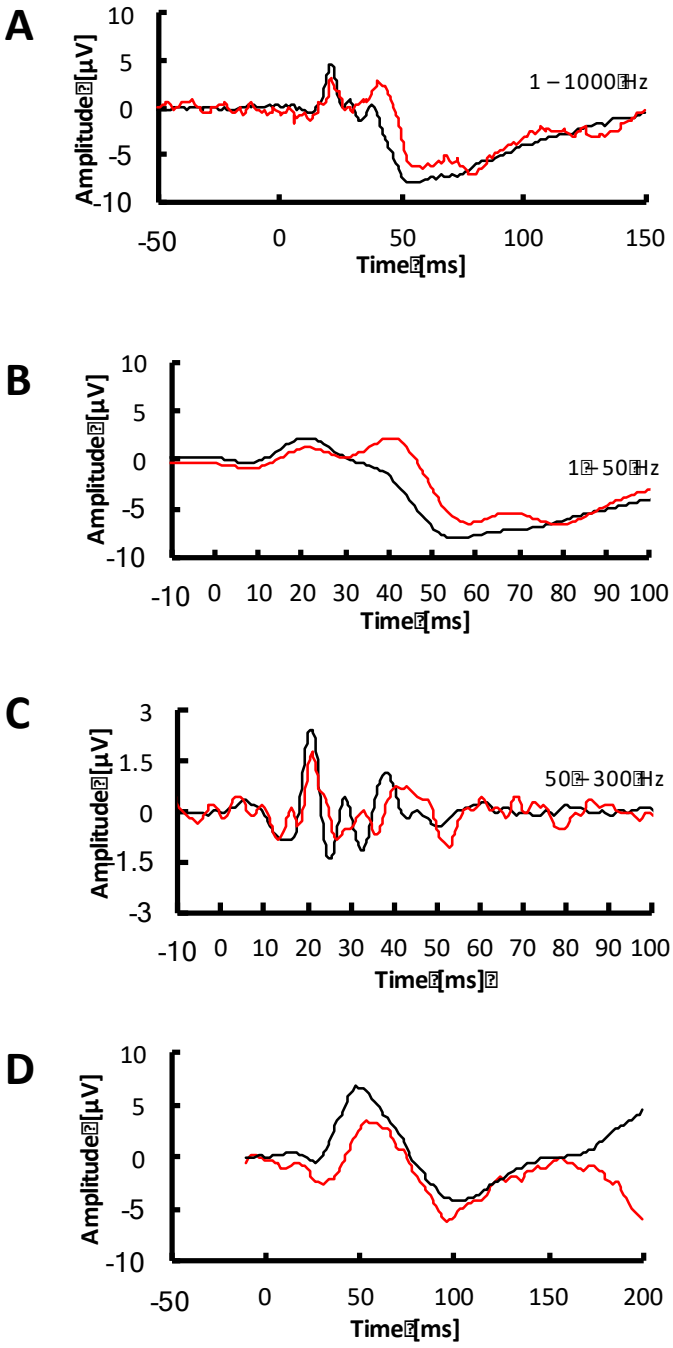

Figure 40. ppERG responses from one diabetic patient. (A) ppERG waveform recorded from normally-sighted subjects (black trace, n = 11) and one diabetic patient (red trace). Responses were recorded with passband 1-1000 Hz at a viewing distance of 30 cm, mean ON-luminance of 1670 ph cd m^{-2}, and a reversal rate of 4.6 RPS. (B) Isolated low-frequency components in the passband 1-50 Hz. (D) Isolated high-frequency components in the passband 50-1000 Hz. (E) Conventional pERG response waveforms obtained under standard ISCEV conditions (Table 2).

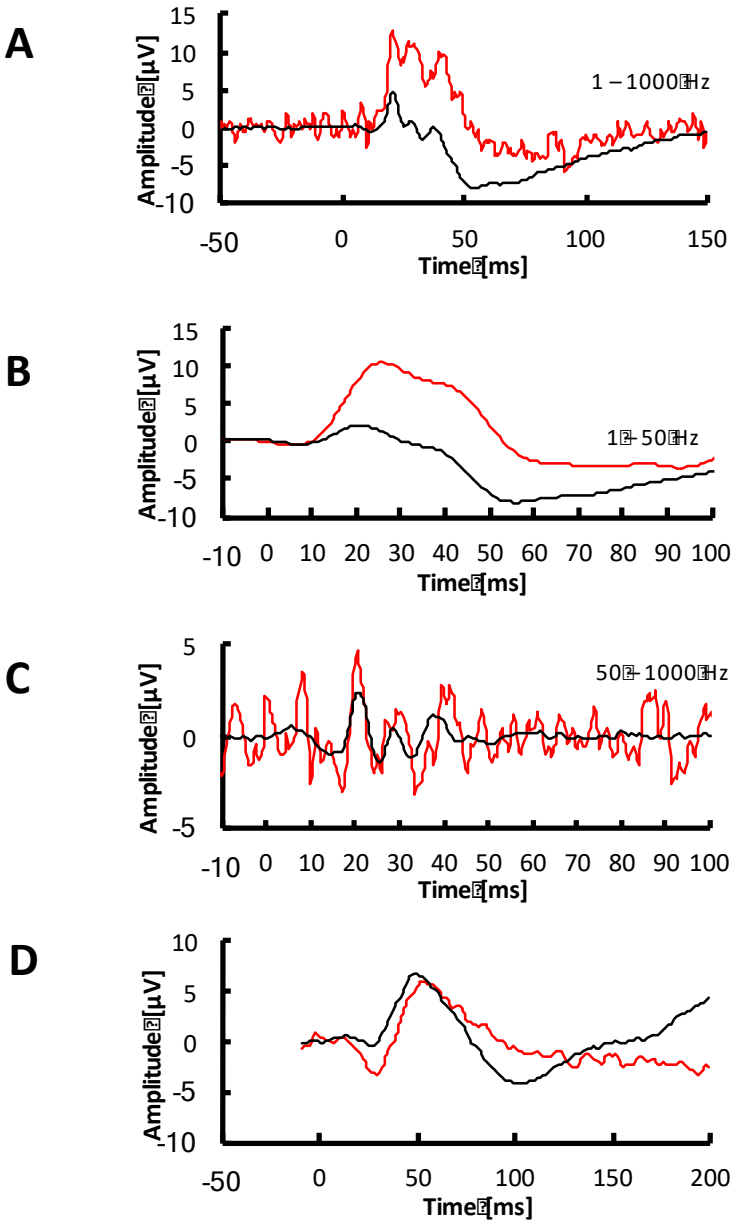

Figure 41 ppERG responses from one IIH patient. (A) ppERG waveform recorded from normally-sighted subjects (black trace, n = 11) and one diabetic patient (red trace). Responses were recorded with passband 1-1000 Hz at a viewing distance of 30 cm, mean ON-luminance of 1670 ph cd m^{-2}, and a reversal rate of 4.6 RPS. (B) Isolated low-frequency components in the passband 1-50 Hz. (C) Isolated high-frequency components in the passband 50-1000 Hz. (D) Conventional pERG response waveforms obtained under standard ISCEV conditions (Table 2).

Specific Aim 3 Discussion

Differences in ganglion cell diversity, density, morphology and connectivity in peripheral retina may make the earliest functional losses more accessible with appropriate peripheral-field testing, where the influence of the relatively preserved foveal contribution is avoided.

The results summarized above show that the ppERG system is sensitive to glaucomatous damage in the periphery. Cluster analysis gave the best separation of patients from normal when the four waveform components (P and N amplitudes and implicit times) are considered. The ppERG N implicit times appear to be the most informative feature in distinguishing the patients from the healthy group. The increase in N implicit time was seen in the DM and IIH patients as well. Results from the IIH patient did not show the expected reduction in ppERG N amplitude [Falsini et al. 1992]. The N implicit time of the late negative component however increased in both tests, pERG (N95) and ppERG (N).

An important potential advantage of the ppERG stimulus source used here is the ability to probe sectors of the peripheral retina – local pattern stimulation. Glaucomatous onset is often said to follow a retinotopic path and damage is said to start within a specific sector (temporal, superior-temporal, inferior-temporal, nasal or macular). The onset of damage however can be arbitrary, effecting any sector before moving on to the next. Local changes in function with in the ~ 50 degrees of the visual field can be detected with the help of standard perimetry tests (HVF, 24-2' protocol). The damage outside this region, primarily in the superior –nasal regions is overlooked because of the limited field [Hood et al., 2013]. The unique capability of the pERG system to probe peripheral local function (beyond the

30-50 degrees of the conventional test) proves advantageous in overcoming the limitations of the HVF test. Measuring local function can also be more sensitive because of the increase in effect size compared to the healthy; because of the advantages mentioned above (target peripheral regions and increased effect size), the local pattern stimulation protocol shows considerable promise in early detection and needs to be established in a larger patient population.

High-frequency components evoked in the high-luminance ppERG response had measurable but limited effect on test sensitivity within a small cohort of glaucoma patients (Figure 34C), but showed a definite reduction in amplitude and shifts in implicit times in the one type 2 diabetic mellitus patient recruited in the study. This suggests that the high frequency components may have greater importance for patients with vascular involvement.

These findings motivate additional testing across a larger and more diverse patient population (with age-matched controls), where the advantages of peripheral-field and high-luminance pattern stimuli can be more thoroughly evaluated.

Part V: Discussion

Discussion

The peripheral pattern ERG system developed in this study has the ability to target the understudied and overlooked peripheral retina. The unique capability of presenting local pattern stimulation can help detect early localized glaucomatous damage. Data collected from a small group of normally sighted subjects was used to validate the system and characterize the ppERG response with respect to luminance, reversal rate and field subtended (Specific Aim 2). Results from the glaucoma patients showed that the test was relatively more sensitive to glaucomatous damage than the conventional pattern ERG test.

The next step would be to explore and validate the system capabilities in other diseases that can affect retinal ganglion cell function in the periphery.

Neuropsychiatric disorders and the peripheral pattern ERG.

Developmentally and anatomically, the retina is known to be an extension of the central nervous system [London et al., 2012]. It has been hypothesized that the retina, specifically retinal ganglion cells, are a site of functional and structural changes in neuropsychiatric disorders, like Parkinson's disease (PD), Alzheimer's disease (AD) and schizophrenia [Silverstein & Rosen., 2015].

The RNFL thickness, a measure of structural ganglion cell damage, is said to reflect neurodegeneration in the brain. Progression of RNFL thinning parallels disease progression in PD [Satue et al., 2014], multiple sclerosis [Ratchford et al., 2014, Graham et al., 2016], AD [Parisi et al., 2001] and schizophrenia [Silverstein & Rosen., 2015].

As functional alterations in the retina precedes structural damage, electroretinography is

ideally suited to reveal subtle losses in early disease. Loss in contrast sensitivity and changes in pERG signals have been observed in PD [Wollner *et al.,* 987; Gottlob et al., 1987; Tagliati et al., 1994; Tagliati et al., 1996; Peppe et al., 1998; Sartucci et al., 2006] and AD [Katz et al., 1989; Karsodomska et al., 2010], with suggestive evidence being found in schizophrenia [Silverstein et al., 2015].

The high-luminance peripheral pattern ERG stimulus source has shown promise in detecting glaucomatous damage in the periphery. It will now be interesting to study changes, if any, occurring in the peripheral retinal regions in neurological and neuropsychiatric disease mentioned above. If successful, the test can provide a clinically advantageous platform to study the extent to which these alterations can act as biomarkers for changes in the brain, and ultimately aid in monitoring at risk individuals or those currently undergoing treatment for neuropsychiatric disorders.

CITED LITERATURE

Arden, G. B., R. M. Carter, and A. Macfarlan. 1984. Pattern and ganzfeld electroretinograms in macular disease. *The British Journal of Ophthalmology* 68 (12) (Dec): 878-84.

Aylward, G. W., V. Billson, and F. A. Billson. 1989. The wide-angle pattern electroretinogram. relation between pattern electroretinogram amplitude and stimulus area using large stimuli. *Documenta Ophthalmologica.Advances in Ophthalmology* 73 (3) (Nov): 275-83.

Bach, M., M. G. Brigell, M. Hawlina, G. E. Holder, M. A. Johnson, D. L. McCulloch, T. Meigen, and S. Viswanathan. 2013. ISCEV standard for clinical pattern electroretinography (PERG): 2012 update. *Documenta Ophthalmologica.Advances in Ophthalmology* 126 (1) (Feb): 1-7.

Bach, M., P. Hiss, and J. Rover. 1988. Check-size specific changes of pattern electroretinogram in patients with early open-angle glaucoma. *Documenta Ophthalmologica.Advances in Ophthalmology* 69 (3) (Jul): 315-22.

Bach, M., and M. B. Hoffmann. 2008. Update on the pattern electroretinogram in glaucoma. *Optometry and Vision Science : Official Publication of the American Academy of Optometry* 85 (6) (Jun): 386-95.

Bach, M., and A. Ramharter-Sereinig. 2013. Pattern electroretinogram to detect glaucoma: Comparing the PERGLA and the PERG ratio protocols. *Documenta Ophthalmologica.Advances in Ophthalmology* 127 (3) (Dec): 227-38.

Bach, M., F. Sulimma, and J. Gerling. 1997. Little correlation of the pattern electroretinogram (PERG) and visual field measures in early glaucoma. *Documenta Ophthalmologica.Advances in Ophthalmology* 94 (3) (-1998): 253-63.

Banitt, M. R., L. M. Ventura, W. J. Feuer, E. Savatovsky, G. Luna, O. Shif, B. Bosse, and V. Porciatti. 2013. Progressive loss of retinal ganglion cell function precedes structural loss by several years in glaucoma suspects. *Investigative Ophthalmology & Visual Science* 54 (3) (Mar 28): 2346-52.

Berninger, T., and R. P. Schuurmans. 1985. Spatial tuning of the pattern ERG across temporal frequency. *Documenta Ophthalmologica.Advances in Ophthalmology* 61 (1) (Oct 30): 17-25.

Berninger, T. A., and G. B. Arden. 1988. The pattern electroretinogram. *Eye (London, England)* 2 Suppl : S257-83.

Bodis-Wollner, I., M. S. Marx, S. Mitra, P. Bobak, L. Mylin, and M. Yahr. 1987. Visual dysfunction in parkinson's disease. loss in spatiotemporal contrast sensitivity. *Brain : A Journal of Neurology* 110 (Pt 6) (Pt 6) (Dec): 1675-98.

Calkins, D. J. 2012. Critical pathogenic events underlying progression of neurodegeneration in glaucoma. *Progress in Retinal and Eye Research* 31 (6) (Nov): 702-19.

Calkins, D. J., and P. J. Horner. 2012. The cell and molecular biology of glaucoma: Axonopathy and the brain. *Investigative Ophthalmology & Visual Science* 53 (5) (May 4): 2482-4.

Chang, E. E., and J. L. Goldberg. 2012. Glaucoma 2.0: Neuroprotection, neuroregeneration, neuroenhancement. *Ophthalmology* 119 (5) (May): 979-86.

Crish, S. D., R. M. Sappington, D. M. Inman, P. J. Horner, and D. J. Calkins. 2010. Distal axonopathy with structural persistence in glaucomatous neurodegeneration. *Proceedings of the National Academy of Sciences of the United States of America* 107 (11) (Mar 16): 5196-201.

Curcio, C. A., and K. A. Allen. 1990. Topography of ganglion cells in human retina. *The Journal of Comparative Neurology* 300 (1) (Oct 1): 5-25.

Davis, B. M., L. Crawley, M. Pahlitzsch, F. Javaid, and M. F. Cordeiro. 2016. Glaucoma: The retina and beyond. *Acta Neuropathologica* 132 (6) (Dec): 807-26.

Dengler-Crish, C. M., M. A. Smith, D. M. Inman, G. N. Wilson, J. W. Young, and S. D. Crish. 2014. Anterograde transport blockade precedes deficits in retrograde transport in the visual projection of the DBA/2J mouse model of glaucoma. *Frontiers in Neuroscience* 8 (Sep 17): 290.

Eke, T., J. F. Talbot, and M. C. Lawden. 1997. Severe persistent visual field constriction associated with vigabatrin. *BMJ (Clinical Research Ed.)* 314 (7075) (Jan 18): 180-1.

Fitzgibbon, T., and S. F. Taylor. 1996. Retinotopy of the human retinal nerve fibre layer and optic nerve head. *The Journal of Comparative Neurology* 375 (2) (Nov 11): 238-51.

Gottlob, I., E. Schneider, W. Heider, and W. Skrandies. 1987. Alteration of visual evoked potentials and electroretinograms in parkinson's disease. *Electroencephalography and Clinical Neurophysiology* 66 (4) (Apr): 349-57.

Graham, Elizabeth C., Yuyi You, Con Yiannikas, Raymond Garrick, John Parratt, Michael H. Barnett, and Alexander Klistorner. 2016. Progressive Loss Of Retinal Ganglion Cells And Axons In Nonoptic Neuritis Eyes In Multiple Sclerosis: A Longitudinal Optical Coherence Tomography Study. Investigative Opthalmology & Visual Science 57 (4): 2311.

Your Bibliography: Graham, Elizabeth C., Yuyi You, Con Yiannikas, Raymond Garrick, John Parratt, Michael H. Barnett, and Alexander Klistorner. 2016. "Progressive Loss Of Retinal Ganglion Cells And Axons In Nonoptic Neuritis Eyes In Multiple Sclerosis: A Longitudinal Optical Coherence Tomography Study". Investigative Opthalmology & Visual Science 57 (4): 2311. doi:10.1167/iovs.15-19047.

Graham, S. L., V. A. Wong, S. M. Drance, and F. S. Mikelberg. 1994. Pattern electroretinograms from hemifields in normal subjects and patients with glaucoma. *Investigative Ophthalmology & Visual Science* 35 (9) (Aug): 3347-56.

Hebert-Lalonde, N., L. Carmant, P. Major, M. S. Roy, M. Lassonde, and D. Saint-Amour. 2016. Electrophysiological evidences of visual field alterations in children exposed to vigabatrin early in life. *Pediatric Neurology* 59 (Jun): 47-53.

Holopigian, K., J. Snow, W. Seiple, and I. Siegel. 1988. Variability of the pattern electroretinogram. *Documenta Ophthalmologica.Advances in Ophthalmology* 70 (1) (Sep): 103-15.

Hood, D. C., V. Greenstein, L. Frishman, K. Holopigian, S. Viswanathan, W. Seiple, J. Ahmed, and J. G. Robson. 1999. Identifying inner retinal contributions to the human multifocal ERG. *Vision Research* 39 (13) (Jun): 2285-91.

Katz, B., S. Rimmer, V. Iragui, and R. Katzman. 1989. Abnormal pattern electroretinogram in alzheimer's disease: Evidence for retinal ganglion cell degeneration? *Annals of Neurology* 26 (2) (Aug): 221-5.

Krasodomska, K., W. Lubinski, A. Potemkowski, and K. Honczarenko. 2010. Pattern electroretinogram (PERG) and pattern visual evoked potential (PVEP) in the early stages of alzheimer's disease. *Documenta Ophthalmologica.Advances in Ophthalmology* 121 (2) (Oct): 111-21.

Liu, M., J. Duggan, T. E. Salt, and M. F. Cordeiro. 2011. Dendritic changes in visual pathways in glaucoma and other neurodegenerative conditions. *Experimental Eye Research* 92 (4) (Apr): 244-50.

London, Anat, Inbal Benhar, and Michal Schwartz. 2012. The Retina As A Window To The Brain—From Eye Research To CNS Disorders. Nature Reviews Neurology 9 (1): 44-53.

Lucy, K. A., and G. Wollstein. 2016. Structural and functional evaluations for the early detection of glaucoma. *Expert Review of Ophthalmology* 11 (5): 367-76.

Luo, X., and L. J. Frishman. 2011. Retinal pathway origins of the pattern electroretinogram (PERG). *Investigative Ophthalmology & Visual Science* 52 (12) (Nov 1): 8571-84.

Luu, C. D., J. A. Szental, S. Y. Lee, R. Lavanya, and T. Y. Wong. 2010. Correlation between retinal oscillatory potentials and retinal vascular caliber in type 2 diabetes. *Investigative Ophthalmology & Visual Science* 51 (1) (Jan): 482-6.

Mafei, L., and A. Fiorentini. 1981. Electroretinographic responses to alternating gratings before and after section of the optic nerve. *Science (New York, N.Y.)* 211 (4485) (Feb 27): 953-5.

Maffei, L., A. Fiorentini, S. Bisti, and H. Hollander. 1985. Pattern ERG in the monkey after section of the optic nerve. *Experimental Brain Research* 59 (2): 423-5.

Miura, G., M. H. Wang, K. M. Ivers, and L. J. Frishman. 2009. Retinal pathway origins of the pattern ERG of the mouse. *Experimental Eye Research* 89 (1) (Jun 15): 49-62.

Morgan, J. E. 2012. Retina ganglion cell degeneration in glaucoma: An opportunity missed? A review. *Clinical & Experimental Ophthalmology* 40 (4) (May-Jun): 364-8.

Morgan, J. E. 2004. Circulation and axonal transport in the optic nerve. *Eye (London, England)* 18 (11) (Nov): 1089-95.

Morquette, J. B., and A. Di Polo. 2008. Dendritic and synaptic protection: Is it enough to save the retinal ganglion cell body and axon? *Journal of Neuro-Ophthalmology : The Official Journal of the North American Neuro-Ophthalmology Society*28 (2) (Jun): 144-54.

Moss, H. E., J. C. Park, and J. J. McAnany. 2015. The photopic negative response in idiopathic intracranial hypertension. *Investigative Ophthalmology & Visual Science* 56 (6) (Jun): 3709-14.

Parisi, V., M. Centofanti, S. Gandolfi, D. Marangoni, L. Rossetti, L. Tanga, M. Tardini, et al. 2014. Effects of coenzyme Q10 in conjunction with vitamin E on retinal-evoked and cortical-evoked responses in patients with open-angle glaucoma. *Journal of Glaucoma* 23 (6) (Aug): 391-404.

Parisi, V., M. Centofanti, L. Ziccardi, L. Tanga, M. Michelessi, G. Roberti, and G. Manni. 2015. Treatment with citicoline eye drops enhances retinal function and neural conduction along the visual pathways in open angle glaucoma. *Graefe's Archive for Clinical and Experimental Ophthalmology = Albrecht Von Graefes Archiv Fur Klinische Und Experimentelle Ophthalmologie* 253 (8) (Aug): 1327-40.

Parisi, V., R. Restuccia, F. Fattapposta, C. Mina, M. G. Bucci, and F. Pierelli. 2001. Morphological and functional retinal impairment in alzheimer's disease patients. *Clinical Neurophysiology : Official Journal of the International Federation of Clinical Neurophysiology* 112 (10) (Oct): 1860-7.

Patangay S, Derafshi Z, Vajaranant TS, Park JC, Ghahari E, McAnany JJ & Hetling JR (2018). Pattern electroretinogram responses elicited with high-luminance patterns in peripheral retina with healthy and glaucomatous eyes. *Translational Vision Science and Technology. The Association for Research in Vision and Ophthalmology is the*

Peppe, A., P. Stanzione, M. Pierantozzi, R. Semprini, A. Bassi, A. M. Santilli, R. Formisano, M. Piccolino, and G. Bernardi. 1998. Does pattern electroretinogram spatial tuning alteration in parkinson's disease depend on motor disturbances or retinal dopaminergic loss? *Electroencephalography and Clinical Neurophysiology* 106 (4) (Apr): 374-82.

Pescosolido, N., A. Barbato, A. Stefanucci, and G. Buomprisco. 2015. Role of electrophysiology in the early diagnosis and follow-up of diabetic retinopathy. *Journal of Diabetes Research* 2015 : 319692.

Porciatti, V., and L. M. Ventura. 2004. Normative data for a user-friendly paradigm for pattern electroretinogram recording. *Ophthalmology* 111 (1) (Jan): 161-8.

Sartucci, F., G. Orlandi, U. Bonuccelli, D. Borghetti, L. Murri, C. Orsini, L. Domenici, and V. Porciatti. 2006. Chromatic pattern-reversal electroretinograms (ChPERGs) are spared in multiple system atrophy compared with parkinson's disease. *Neurological Sciences : Official Journal of the Italian Neurological Society and of the Italian Society of Clinical Neurophysiology* 26 (6) (Feb): 395-401.

Satue, M., M. Seral, S. Otin, R. Alarcia, R. Herrero, M. P. Bambo, M. I. Fuertes, L. E. Pablo, and E. Garcia-Martin. 2014. Retinal thinning and correlation with functional disability in patients with parkinson's disease. *The British Journal of Ophthalmology* 98 (3) (Mar): 350-5.

Sehi, M., M. Pinzon-Plazas, W. J. Feuer, and D. S. Greenfield. 2009. Relationship between pattern electroretinogram, standard automated perimetry, and optic nerve structural assessments. *Journal of Glaucoma* 18 (8) (Oct-Nov): 608-17.

Shorstein, N. H., W. W. Dawson, and M. B. Sherwood. 1999. Mid-peripheral pattern electrical retinal responses in normals, glaucoma suspects, and glaucoma patients. *The British Journal of Ophthalmology* 83 (1) (Jan): 15-23.

Silverstein, S. M., and R. Rosen. 2015. Schizophrenia and the eye. *Schizophrenia Research.Cognition* 2 (2) (Jun): 46-55.

Smith, M. A., C. Z. Xia, C. M. Dengler-Crish, K. M. Fening, D. M. Inman, B. R. Schofield, and S. D. Crish. 2016. Persistence of intact retinal ganglion cell terminals after axonal transport loss in the DBA/2J mouse model of glaucoma. *The Journal of Comparative Neurology* 524 (17) (Dec 1): 3503-17.

Tagliati, M., I. Bodis-Wollner, I. Kovanecz, and P. Stanzione. 1994. Spatial frequency tuning of the monkey pattern ERG depends on D2 receptor-linked action of dopamine. *Vision Research* 34 (16) (Aug): 2051-7.

Tagliati, M., I. Bodis-Wollner, and M. D. Yahr. 1996. The pattern electroretinogram in parkinson's disease reveals lack of retinal spatial tuning. *Electroencephalography and Clinical Neurophysiology* 100 (1) (Jan): 1-11.

Thompson, D. A., and N. Drasdo. 1994. The origins of luminance and pattern responses of the pattern electroretinogram. *International Journal of Psychophysiology : Official Journal of the International Organization of Psychophysiology* 16 (2-3) (May): 219-27.

Trick, G. L. 1985. Retinal potentials in patients with primary open-angle glaucoma: Physiological evidence for temporal frequency tuning deficits. *Investigative Ophthalmology & Visual Science* 26 (12) (Dec): 1750-8.

Tzekov, R., and G. B. Arden. 1999. The electroretinogram in diabetic retinopathy. *Survey of Ophthalmology* 44 (1) (Jul-Aug): 53-60.

Varma, R., P. P. Lee, I. Goldberg, and S. Kotak. 2011. An assessment of the health and economic burdens of glaucoma. *American Journal of Ophthalmology* 152 (4) (Oct): 515-22.

Ventura, L. M., N. Sorokac, R. De Los Santos, W. J. Feuer, and V. Porciatti. 2006. The relationship between retinal ganglion cell function and retinal nerve fiber thickness in early glaucoma. *Investigative Ophthalmology & Visual Science* 47 (9) (Sep): 3904-11.

Viswanathan, S., L. J. Frishman, and J. G. Robson. 2000. The uniform field and pattern ERG in macaques with experimental glaucoma: Removal of spiking activity. *Investigative Ophthalmology & Visual Science* 41 (9) (Aug): 2797-810.

Wachtmeister, L. 1998. Oscillatory potentials in the retina: What do they reveal. *Progress in Retinal and Eye Research* 17 (4) (Oct): 485-521.

Weinreb, R. N., T. Aung, and F. A. Medeiros. 2014. The pathophysiology and treatment of glaucoma: A review. *Jama* 311 (18) (May 14): 1901-11.

Bodis-Wollner, Ivan, Marcia S. Marx, Sundana m, Phyllis B, Leland M, and Melvin Y. 1987. Visual dysfunction in Parkinson's disease. Brain 110 (6): 1675-1698.

Xia, X., R. Wen, T. H. Chou, Y. Li, Z. Wang, and V. Porciatti. 2014. Protection of pattern electroretinogram and retinal ganglion cells by oncostatin M after optic nerve injury. *PloS One* 9 (9) (Sep 22): e108524.

Xu, L., S. L. Ball, K. R. Alexander, and N. S. Peachey. 2003. Pharmacological analysis of the rat cone electroretinogram. *Visual Neuroscience* 20 (3) (May-Jun): 297-306.

Zapf, H. R., and M. Bach. 1999. The contrast characteristic of the pattern electroretinogram depends on temporal frequency. *Graefe's Archive for Clinical and Experimental Ophthalmology = Albrecht Von Graefes Archiv Fur Klinische Und Experimentelle Ophthalmologie* 237 (2) (Feb): 93-9.

APPENDIX

Sections of Part III, excluding “Effect of NMDA on High Luminance pERG” and “Local Pattern Stimulation” of this document are published in the manuscript Patangay et al.; The Association for Research in Vision and Ophthalmology is the copyright holder of this article. This work is licensed under a Creative Commons Attribution-NonCommercial-NoDerivatives 4.0 International License.

Education

Doctor of Philosophy, Bioengineering
University of Illinois at Chicago, USA 2012 - 2017
Bachelor of Technology, Biotechnology
Jawaharlal Nehru Technological University, Hyderabad, India 2007 - 2011

Publications

Patangay S, Derafshi Z, Vajaranant TS, Park JC, Ghahari E, McAnany JJ & Hetling JR (2018). Pattern electroretinogram responses elicited with high-luminance patterns in peripheral retina with healthy and glaucomatous eyes. Translational Vision Science and Technology.
Patangay S, Derafshi Z, J.C Park, Ghahari E, Vajaranant T, J.J McAnany, Hetling J.R. Assessment of peripheral pattern electroretinogram (ppERG) test sensitivity in glaucoma patients. (*In final preparation*)

Patents

Hetling JR, **Patangay S,** Ouy M. Pixelated Full-Field Multi-Purpose Stimulus Source Apparatus, Method and System for Probing Visual Pathway Function. PCT US2016, 048129, filed Aug 2016, *pending*.
Hetling JR, **Patangay S**, Derafshi Z. Pattern Stimulus Source for Visual Electrophysiology. PCT/US2014/034636, filed Jul 2013, *pending*.

Conferences and Talks

Patangay S, Park JC, Vajaranant T, McAnany JJ, Hetling JR (2017). pERG responses from the peripheral retina: correlation of field sector PERG responses with standard automated perimetry and circumpapillary retinal nerve fiber layer thickness in glaucoma patients. International Society for Clinical Electrophysiology of Vision annual meeting, Bascom Palmer Eye Institute, Miami, Florida. 2017 Oct 21-26. Oral Presentation.
JR Hetling, **S Patangay**, JC Park, S Rahmani, T Ban, JJ McAnany (2017). Evaluation of a soft, disposable ERG electrode prototype. International Society for Clinical Electrophysiology of Vision annual meeting, Bascom Palmer Eye Institute, Miami, Florida. 2017 Oct 21-26. Winner: The Marmor Award for Clinical Innovation in Visual Electrophysiology.
Patangay S, Park JC, Ghahari E, Vajaranant T, McAnany JJ, Hetling JR (2017). Pattern electroretinogram responses from the far-peripheral retina (ring and sector stimuli) in healthy eyes and in eyes with glaucoma. Poster presented at: The Association for Research in Vision and Ophthalmology, Baltimore, Maryland. 2017 May 7-11
Safa Rahmani, Tamas Ban, **Shresta Patangay**, Jason C. Park, J. Jason McAnany, John Hetling (2017). Evaluation of a soft, disposable, conformal ERG lens electrode prototype vs. Burian-Allen lens and DTL fiber electrodes. (**Presenting Author**). Poster presented at: The Association for Research in Vision and Ophthalmology, Baltimore, Maryland. 2017 May 7-11.
Patangay S, Derafshi Z, Park JC, Ghahari E, Vajaranant T, McAnany JJ, Hetling JR (2016). Reversal rate dependence and nasal-temporal field differences in high luminance peripheral pattern electroretinogram (ppERG) responses in healthy human eyes. Poster presented at: The Association for Research in Vision and Ophthalmology, Seattle, Washington. 2016 May 1-5.

Patangay S, Derafshi Z, Park JC, Vajaranant T, McAnany JJ, Hetling JR. (2015). Pattern electroretinogram (pERG) responses evoked by a novel high-luminance three-dimensional stimulus source that targets the peripheral retina. Poster presented at: The Association for Research in Vision and Ophthalmology, Denver, Colorado. 2015 May 3-7.
Patangay S. (2015, 2016, 2017). Clinical testing of the peripheral retina. Invited guest lectures in the course Freshman Seminar in Bioengineering (BIOE 102).

Awards and Honors

The Marmor Award for Clinical Innovation in Visual Electrophysiology (ISCEV) Oct 2017
Honorable mention, The Image of Research, UIC Sept 2017
The Association for Research in Vision and Ophthalmology (ARVO): Hot Topic May 2017
Joseph M. and Eula C. Lawrence Travel Grant – Retina research foundation (ARVO) May 2016
The Association for Research in Vision and Ophthalmology (ARVO): Hot Topic May 2015
Proof of concept awards program – UIC Chancellor's Innovation Fund. Aug 2013

Research

Dissertation: Pattern Electroretinograpy in Peripheral Retina: System Development and Validation in Human Subjects.
Research summary: Evaluating health of the peripheral retina is critical to diagnosis and management of degenerative eye diseases such as glaucoma. Peripheral retina cannot be effectively tested with existing clinical tools. We developed, from the ground up, a system to test ganglion cell function in peripheral retina, established a normative database, and evaluated efficacy in glaucoma patients, with comparison to current clinical gold standard tests. This new testing protocol, ***peripheral pattern electroretinigraphy*** (ppERG) was more sensitive to early glaucomatous damage than conventional central-field pERG in most patients. This technology can significantly improve early diagnosis of glaucoma, leading to decreased lifetime vision loss for glaucoma patients. This work was recognized as a Hot Topic for two years by the *Association for Research in Vision and Ophthalmology*, and the enabling technology is described in two pending patents.

Other Responsibilities

- Trained for and carried out experiments in rodent and human multi-electrode electroretinography.
- Helped establish SOP for preparing contact lens electrode arrays.
- Key role in pre-clinical testing of novel human electroretinogram sensors.
- Substantially contributed to NSF STTR Phase I proposal: RetMap ERG Electrode: Safe, Disposable, Stable (submitted 2016, not funded)
- Substantially contributed to the BrightFocus Foundation Glaucoma Research proposal: Diagnosing glaucoma in the therapeutic window of opportunity. (submitted 2016, not funded; resubmitted 2017).

- Led the effort to secure UIC IRB approved research protocol: Novel electroretinogram protocols for assessing neurodegenerative disease. Approved 2016, continuing review approved 2017.
- Mentored an undergraduate Senior Design team, project title: Full-Field Stimulus Source for Vision Testing (2016-2017)
- Mentored undergraduate research student in design of a video fixation target for pediatric vision testing (2016-present)
- Jury member: BIOE 250 Symposium - Clinical Problems in Bioengineering. 2015 May.

Workshops and Training

- Institutional training in the use of animals in research: Animal Research at UIC, 2014 Oct 28; Working with Mice and Rats at UIC, 2014 Nov 26.
- Educational courses: Applying Visual Electrophysiology for Clinical Evaluation and Vision Research. The Association for Research in Vision and Ophthalmology , Seattle, Washington. 2016 May 1-5
- Institutional training in human subjects research: Group 1, HSP, Biomedical Research Investigators and Key Personnel, 2017 Jan 24.
- Two-day hands-on course, *Human Clinical Visual Electrophysiology*, International Society for Clinical Electrophysiology of Vision annual meeting, Bascom Palmer Eye Institute, Miami, Florida. 2017 Oct 21-26

Positions Held

Teaching Assistant 2015 - 2017

Introduction to Bioengineering: BIOE 101

- Mentored students extensively in the use of SolidWorks and Arduino

Modeling Physiological Data and Systems: BIOE 240

- Mentored students extensively in the use of Matlab

Clinical Problems in Bioengineering: BIOE 250
Neural Engineering I: Introduction to Hybrid Neural Systems: BIOE 475
Neural Engineering I Laboratory: BIOE 476

- Co-developed laboratory module Electroretinogram Recording and Analysis
- Co-developed laboratory module Biopotential Control of Robotics
- Mentored students extensively in neural engineering system design and troubleshooting, especially with LabView-based data acquisition, analog circuit design and Arduino

Clinical Study Coordinator 2015 - Present

Responsibilities

- Recruiting consenting and testing healthy subjects.
- Recruiting consenting and testing patients from the Glaucoma and General Eye Clinics at UIC, and at the Chicago Lighthouse for the Blind and Visually Impaired.

Research Intern, RetMap, Inc. 2016 - Present

Responsibilities

- Supported market assessment
- Management of company image
- Product technical support
- Fundraising (including investor pitch meetings and SBIR proposal preparation).

Technical Skills

Matlab | LabView | Arduino | Python | Technical Photography and Illustration | Web Design | SolidWorks (beginner) |

Memberships

- The Association for Research in Vision and Ophthalmology (ARVO) - Member in Training
- International Society for Clinical Electrophysiology and Vision Science (ISCEV) - Student member
- Young International Society for Clinical Electrophysiology and Vision Science (YSCEV)

Languages

English | Hindi | Telugu | Marathi | Parseltongue